

23

CENTRAL RESEARCH LIBRARY  
DOCUMENT COLLECTION

OAK RIDGE NATIONAL LABORATORY LIBRARY



3 4456 0021563 9

ORNL-3390  
UC-4 - Chemistry  
TID-4500 (24th ed.)

THE EXPERIMENTAL DETERMINATION OF  
THE THERMAL CONDUCTIVITY OF  
MOLTEN LITHIUM FROM 600 TO  
1550 DEGREES FAHRENHEIT

J. W. Cooke  
*(thesis)*

CENTRAL RESEARCH LIBRARY  
DOCUMENT COLLECTION  
**LIBRARY LOAN COPY**  
**DO NOT TRANSFER TO ANOTHER PERSON**  
If you wish someone else to see this  
document, send in name with document  
and the library will arrange a loan.



**OAK RIDGE NATIONAL LABORATORY**  
operated by  
**UNION CARBIDE CORPORATION**  
for the  
**U.S. ATOMIC ENERGY COMMISSION**

Printed in USA. Price: \$2.75 Available from the  
Office of Technical Services  
U. S. Department of Commerce  
Washington 25, D. C.

LEGAL NOTICE

This report was prepared as an account of Government sponsored work. Neither the United States, nor the Commission, nor any person acting on behalf of the Commission:

- A. Makes any warranty or representation, expressed or implied, with respect to the accuracy, completeness, or usefulness of the information contained in this report, or that the use of any information, apparatus, method, or process disclosed in this report may not infringe privately owned rights; or
- B. Assumes any liabilities with respect to the use of, or for damages resulting from the use of any information, apparatus, method, or process disclosed in this report.

As used in the above, "person acting on behalf of the Commission" includes any employee or contractor of the Commission, or employee of such contractor, to the extent that such employee or contractor of the Commission, or employee of such contractor prepares, disseminates, or provides access to, any information pursuant to his employment or contract with the Commission, or his employment with such contractor.

Contract No. W-7405-eng-26

Reactor Division

THE EXPERIMENTAL DETERMINATION OF THE THERMAL  
CONDUCTIVITY OF MOLTEN LITHIUM FROM  
600 TO 1550 DEGREES FAHRENHEIT

J. W. Cooke

Submitted as a thesis to the Graduate Council of  
The University of Tennessee in partial fulfillment of  
the requirements for the degree of Master of Science.

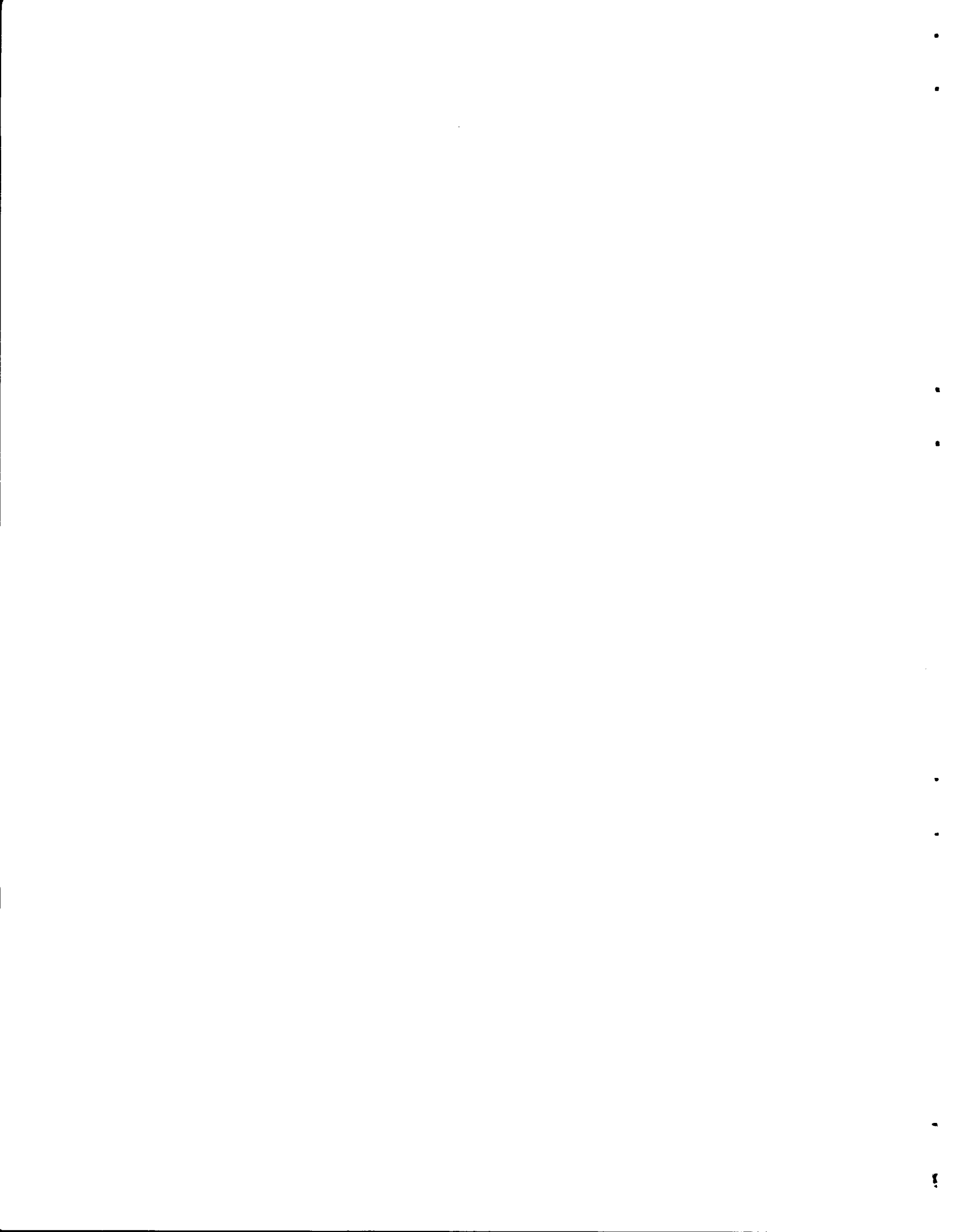
Date Issued

JAN 22 1964

OAK RIDGE NATIONAL LABORATORY  
Oak Ridge, Tennessee  
operated by  
UNION CARBIDE CORPORATION  
for the  
U. S. ATOMIC ENERGY COMMISSION

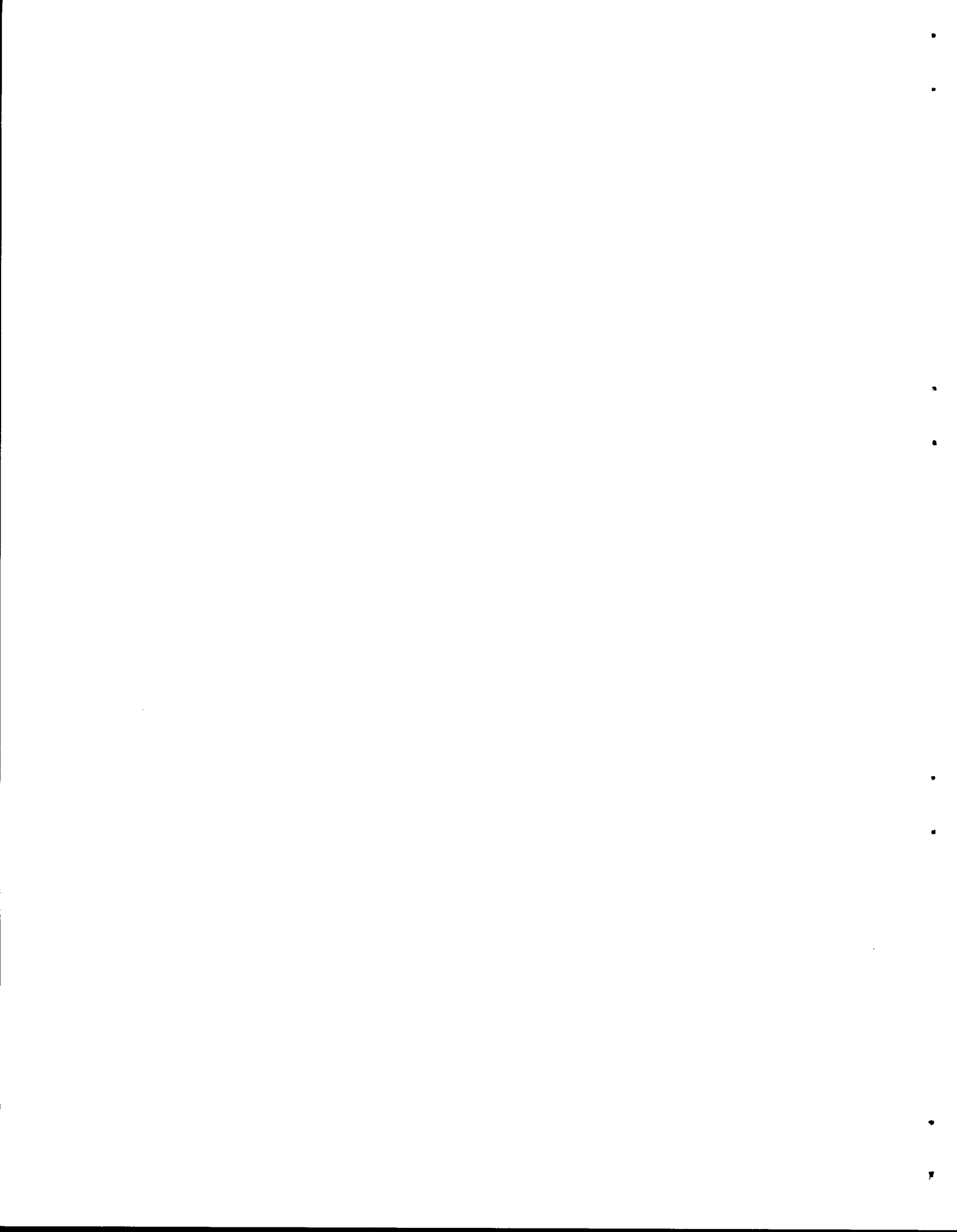


3 4456 0021563 9



## ACKNOWLEDGMENTS

The investigation described herein was performed at the Oak Ridge National Laboratory, and the author is grateful for the invaluable assistance of many of his associates. In particular, the author wishes to express his appreciation to the following persons: Dr. H. W. Hoffman for his initiation and guidance of this investigation during its early stages, Mr. W. R. Gambill for his patient advice and encouragement, Mr. S. J. Claiborne, project technician, for his valuable assistance in constructing and operating the apparatus, Mr. W. C. Colwell's Graphic Arts Section for their skillful preparation of the illustrations used in this report, and Miss Dolores Eden for her conscientious typing of this report. The author would also like to acknowledge the timely suggestions and careful review of this report by Professor P. F. Pasqua, Head of the Nuclear Engineering Department at the University of Tennessee.



## SUMMARY

Molten lithium has long appeared attractive as a high-temperature, high-efficiency heat-transfer medium. As more knowledge is gained of its compatibility with various container materials, molten lithium seems certain to find application as a coolant for space-power reactors and other high-performance reactor systems. However, knowledge of its physical properties, particularly thermal conductivity, is still limited with regard to temperature range and agreement of experimental data. For example, the results of three previous investigations of the thermal conductivity of molten lithium disagree by as much as 60% in absolute magnitude. In an attempt to resolve these disagreements and to extend the data to higher temperatures, an apparatus was developed to determine the conductivity of molten lithium from 600 to 1550°F.

A comparative, axial-heat-flow thermal conductivity apparatus utilizing compensating guard heating was developed for the investigation. By this method, heat flowed downward through a heat meter, through a cavity containing the lithium sample, through another heat meter, and into a water-cooled sink. Heat flow in the radial direction was minimized by maintaining with guard heaters an axial temperature profile in a coaxial guard tube which matched the axial temperature profile along the centerline of the apparatus. The lithium conductivity was determined from the known conductivity of the heat meters and from the axial temperature gradients and cross-sectional areas of the heat meters and lithium sample. The temperature gradients were determined using Pt/90Pt+10Rh thermocouples, and type 347 stainless steel was used for the heat meters. Initial filling difficulties caused by the high-surface tension, large heat of fusion, and low density of the

lithium were overcome, and the cavity was successfully filled with a void-free sample of 99.8+ wt % lithium metal. Careful assembly and operation of the apparatus insured against extraneous thermal and electrical emfs, sample contamination, radial heat flow, thermocouple drift, and nonsteady state.

Twenty-six determinations were made of the conductivity of the molten lithium sample. From 600 to 1550°F, the results can be represented to within  $\pm 2.2\%$  rms deviation by the least-squares equation:

$$k \text{ (Btu/hr}\cdot\text{ft}\cdot\text{°F)} = 19.76 [1 + 5.01 \times 10^{-4} t \text{ (°F)}] .$$

From consideration of many possible sources of error, the total uncertainty in the results was conservatively estimated to be less than  $\pm 8$  to  $\pm 15\%$  from the lower to the higher temperatures. That the actual uncertainty was probably less than the total uncertainty is evidenced by (a) the good agreement between the two independent axial-heat-flow measurements [the difference varying from 0.1 to 3.8%], (b) the modest amount of radial heat exchange [always  $\leq 0.9\%$  of the axial-heat flow], and (c) the consistency of the axial temperature profiles.

Extrapolations to the melting point of the present data, previous results, and values predicted by the Wiedemann-Franz relationship agree to within  $\pm 7\%$ ; whereas above 1000°F, the present results compare well only with predicted values, particularly in temperature dependency. The temperature dependency of the present results is positive, which is contrary to the data of either molten sodium or potassium, but is consistent with the volumetric coefficient of thermal expansion of molten lithium being almost half that of either molten sodium or potassium.

From a broad extrapolation of the present data to the calculated critical conductivity, the conductivity of the molten lithium appears to reach a maximum of 45 Btu/hr·ft·°F at 3200°F. This will require further investigation at high temperatures for verification. By substituting a niobium alloy for the stainless steel, the present apparatus could be used to extend the conductivity data to the normal boiling point (2403°F).

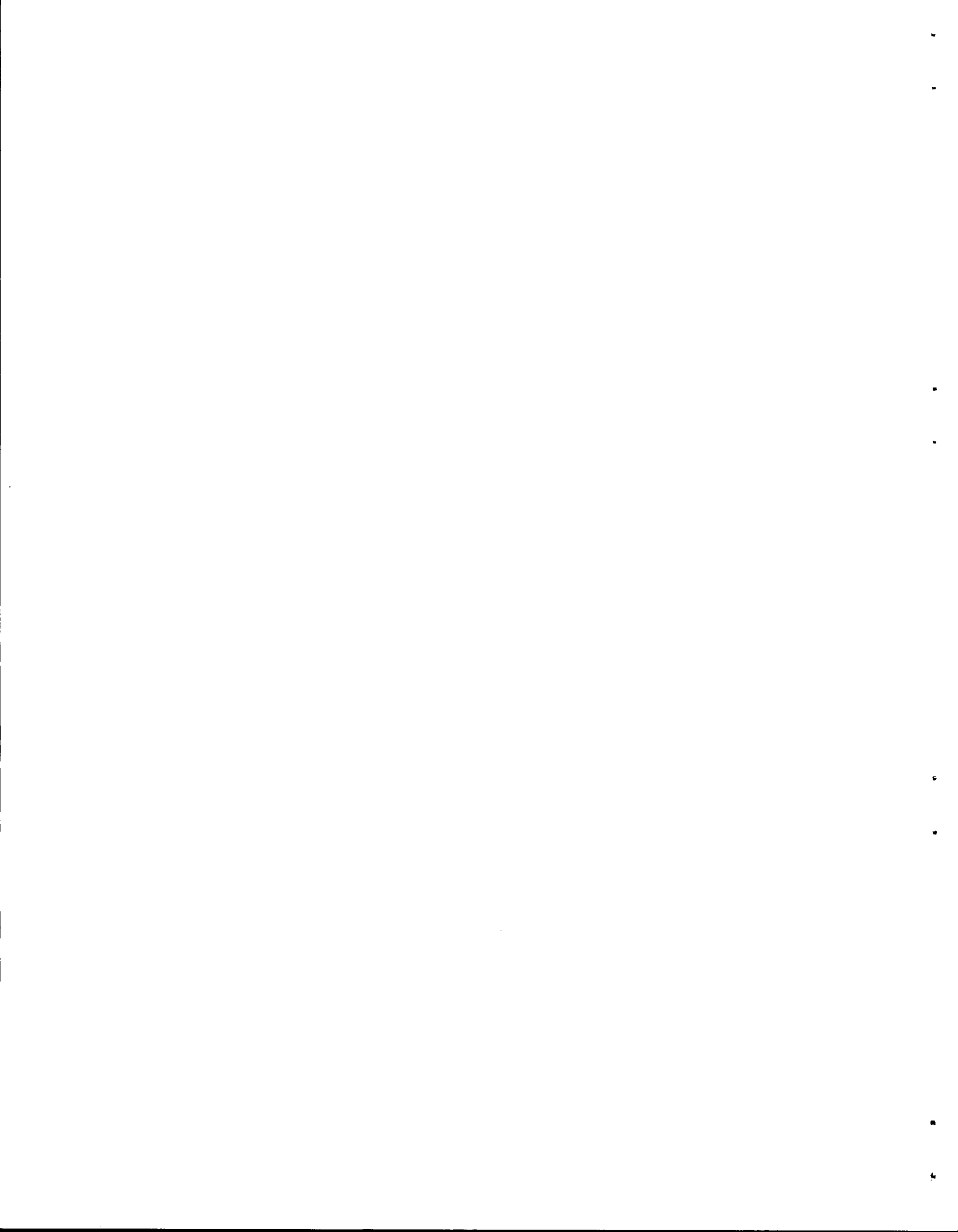


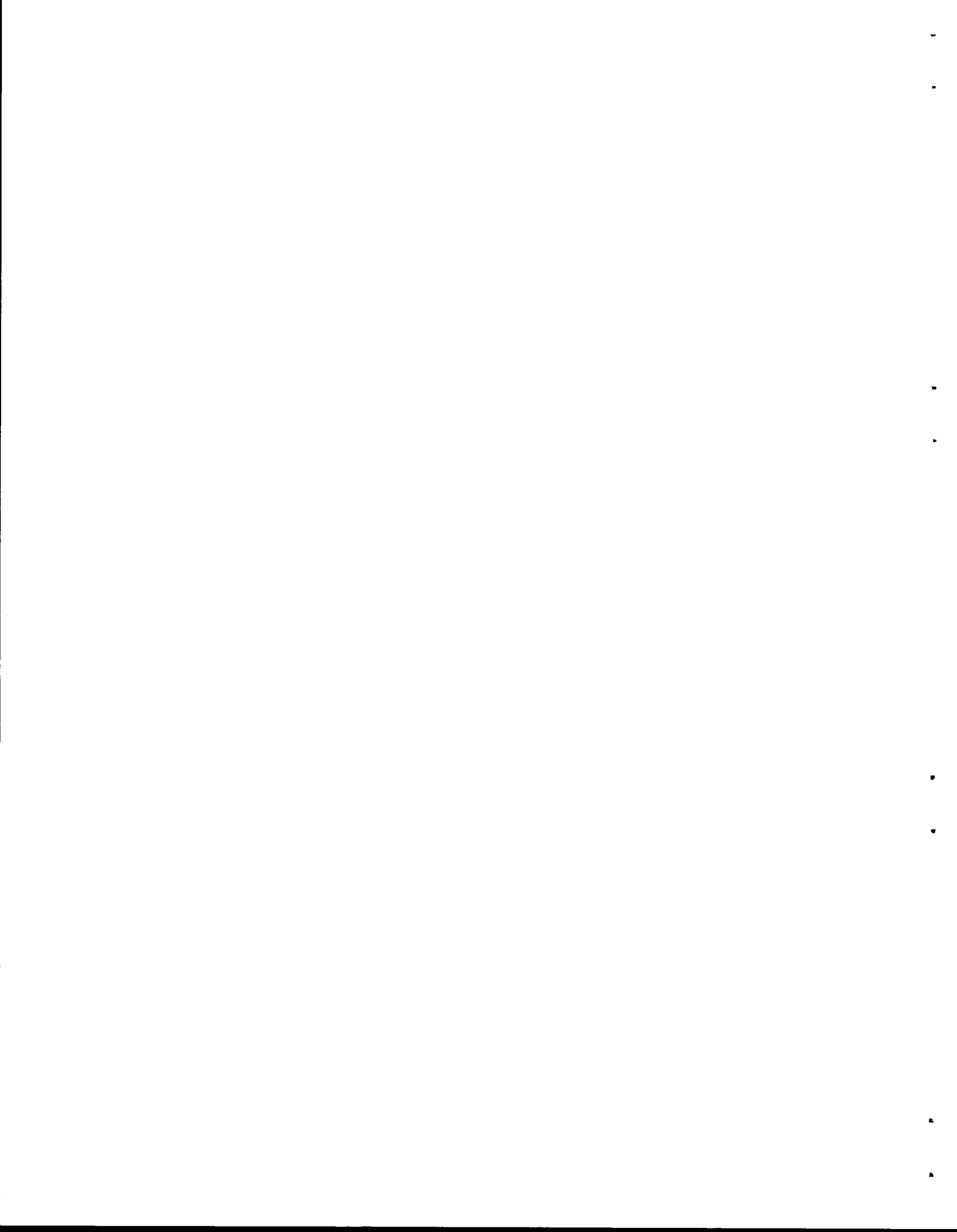
## TABLE OF CONTENTS

CHAPTER	PAGE
I. INTRODUCTION . . . . .	1
II. THEORY . . . . .	2
Mechanism of liquid-metal thermal conductivity . . . . .	2
Correlations for predicting thermal conductivity . . . . .	6
Methods for determining the thermal conductivity of liquid metals . . . . .	9
Method of determination used in the present investigation . . . . .	12
Method of calculation used in the present investigation . . . . .	14
III. EXPERIMENTAL EQUIPMENT . . . . .	19
Complete system . . . . .	19
Test piece . . . . .	19
Coaxial guard tube . . . . .	24
Guard heaters . . . . .	26
Sink heating and cooling . . . . .	27
Furnace . . . . .	28
Electrical system . . . . .	28
Instrumentation . . . . .	30
Vacuum system . . . . .	32
IV. PROCEDURE . . . . .	33
Filling the test piece . . . . .	33
Calibration and installation of thermocouples . . . . .	40

CHAPTER	PAGE
Operating procedure . . . . .	41
V. RESULTS . . . . .	45
Values of the thermal conductivity of molten lithium . . . . .	45
Axial and radial heat flow along the test piece . . . . .	48
Axial temperature measurements and profiles . . . . .	49
Axial location of thermocouple junctions . . . . .	50
Miscellaneous observations . . . . .	54
VI. DISCUSSION OF RESULTS . . . . .	55
Errors in the present determinations . . . . .	55
Comparisons with previous determinations . . . . .	60
Comparisons with predicted values and theory . . . . .	65
Adequacy of experimental apparatus . . . . .	70
VII. CONCLUSIONS . . . . .	72
REFERENCES . . . . .	74
APPENDIX . . . . .	79
A. PREVIOUS DETERMINATIONS OF THE THERMAL CONDUCTIVITY OF MOLTEN LITHIUM . . . . .	79
B. ADDITIONAL DETAILS OF THE DESIGN OF THE APPARATUS . . . . .	95
C. EXPERIMENTAL DATA AND CALCULATIONS . . . . .	103
D. PRECISION AND ERROR ANALYSES; FACTORS AFFECTING THE ACCURACY OF THE RESULTS . . . . .	117
E. PROPERTIES OF MATERIALS USED IN APPARATUS . . . . .	140
F. NOTATION . . . . .	148

## LIST OF TABLES

TABLE	PAGE
I. Spectrochemical Analyses of the Lithium Sample Before and After Thermal Conductivity Determinations . . . . .	34
II. Summary of Lithium Thermal Conductivity Calculations . . . . .	46
III. Summary of Calculated Thermocouple Locations . . . . .	53
IV. Source and Estimated Magnitude of Experimental Errors . . . . .	56
V. List of Experimental Equipment Used with Capacities, Ranges, and Accuracies Given When Known . . . . .	102
VI. Uncorrected Experimental Data . . . . .	104
VII. Corrected Experimental Data . . . . .	107
VIII. Critical "As Built" Dimensions of the Apparatus . . . . .	109
IX. Summary of Error and Precision Analyses . . . . .	139

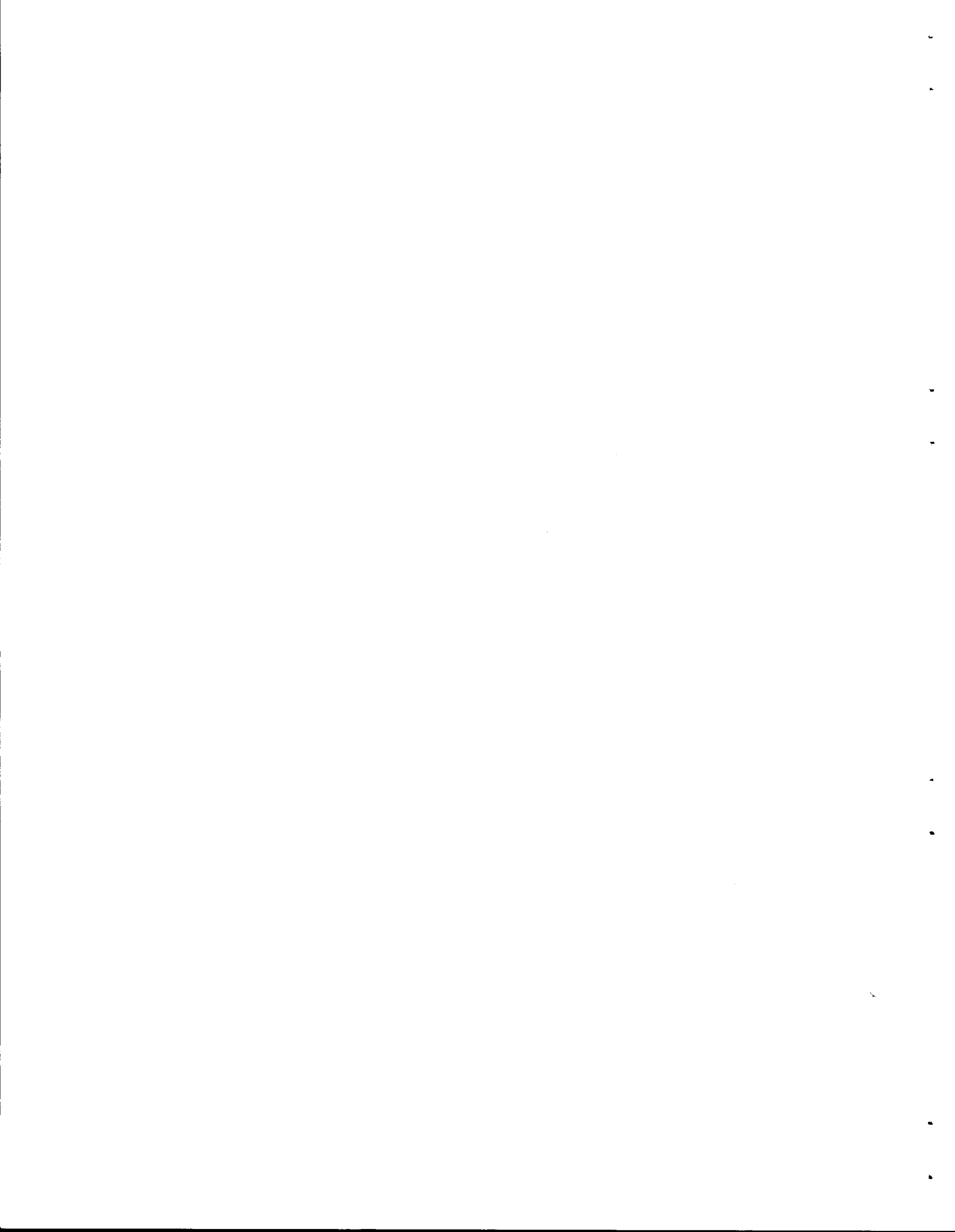


## LIST OF FIGURES

FIGURE	PAGE
1. Apparatus Assembly . . . . .	13
2. Reference Planes for Heat Balances Along Test Piece and Coaxial Guard Tube . . . . .	15
3. Schematic Diagram of Complete System . . . . .	20
4. Front View of Apparatus . . . . .	21
5. Rear View of Apparatus . . . . .	22
6. Test Piece Assembly . . . . .	23
7. Thermocouple Locations . . . . .	25
8. Electrical System for Heaters . . . . .	29
9. Thermocouple Circuit Diagram . . . . .	31
10. Details and Schematic Flow Diagram of Fill System . . . . .	35
11. X-Ray Photographs of Test Piece Showing Void in Lithium Sample for Test Piece No. 1 (a) After Filling and (b) After 20 gees Acceleration; and for Test Piece No. 2 (c) After Filling, (d) At 550°F, (e) At 650°F, and (f) As Installed in Apparatus . . . . .	38
12. Method of Thermocouple Installation . . . . .	42
13. Thermal Conductivity of Molten Lithium as a Function of Temperature - Present Results . . . . .	47
14. In Place, Relative Calibration of System Thermocouples After Completion of Data Runs . . . . .	51
15. Typical Axial Temperature Profile Along Test Piece and Guard Tube - Run No. 8 . . . . .	52

FIGURE	PAGE
16. Thermal Conductivity of Molten Lithium as a Function of Temperature - Present, Previous, and Predicted Values . . . . .	62
17. Thermal Conductivity of Molten Lithium as a Function of Temperature - Comparisons Between Recent Russian Data and the Present Results . . . . .	64
18. Thermal Conductivity Device Used by Yaggee and Untermyer . . .	80
19. Apparatus Used by Ewing, <u>et al.</u> , to Measure the Thermal Conductivity of Molten Metals . . . . .	83
20. Apparatus Used by Webber, <u>et al.</u> , to Measure the Thermal Conductivity of Molten Lithium . . . . .	87
21. Thermal Conductivity Apparatus Used by Nikolskii, <u>et al.</u> . . .	92
22. Details of Lower Heat Meter and Sample Container . . . . .	96
23. Details of Upper Heat Meter and Expansion Tank . . . . .	97
24. Details of Coaxial Guard Tube . . . . .	100
25. Details of Guard Heaters and Main Heater . . . . .	101
26. One-Dimensional Representation of the Temperature Distri- bution Along the Test Piece and Attached Thermocouple Lead Wire . . . . .	131
27. Properties of Lithium as a Function of Temperature - Electrical Resistivity, Viscosity, and Heat Capacity . . . . .	141
28. Properties of Lithium as a Function of Temperature - Density and Coefficient of Volumetric Thermal Expansion . . . . .	142
29. Properties of Type 347 Stainless Steel as a Function of Temperature - Density, Coefficient of Linear Thermal Expansion, and Heat Capacity . . . . .	143

FIGURE	PAGE
30. Thermal Conductivity of Type 347 Stainless Steel as a Function of Temperature . . . . .	144
31. Thermal Conductivity of Fiberfrax Insulation . . . . .	145



## CHAPTER I

## INTRODUCTION

Considering the potential value of molten lithium as a high-temperature, high-efficiency heat-transfer medium, it is surprising to find only a meager amount of inconsistent data for its thermal conductivity. For example, of three investigations previously available, one showed a sharp decline in the thermal conductivity for molten lithium with increasing temperature,<sup>1\*</sup> one found it to be almost constant,<sup>2</sup> and the other indicated that the conductivity increased with temperature.<sup>3</sup> In addition, these three investigations disagreed by as much as 60 per cent in absolute magnitude. In an attempt to resolve these disagreements and to extend the data to higher temperatures, an apparatus was developed to determine the thermal conductivity of molten lithium from 600 to 1550°F.

A detailed description of the thermal conductivity apparatus and of the procedures used in its operation is given in this report. The results and an estimation of their accuracy are presented and compared with theory and existing data. Recently obtained electrical resistivity measurements for molten lithium<sup>4,5</sup> are used in conjunction with various electrical-thermal conductivity correlations<sup>6-9</sup> to show their relative worth in predicting the thermal conductivity of molten lithium.

---

\* Superscript numbers refer to similarly numbered References at the end of the report.

## CHAPTER II

## THEORY

The theory and methods of determination of the thermal conductivity of liquid metals and the method used in the present investigation to calculate the thermal conductivity of molten lithium are discussed in this chapter.

Mechanism of liquid-metal thermal conductivity. A mathematical expression for the propagation of thermal energy through a solid material was first proposed by Biot in 1804 and amplified by Fourier in 1822.<sup>10</sup> The expression stated that the quantity of heat flowing through a given area in a given time was equal to the temperature gradient normal to the area times a coefficient of thermal conductivity. This expression simplified a complex problem. The term coefficient of thermal conductivity itself combined many complex atomic processes which governed the transmittal of heat through a substance and which at that time were not understood and in many cases unknown.

Since 1822, every major advance in atomic physics has led to an advance in the theory of conduction. By 1930, it was known that two processes, the interaction of atoms or molecules and the interaction of free electrons, transferred the thermal energy through a substance from a higher to a lower temperature region. The degree to which either of these two processes predominated depended to a large extent on the number and mobility of the free electrons. In the case of metals, such as copper, it was believed that as much as 80 to 90 per cent of the thermal

energy was transferred by the interaction of free electrons. Whereas for nonmetallic materials, such as water, almost all of the heat was transferred by atomic or molecular interaction.

In 1930, the breakthrough of the quantum mechanic theory led to greater insight and more restrictions on the theory of conduction. First, the free or mobile electrons of a metal were found to obey the Fermi-Dirac statistics; i.e., the electrons have only a very small heat capacity. Second, if the atoms or molecules of a metal were arranged in a perfect array, the free electrons would not be scattered and would thus have an almost infinite mean-free path resulting in perfect thermal conduction, i.e., propagation of thermal energy with negligible temperature gradient. However, such perfect arrays of atoms do not exist as the atoms are displaced from their mean positions by (1) thermal energy, (2) foreign atoms, and (3) mechanical stresses.

Expressions for the thermal conductivity, more or less crude, have been developed based on these concepts. For a pure, high-conduction metal, the thermal conductivity can be expressed in terms of the thermal capacity, mean-free path, and velocity of the electrons as:<sup>11</sup>

$$k = \frac{C_e \ell v}{3}$$

or, after evaluating the thermal capacity from Fermi-Dirac statistics, as:

$$k = \frac{\pi^2 \kappa^2 n T \ell}{6 m v} \quad (1)$$

When the influence of lattice imperfections and lattice conduction are considered, the complexity of an expression for thermal conductivity is

greatly increased. One way to express this added complexity would be:<sup>11</sup>

$$k = \frac{\pi^2 \kappa^2 n T}{6 m v} \left( \frac{1}{(1/\ell)_{\text{Thermal}} + (1/\ell)_{\text{Structure}}} \right) + k_{\text{Lattice}} \quad , \quad (2)$$

where the contribution of lattice conduction has been added, and where the impedance to the mean-free path has been separated into two parts; i.e., thermal motion of the atoms and structural defects of the atomic lattice. Realizing that  $\ell_{\text{Thermal}} = cT^{-1}$  and letting  $(1/\ell)_{\text{Structure}} = \Gamma$ , Equations (1) and (2) can be simplified to:

$$k = \frac{c \pi^2 \kappa^2 n}{6 m v} \quad , \quad (1a)$$

and

$$k = \left( \frac{\pi^2 \kappa^2 n T}{6 m v} \right) \left( \frac{1}{cT + \Gamma} \right) + k_{\text{Lattice}} \quad . \quad (2a)$$

At first glance, it would appear that  $v$  should be proportional to  $T^{1/2}$ ; however, the velocity of the electrons must be calculated from the Fermi-Dirac statistics and is found to increase only slowly with temperature. Thus Equation (1a) does agree qualitatively with experimental results; i.e., the thermal conductivity of pure, high-conducting materials (such as copper and silver) decreases slowly with increasing temperature and in general the thermal conductivity of most metals is relatively independent of temperature compared with other properties such as electrical conductivity.

Thus far, the discussion has essentially centered only on the solid state. In going from the solid to the liquid and then to the gaseous state, the atomic or molecular structure becomes increasingly random.

Fortunately, the arrangement of the molecular structure in the gaseous state is so completely random that statistical theories, such as the kinetic theory of gases, can be used with good success in predicting the physical properties of a gaseous substance. Unfortunately, liquids lie in a state which consists of some intermediate degree of molecular order between that of the solid and gaseous states. As a solid melts, although the long-range order of the crystal lattice is destroyed, a residue of local order persists in the liquid state in which each molecule maintains a partially ordered arrangement of its neighbors which is a blurred replica of the crystal lattice. This vestigial order lacks the long-range character of that of the crystal lattice and becomes imperceptible at distances greater than several molecular diameters. With this added complexity, the thermal conductivity of a liquid becomes even more difficult to predict and understand than either gases or solids.

Recently, several new studies have been made of the liquid state of molten alkaline metals. Gingrich and Heaton<sup>12</sup> have made neutron diffraction studies of the structure of molten alkali metals. Their results showed that the nearest neighbor distances varied from 3.15 Å for lithium to 4.97 Å for rubidium with the average number of nearest neighbors varying from 9 to 9.5. Freedman and Robertson<sup>5</sup> have made electrical resistivity measurements of dilute liquid sodium solutions to which small atomic per cents of the solutes lithium, potassium, cesium, rubidium, silver, gold, cadmium, lead, and tin had been added. They concluded that the three factors (atomic size, ion core potential, and charge) contributing to the resistivity of a monovalent, metallic, liquid solution could be separated and experimentally evaluated; and that the separation could to

some extent be justified in terms of ideas and relationships developed for application to solid solutions. Thus it appears from their data that the manner and degree to which the electrical resistivity of a monovalent, metallic, liquid solution was changed, by the addition of small atomic per cent impurities, was not significantly different than would be expected for the same atomic per cent impurities added to the solid state.

Correlations for predicting thermal conductivity. Numerous attempts have been made to correlate thermal conductivity with other more easily measured properties of a substance. In most cases, these attempts have been more or less successful only for metallic substances. One such relationship due to Mott<sup>13</sup> and Rao<sup>14</sup> relates the change of the thermal conductivity at fusion to the latent heat of fusion by the equation:

$$k_S/k_L = e^{2.330 L_m/T_m}, \quad (3)$$

or, more exactly to the ratio of atomic frequencies at the melting point by the relationship:

$$k_S/k_L = (f_S/f_L)^2, \quad (4)$$

where  $f_S$  is obtained from the characteristic temperature of the solid by:

$$f_S = \phi_S \kappa/h, \quad (5)$$

and  $f_L$  is determined from the expression,

$$\frac{e^{\phi_S/T_m} - 1}{e^{hf_L/\kappa T_m} - 1} = e^{1.165 L_m/T_m}. \quad (6)$$

Equation (6) is based on the average energy change at fusion of the atoms

which are assumed to behave as harmonic oscillators with quantized energy levels. For some metals, the melting temperature is much greater than the Debye characteristic temperature and Equations (4), (5), and (6) reduce to Equation (3). The theoretical basis for these relationships is the increased amplitude of the atomic oscillations upon melting which hinders the free movement of the electrons. A tabulation by Powell<sup>15</sup> showed that Equation (3) gave results that were on the average 25 per cent greater than the experimental results for seven liquid metals.

Another correlation due to Bidwell<sup>16</sup> relates the thermal conductivity to the atomic heat by the equation:

$$k/AC = c_1/T + c_2, \quad (7)$$

where  $c_1$  and  $c_2$  are constants. According to Bidwell many metals fit Equation (7) in that a plot of  $k/AC$  versus  $1/T$  gives a straight line. An extension of this straight line to  $1/T = 0$  (corresponding to  $T = \infty$ ) would give the value of the intercept,  $c_2$ . Bidwell went further to show, from the results of Wilson,<sup>17</sup> that the first term on the right of Equation (7) should relate to conduction by the crystal lattice, and the second term to conduction by electrons. Since lattice conduction is largely reduced in the molten state, the second term (the intercept) should give the value  $k/AC$  for the molten state. Powell<sup>15</sup> made a thorough study of Bidwell's work and concluded that Bidwell had apparently selected the experimental data to fit his theory and that there was clearly a need for more experimental work before any relationship such as Bidwell's could be accepted.

One of the first and most successful relationships developed has been the correlation between thermal and electrical conductivities due to

Wiedemann, Franz, Lorenz, and Sommerfeld. In 1853, Wiedemann and Franz<sup>6</sup> observed that the ratio of the thermal to the electrical conductivity at a given temperature was approximately constant for certain normal metals whose thermal conductivity is now thought to be due predominantly to the interaction of free electrons. In 1872, Lorenz<sup>7</sup> derived an expression which indicated that the ratio should be proportional to the absolute temperature, so that

$$k \rho_e / T = L_0 . \quad (8)$$

Later, Sommerfeld<sup>8</sup> (using quantum mechanical theory) deduced that

$$L_0 = \pi^2 \kappa^2 / 3 e^2 = 2.57 \times 10^{-8} \text{ Btu}\cdot\text{ohm/hr}\cdot(^{\circ}\text{R})^2 . \quad (9)$$

Since all metals have some lattice component of thermal conductivity, the thermal conductivity as calculated from Equation (8) should be lower than the actual values. In the case of molten metals where the lattice component is reduced upon fusion, Equation (8) should give the thermal conductivity close to the actual value. Unfortunately, for a number of the liquid metals, whose electrical and thermal conductivities are commonly accepted and referred to, Equation (8) gives thermal conductivities which are higher than the experimental values. It has yet to be resolved whether this is caused by the theory breaking down or by inaccuracies in the electrical and thermal conductivities.

Ewing, et al.,<sup>9</sup> have attempted to extend Equation (8) to account for lattice and molecular conduction by empirical correlations of existing data. Their general equation for metals derived in this manner is:

$$k = 2.74 \times 10^{-8} T / \rho_e - 2.4 \times 10^{-17} (T / \rho_e)^2 / c_p \gamma + 2.6 c_p \gamma^2 / MT . \quad (10)$$

The first term on the right of Equation (10) is essentially Equation (8) and thus gives the electronic portion of the thermal conductivity. The second term, according to Ewing, et al., appears to correct for the general situation that electrical conductivities are measured under isothermal conditions; whereas, thermal coefficients are measured with thermal gradients existing in the material. The third term in Equation (10) represents the lattice or molecular contribution to the thermal conduction. The mean deviation of the thermal conductivity calculated by Equation (10) from the observed value for sixteen liquid metals was  $\pm 10$  per cent; for twenty-five solid metals,  $\pm 7$  per cent; for numerous solid metal alloys,  $\pm 5$  per cent; and for thirty-two simple organic liquids, including water,  $\pm 30$  per cent. These, of course, were mean deviations; the deviations for specific materials varied from 1 to 300 per cent.

Methods for determining the thermal conductivity of liquid metals.

From the above discussions, it should be obvious that at the present state of knowledge of thermal conductivity many parameters still need to be investigated and evaluated. Thus to be assured of better than  $\pm 20$  per cent accuracy in the thermal conductivity of most liquids, and for that matter many solids, resort must be made to accurate experimental determinations.

The methods for determining the thermal conductivity of substances are numerous. All the experimental methods for the steady-state determination of thermal conductivity are concerned with the attainment of suitable boundary conditions such that the Laplace equation can be solved for the temperature gradient normal to a given area with a simultaneous measurement of the heat flowing through the area. The thermal conductivity

is then calculated from the Fourier heat-transfer equation. The experimental methods for the transient determination of thermal conductivity are based on the solution of the diffusion equation with suitable initial and boundary conditions for the thermal diffusivity coefficient. The thermal conductivity is then calculated from the thermal diffusivity coefficient using the density and heat capacity.

The methods for determining the thermal conductivity of liquids are limited due to the difficulty in separating the conductive from the convective heat-transfer mechanism. Thus the geometry is usually chosen so that the natural-convective heat transfer is negligible compared with the conductive transfer. One way to accomplish this is to use small sample thicknesses so that the conductive mechanism, which depends directly on the thermal gradient, will be much larger than the convective mechanism. Of course, with a small sample thickness, it is usually difficult to determine the temperature gradient with normal heat fluxes unless the thermal conductivity of the sample is sufficiently small (usually  $<5$  Btu/hr·ft·°F). Another approach is to use downward directed, one-dimensional heat flow which would, theoretically, avoid any natural convection.

There are several established methods for determining the thermal conductivity of liquids which make use of the above points. The variable-gap method determines the heat flow and temperature drop across various specimen thicknesses and eliminates most of the effects of interfacial temperature drops and natural convection by extrapolating to zero sample thicknesses. This method is most suitable for determining the thermal

conductivity of corrosive liquids\* whose thermal conductivities lie between 0.1 to 10 Btu/hr.ft.°F. Another method uses the concentric annulus radial-heat-flow device, which is most suited to noncorrosive liquids\* whose thermal conductivities lie between 0.1 to 2 Btu/hr.ft.°F. A third method, the axial-heat-flow or longitudinal method, is useful for corrosive liquids\* whose thermal conductivities are greater than 10 Btu/hr.ft.°F.

Among the most common transient methods which make use of the diffusion equation is the sinusoidally heated hot-wire device. Usually, the resistance-heated wire is a butt-welded thermocouple stretched in a pool of the liquid sample. Thus it is most suited for noncorrosive, dielectric liquids in the temperature range below 1000°F. In general, transient methods for determining thermal conductivity are less accurate than steady-state methods primarily because any errors in the density and heat capacity are also included in the result.

All methods for determining the thermal conductivity require the attainment of definite initial and boundary conditions. However, in actual practice these conditions cannot be established with certainty and systematic errors arise whose magnitude cannot be estimated. Thus, in most cases, the accuracy of the determinations are directly proportional to the skill of the experimenter and the adequacy of the experimental equipment.

---

\*The increased interfacial thermal resistance caused by corrosion of the container walls will, in most cases, reduce the accuracy of the temperature gradient determination in the sample more for the concentric annulus device than the variable-gap or axial-heat-flow methods.

Method of determination used in the present investigation. From previous determinations,<sup>18</sup> it was clear that the thermal conductivity of molten lithium would be sufficiently high ( $>10$  Btu/hr·ft·°F) that it would be necessary to use the axial-heat-flow method. A comparative method using heat meters of known thermal conductivity in series with the lithium sample was chosen instead of an absolute method with its usual disadvantage of a complex heater design. Type 347 stainless steel was used for the heat meters because of its high-temperature strength, proven compatibility with pure lithium, and accurately known thermal conductivity.<sup>19</sup> Compensating guard heating was used to minimize radial heat flow.

The essential features of the apparatus used in this investigation are shown in Figure 1. The central part of the apparatus (the test piece) consisted of an expansion tank, main heater, upper heat meter, sample container, and lower heat meter. Heat from the main heater flowed down the test piece and into the water-cooled sink. Surrounding the test piece were a coaxial guard tube and an Alundum cylinder which supported the guard heaters. Temperature measurements were made along the test piece and coaxial guard tube using thermocouples made from platinum and platinum plus ten per cent rhodium alloy wires. Heat flow in the radial direction was minimized by maintaining, with the guard heaters, an axial temperature profile in the coaxial guard tube which matched the axial temperature profile of the test piece. The coaxial guard tube consisted of three tubes of the same inside and outside diameter brazed end to end at two levels corresponding to the sample heat-meter interfaces. The upper and lower tubes were type 347 stainless steel to match the thermal conductivity of the heat meters. The middle section was of nickel alloy to approximately

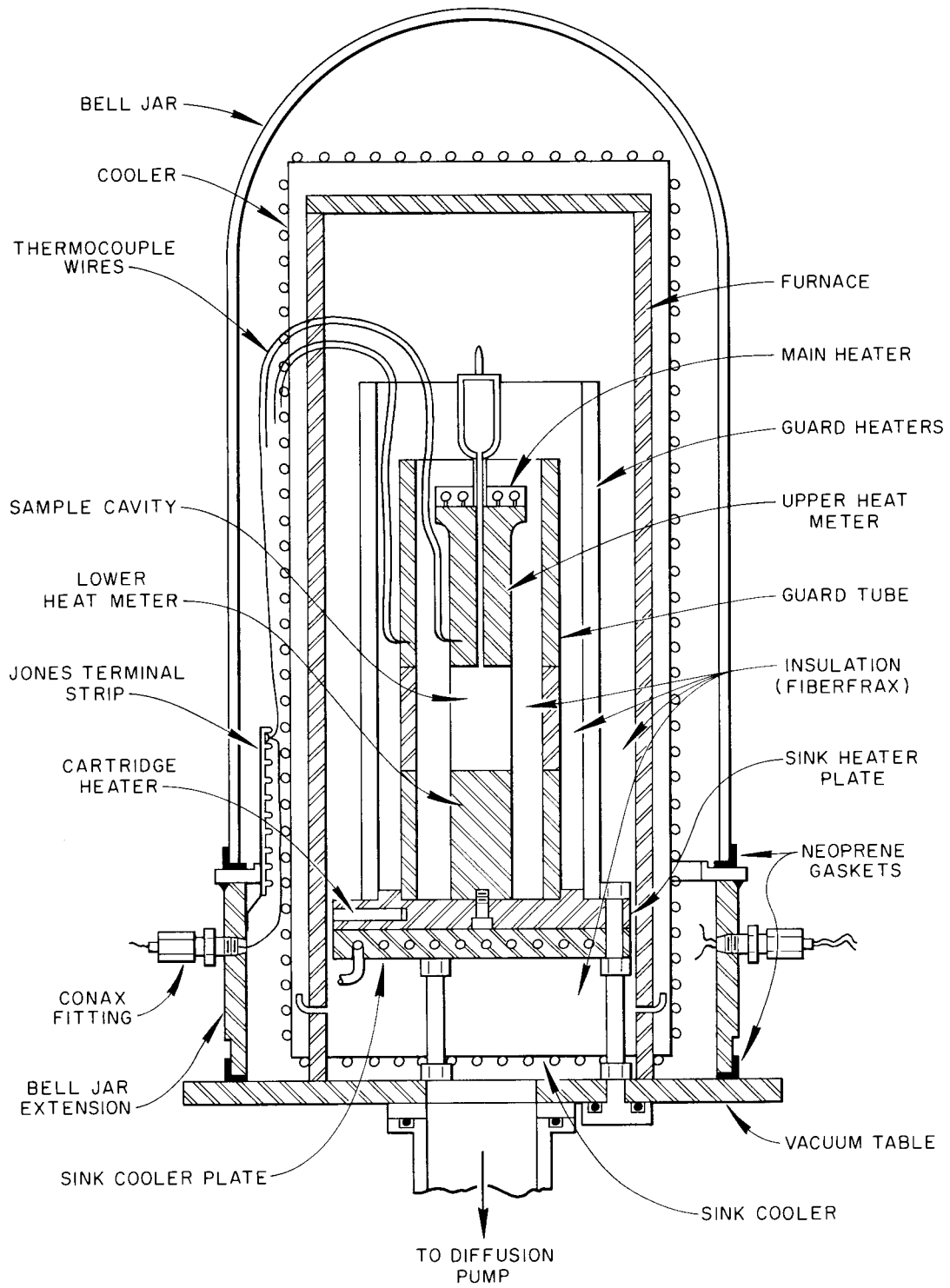


Figure 1. Apparatus Assembly.

match the estimated thermal conductivity of the sample region of the test piece.

The apparatus was placed in a furnace which maintained the surroundings at a temperature level to further reduce any radial heat flow and to assist in calibrating the thermocouples in place. Fiberfrax insulation was carefully placed in all void regions within the furnace. The entire system was maintained in a high vacuum ( $3$  to  $8 \times 10^{-5}$  mm of Hg) to minimize the convective, conductive, and corrosive effects of an atmosphere.

Method of calculation used in the present investigation. By the usual comparative, axial-heat-flow method, the thermal conductivity is calculated from a heat balance between a plane in the central region of the heat meter and a plane in the central region of the sample. Assuming the establishment of steady state and the absence of radial heat flow, a heat balance between the upper heat meter (plane a in Figure 2) and the sample (plane b in Figure 2) can be written as

$$(k A dt/dx)_{H_a} = (k A dt/dx)_{W_b} + (k A dt/dx)_{Li_b} \quad (11)$$

In actual practice, a small radial temperature gradient and a slight, but steady, drift in system temperature levels will usually exist. Thus Equation (11) must be corrected for radial heat flow and heat stored or released between planes a and b, so that

$$(k A dt/dx)_{H_a} = (k A dt/dx)_{W_b} + (k A dt/dx)_{Li_b} + Q_R + Q_\theta \quad (12)$$

A similar equation can be written for a heat balance between the sample

UNCLASSIFIED  
ORNL-LR-DWG 75324

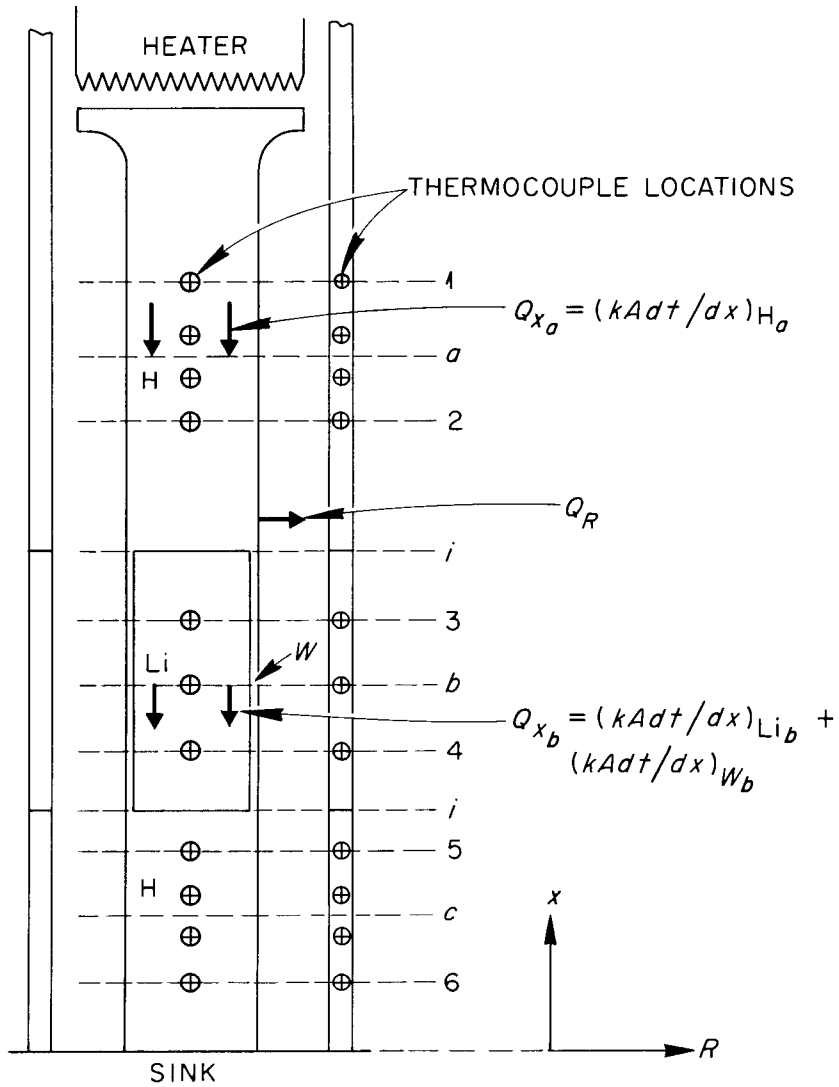


Figure 2. Reference Planes for Heat Balances Along Test Piece and Coaxial Guard Tube.

and the lower heat meter (plane c).

For the present investigation, Equation (12) was simplified by assuming that the temperature distribution along the sample container wall and along the axial centerline of the sample were identical. This assumption was valid because (1) the interfacial thermal resistance between the lithium sample and the type 347 stainless steel wall was quite small, (2) the cross-sectional area of the wall represented only 16 per cent of the cross-sectional area of the test piece, and (3) the thermal conductivity of the type 347 stainless steel was only one-half that of molten lithium. A further simplification was achieved by moving the positions of heat balance from planes a and b to a common plane i (the interface between the upper heat meter and the lithium sample) which eliminated  $Q_R$  and  $Q_\theta$  from Equation (12). With these two simplifications, the thermal conductivity of the lithium sample was calculated from Equation (12) as:

$$k_{Li} = \frac{(k A dt/dx)_{H_i}}{(A dt/dx)_{Li_i}} - k_{H_i} \left( \frac{A_W}{A_{Li}} \right), \quad (13)$$

where, in the present case,  $k_{W_i} = k_{H_i}$ . The conductivity was also calculated by Equation (13) at the interface of the lithium sample and the lower heat meter.

The temperature and temperature gradients at the interfaces were calculated from an equation,

$$t = ax^2 + bx + c, \quad (14)$$

which was least-squares fitted to the temperature data of the three respective regions of the test piece. To adequately establish "a" in

Equation (14) for each region by least-square analysis would require many more temperature measurements than were provided. Thus, "a" in Equation (14) was calculated by the following procedure; taking the second derivative of Equation (14) gives:

$$a = (1/2) d^2t/dx^2 . \quad (15)$$

By definition, the second derivative can also be expressed as

$$d^2t/dx^2 \approx \frac{dt/dx|_{x+\Delta x} - dt/dx|_x}{\Delta x} , \text{ for small } \Delta x. \quad (16)$$

The first derivative can be obtained from Fourier's equation as

$$dt/dx = Q/k A . \quad (17)$$

Therefore, substituting Equations (16) and (17) into Equation (15) results in

$$a = \frac{1}{2 (x_1 - x_2)} \left[ \frac{Q}{k A} \Big|_{x=x_1} - \frac{Q}{k A} \Big|_{x=x_2} \right] , \quad (18)$$

where the subscripts refer to planes 1 and 2 of the upper-heat-meter region as shown in Figure 2. Similar expressions for "a" were derived for the sample region (planes 3 and 4) and the lower-heat-meter region (planes 5 and 6).

The values of  $x_1 - x_2$ ,  $k$ , and  $A$  in Equation (18) were determined from previous and reference measurements corrected for linear temperature dependences. The average heat flow down the apparatus was used for  $Q$  at  $x_1$  in Equation (18). The heat flow at  $x_2$  was determined as  $Q$  at  $x_1$ , plus

any radial heat gained (or lost) between  $x_1$  and  $x_2$ , and plus any heat released (or retained) in the test piece between  $x_1$  and  $x_2$  due to the transient heat-capacity effect. The radial heat flow was calculated from the temperature difference between the test piece and the guard tube and from the conductivity of the Fiberfrax insulation, corrected for the high vacuum (see Figure 31 in Appendix E), so that

$$Q_R = \frac{-2 \pi k_I (x_1 - x_2)(t_T - t_G)}{\ln (r_T/r_G)} \quad (19)$$

The enthalpy change due to a slight, but steady, drift in system temperature levels encountered in the experiment was calculated from the volume, density, heat capacity, and measured temperature drift of the test piece so that

$$Q_\theta = -(V \gamma c_p) \Delta t / \Delta \theta \quad (20)$$

Two steps were taken to better define the axial position of the thermocouple junctions within the thermowells. First, the thermocouple junctions were arc welded to the bottom of the thermowells to fix their location for the duration of the experiment. Second, in the same manner as that described above, an equation of the form:

$$x = Bt^2 + Ct + F \quad (21)$$

was least-squares fitted to the temperature data of the first three data runs. The thermocouple positions were then calculated from Equation (21) for each of the three data runs and averaged. This method of thermocouple location is exactly analogous to the more common method of applying an electrical potential along the test piece. However, it was not convenient to use the electrical potential method for the present case because of a void in the lithium cavity existing at room temperature.

## CHAPTER III

## EXPERIMENTAL EQUIPMENT

The design and construction of the apparatus, including auxiliary equipment, are discussed in this chapter. The description of the test piece, guard tube, and guard heaters - the heart of the apparatus - is sufficiently complete to permit duplication. However, only unusual auxiliary equipment is discussed in detail. Many illustrations and detailed explanations are relegated to the Appendix.

Complete system. The complete system can be considered to consist of eight parts: test piece, coaxial guard tube, guard heaters, cooling system, furnace, electrical system, instrument network, and vacuum system. The connections and relationships between the various components are shown schematically in Figure 3. Photographs taken from the front and rear of the apparatus are shown in Figures 4 and 5.

Test piece. The test piece is shown in Figure 6 and in detail in Figures 22 and 23 in Appendix B. It consists of an expansion tank, main heater, upper heat meter, sample container, and lower heat meter.

The test piece was machined as two parts from a 2.5-in.-dia rod of type 347 stainless steel. The lower part of the test piece was 1.500 in. in diameter and 7 in. long with a 4-in.-deep cavity bored into the upper end to contain the lithium sample. The wall thickness of this cavity was 0.0625 in. Two holes in each of four planes spaced 0.50 in. apart were drilled into the lower heat meter for the insertion of eight thermocouples

UNCLASSIFIED  
ORNL-LR-DWG 58253R

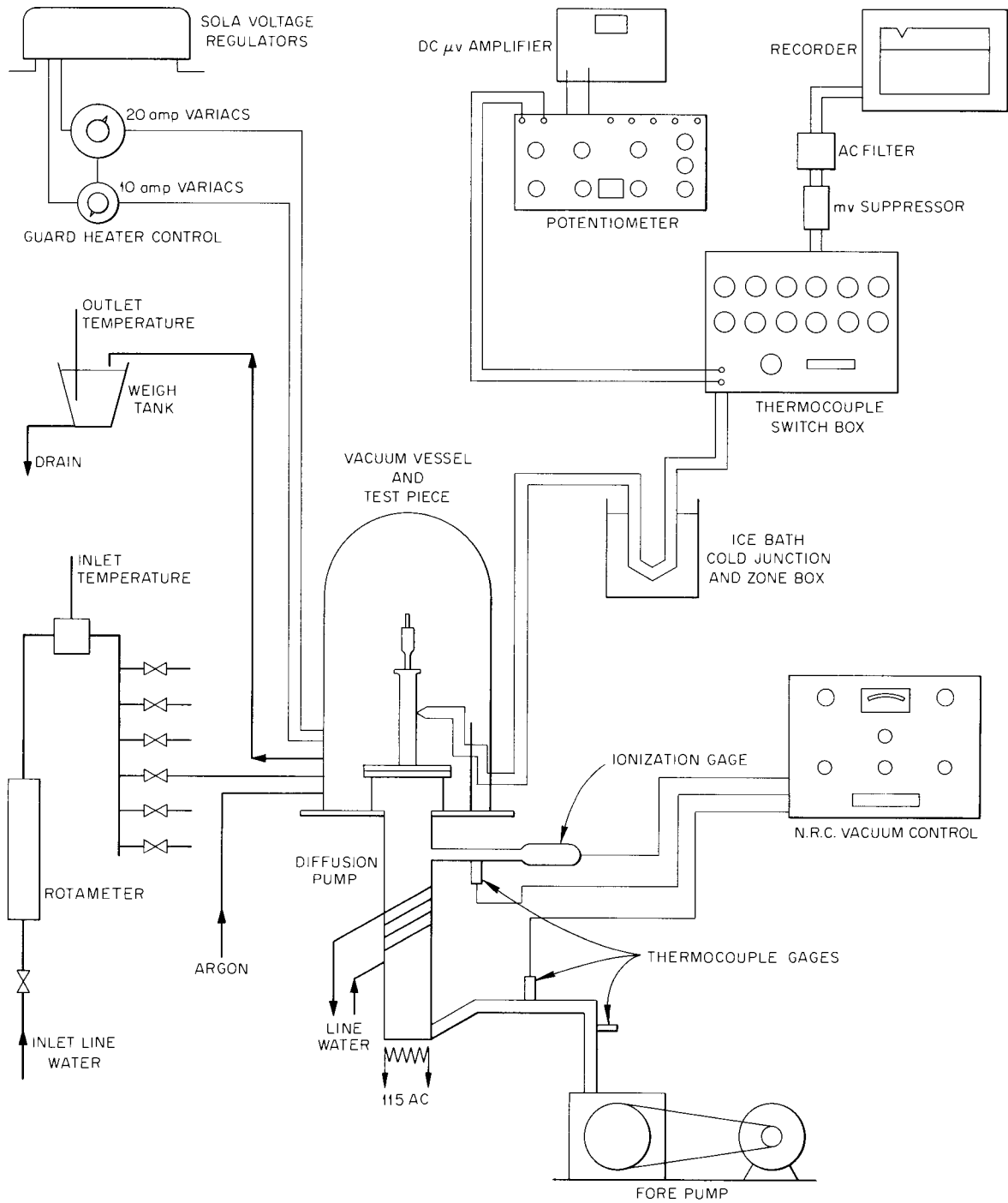


Figure 3. Schematic Diagram of Complete System.

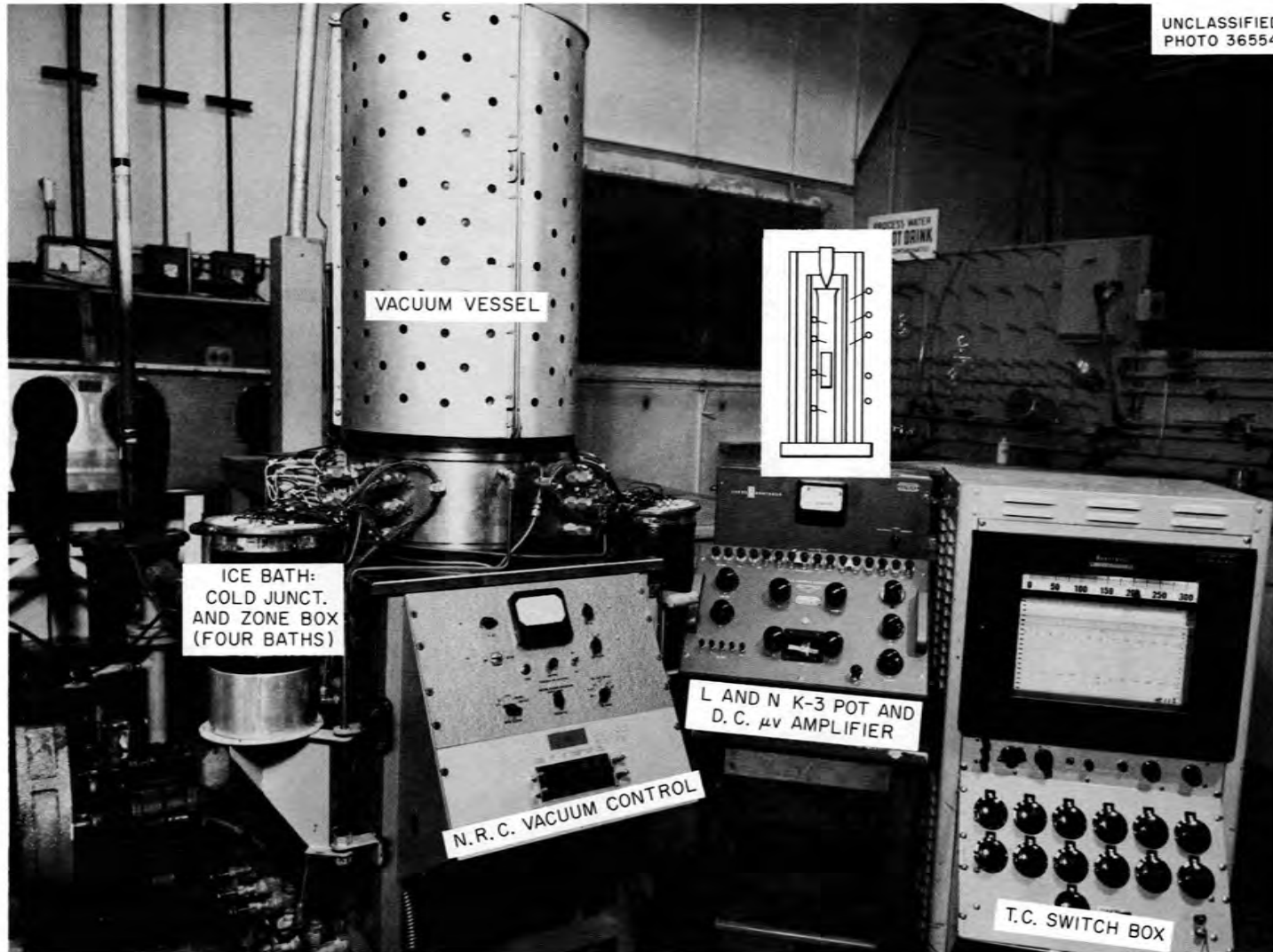


Figure 4. Front View of Apparatus.

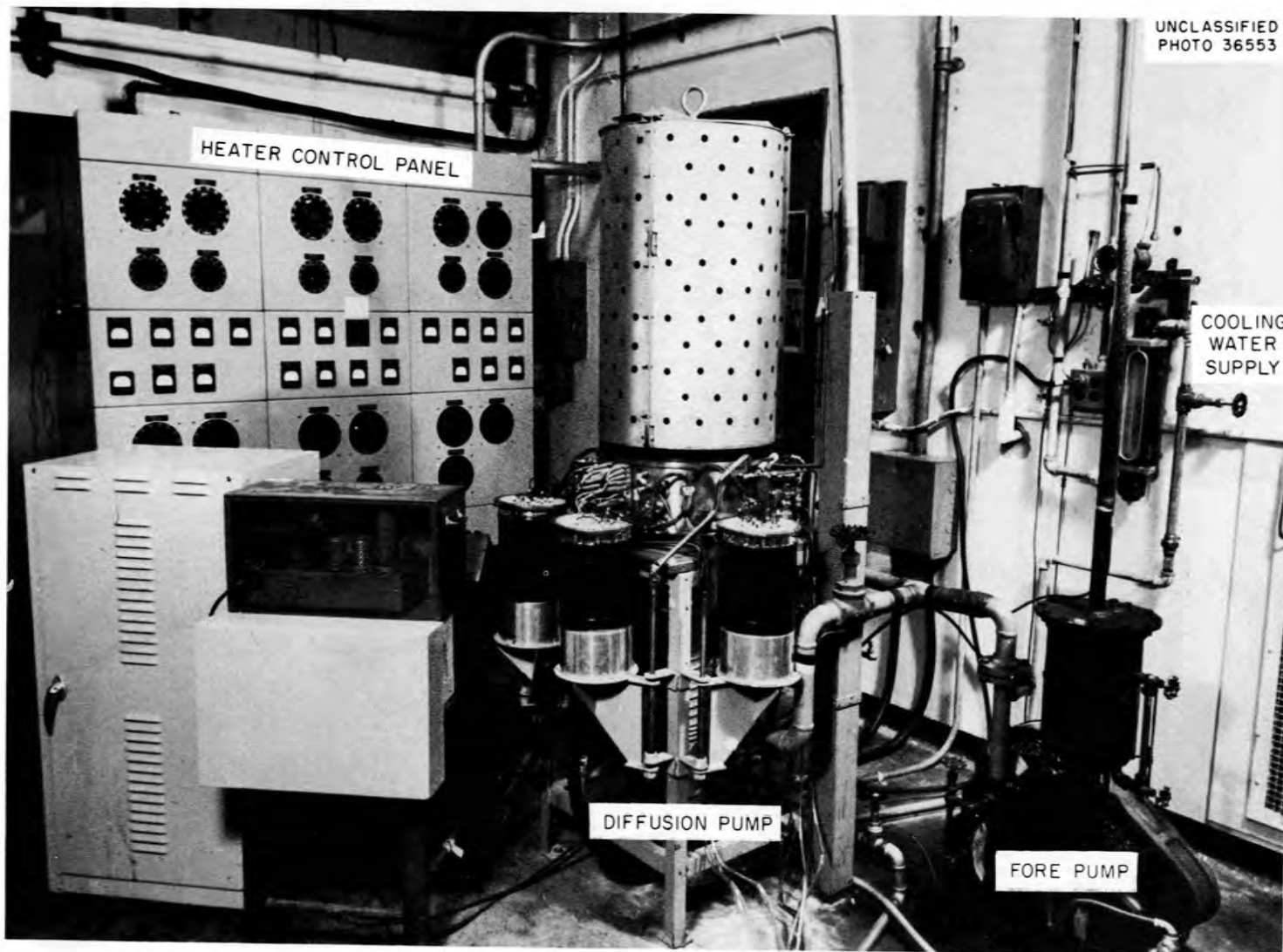


Figure 5. Rear View of Apparatus.

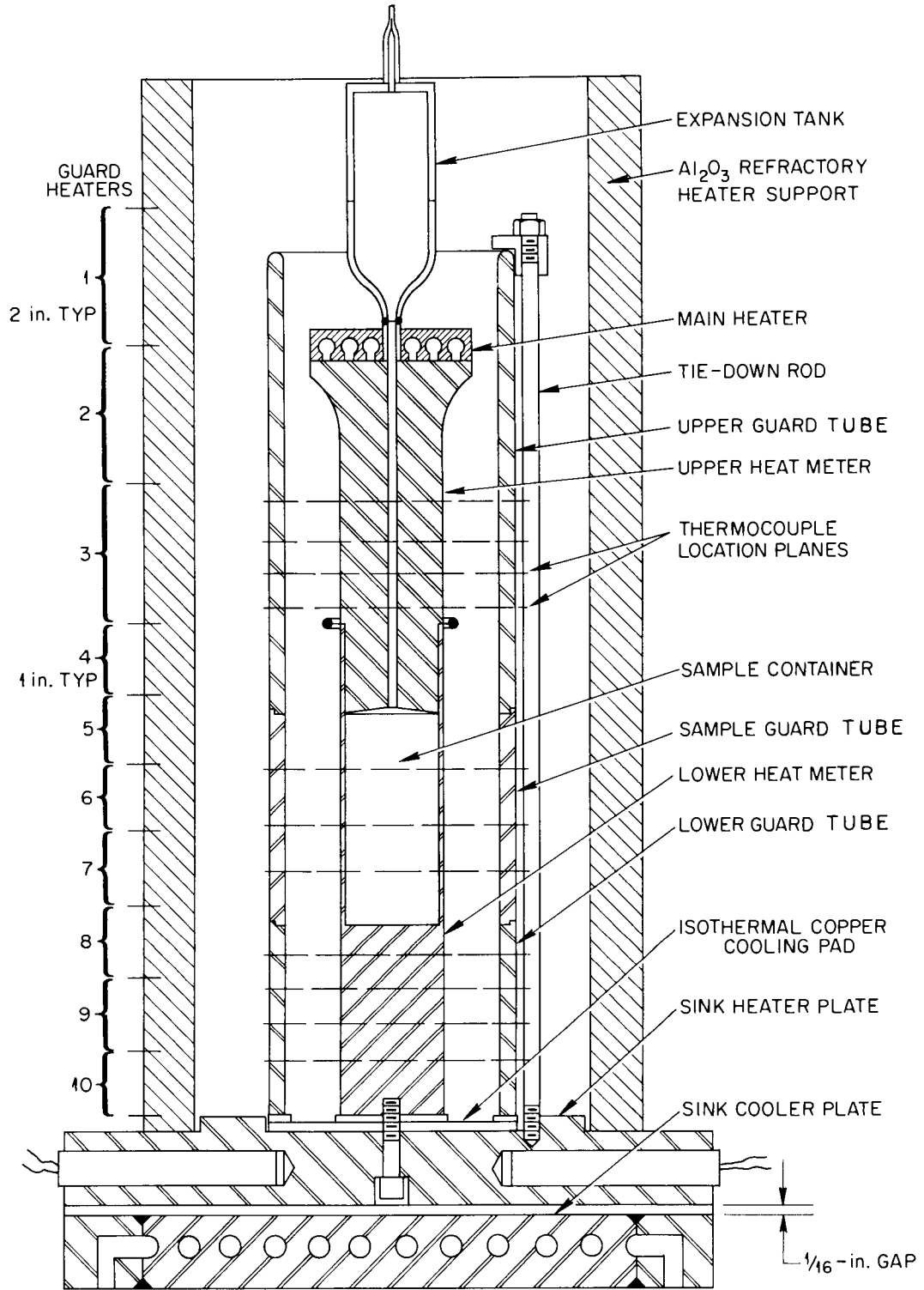


Figure 6. Test Piece Assembly.

(see Figure 7). Three thermowells penetrated into the sample container in three planes spaced 0.75 in. apart and were welded onto the sample container wall (see Figure 22 in Appendix B). A copper pad was brazed to the bottom of the lower heat meter and was polished to a surface roughness of 10  $\mu$ in. rms. As shown in Figure 6, the lower heat meter was bolted with a single screw to a similarly finished copper pad brazed to the sink heater plate.

The upper part of the test piece was 1.500 in. in diameter, 6 in. long, and was flared out to 2.25 in. in diameter at the top to reduce the heat flux at the main heater. Four holes spaced 0.50 in. apart were drilled into the upper heat meter for the insertion of four thermocouples (see Figure 7). The bottom portion of the upper part was machined to fit 1 in. deep into the cavity of the lower part. The two parts were sealed together by a Heliarc fusion weld. Filling and thermal expansion of the lithium sample were provided for by a 0.125-in.-dia hole along the centerline of the upper part which was connected to the expansion tank.

Coaxial guard tube. The coaxial guard tube, shown in Figure 6 and in detail in Figure 24 in Appendix B, consisted of three tubes with 3.087-in. inside and 3.470-in. outside diameters brazed end to end at two levels corresponding to the sample heat-meter interfaces. The upper and lower tubes were type 347 stainless steel to match the thermal conductivity of the heat meters. The middle section was of nickel alloy to approximately match the estimated thermal conductivity of the sample region of the test piece. Any deviations in the temperature gradient caused by a slight mismatch of the thermal conductivity of the sample region and the nickel alloy were made up by selective guard heating in this region. Eleven

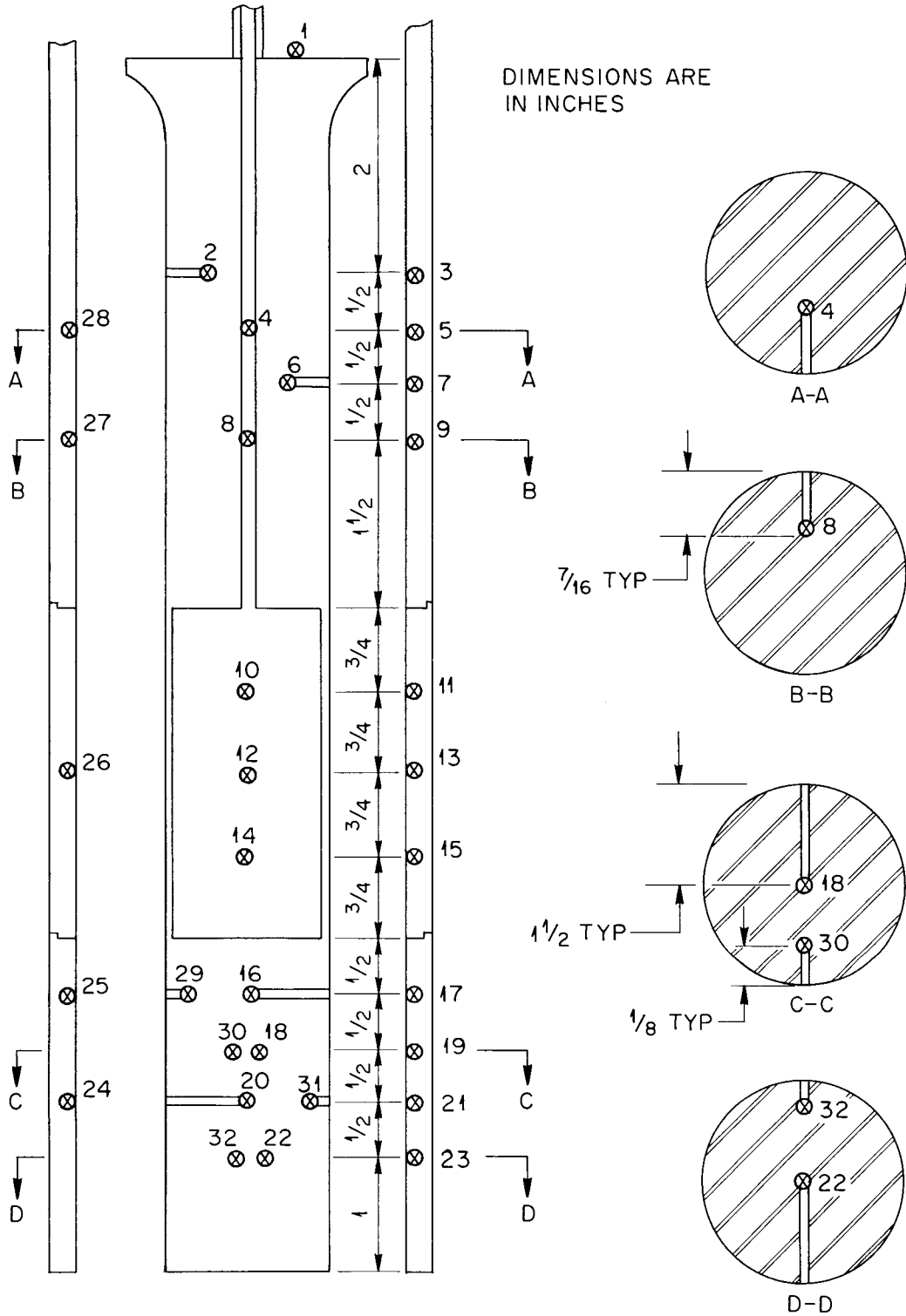


Figure 7. Thermocouple Locations.

axially spaced planes of the guard tube, each containing one thermocouple, were carefully positioned to align with the corresponding eleven thermocouple planes of the test piece. In addition, five other thermocouples were positioned 180 degrees on the opposite side of the guard tube to check for circumferential nonuniformities of heat flow (see Figure 7).

A copper pad was also brazed to the bottom of the guard tube and polished to a surface roughness of 10  $\mu$ in. rms. The guard tube was clamped to the copper pad brazed to the sink heater plate with three tie-down rods as shown in Figure 6. With both the test piece and guard tube clamped to the same copper pad, no adjustment was necessary to maintain equal temperatures at the lower ends of the test piece and guard tube.

The annular space between the test piece and guard tube was filled with Fiberfrax insulation whose thermal conductivity is shown in Figure 31 in Appendix E. Without insulation in the annular space, the heat exchange between the test piece and guard tube due to radiation would have been several times greater than for conduction through the Fiberfrax insulation.

Guard heaters. The axial temperature distribution along the test piece and guard tube was controlled by seven 1-in. long and three 2-in. long by 5.75-in.-dia individually controlled heater sections as shown in Figure 6. Each heater section was made of 22-gauge tantalum wire wound with a spacing of ten turns per inch on the outside of a 5.75-in. OD  $\times$  5.0-in. ID  $\times$  15 in. long high-purity Alundum cylinder (see Figure 25 in Appendix B). Care was taken in beginning and ending each section that over-all circumferential symmetry would be maintained. Tantalum heater wire was selected because of its high-melting point, good ductility, and

high-melting point of its oxide. The high-melting points were desirable in order that the operation of the system would not be limited by a sluggish, asymptotic approach to the maximum design temperature. As the windings were not bifilar, an electrically grounded induction shield of 0.0625-in.-thick stainless steel tubing was placed between the guard heater cylinder and the guard tube (see Figure 25). The annular space between the guard heater cylinder and guard tube was filled with Fiberfrax insulation.

The main heater consisted of a 0.207-in.-OD coil of 22-gauge tantalum heater wire supported by a circular section cut from a standard flat-plate porcelain heater support (see Figure 25).

Sink heating and cooling. Control of the sink temperature was necessary to maintain approximately the same axial temperature gradient over the wide range of temperature levels used in the experiment. Also, the sink had to provide steady, uniform cooling to maintain steady state at any one temperature level. Water was chosen to cool the sink since its large heat capacity limits its temperature response to minor fluctuations in flow rate. Building supply water was used after careful checks showed that its temperature level would not vary significantly ( $\pm 0.2^{\circ}\text{F}$  over periods of one week).

Regulation of the temperature gradient and temperature level of the apparatus was provided by a sink heater and a series arrangement of two water-cooled sinks (see Figure 1 in Chapter II). With water flowing through the upper water-cooled sink (sink-cooler plate), the power to the sink heater plate could be adjusted to regulate the temperature level of

the apparatus up to 1100°F. Above 1100°F, the water and power to the sink cooler and sink heater plates were turned off. Since the thermal resistance between the sink heater plate and the lower water-cooled sink was greater than before (see Figure 1), the power to the sink heater plate could be adjusted to regulate the temperature level of the apparatus up to 1800°F. By this arrangement, the temperature gradient and level of the apparatus could be regulated without resort to the usual method of disrupting the system operation to insert various thicknesses of thermal insulation.

Furnace. Surrounding the test piece assembly was a 10-in.-dia furnace (see Figure 1 in Chapter II). The furnace was made of a hexagonal array of twelve standard 5-in. × 14-in. flat-plate porcelain heaters wound with Nichrome V heater wire. The furnace was capable of bringing the test piece assembly to a steady-state isothermal temperature of 1200°F. Around the furnace was a water-cooled copper heat shield which removed most of the 1.5 kw maximum heat output.

Electrical system. A diagram for the heater electrical system is shown in Figure 8. Six 2 kva and one 1 kva Sola transformers (see Table V in Appendix B for specifications) provided the necessary regulation of the voltage to the guard, main, and sink heaters. The voltage to the furnace was not regulated. The adjustment of each voltage to the guard, main, and sink heaters was provided by two variacs. The input voltage to the fine adjustment 10-amp variac was reduced to 30 volts by tapping the output winding of the course adjustment 20-amp variac. By this arrangement, the 10-amp variac could increment any 20-amp variac setting (sensitivity 0.2

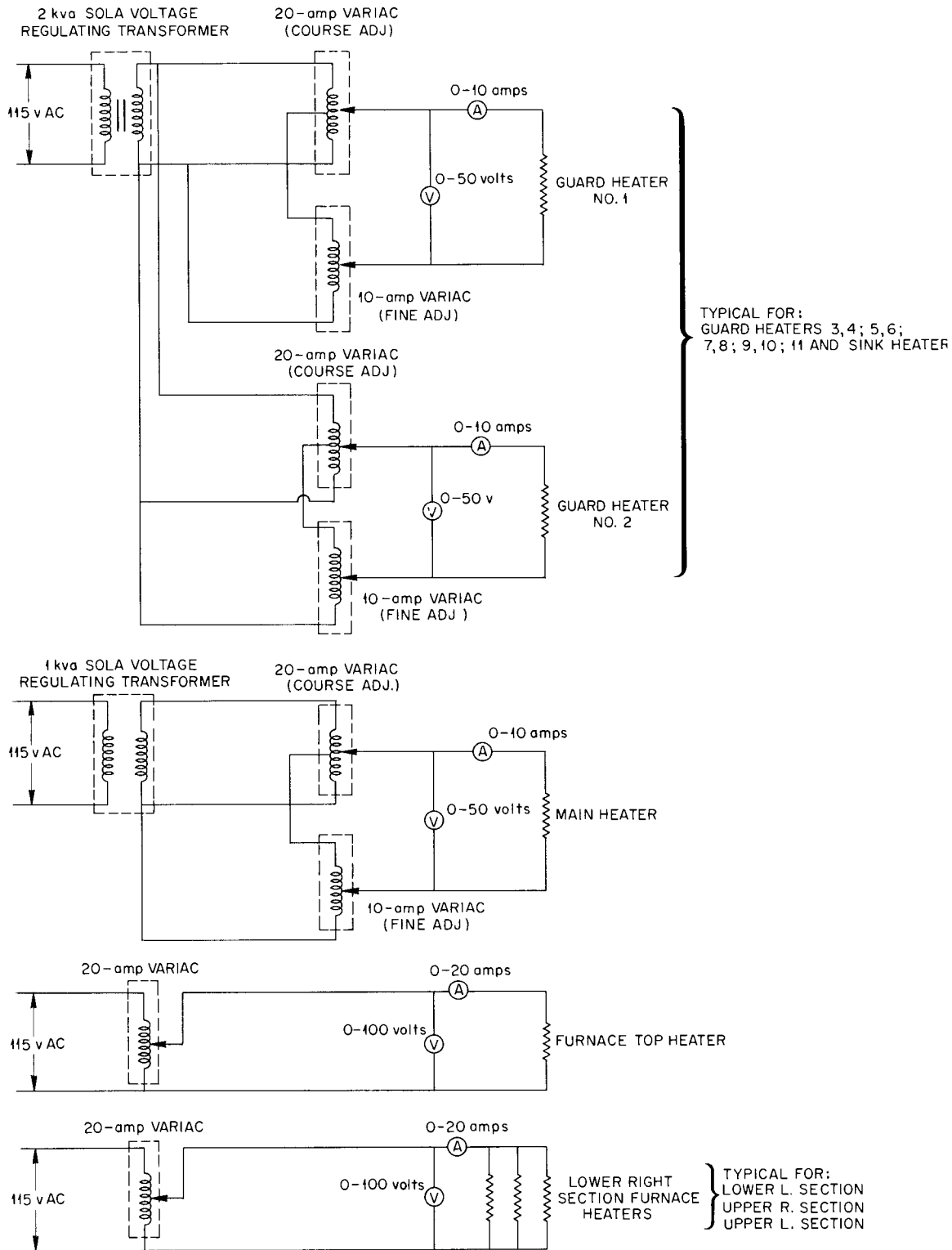


Figure 8. Electrical System for Heaters.

volts) with 30 additional volts at a sensitivity of 0.01 volts. The furnace voltages were adjusted by five 20-amp variacs in the usual manner.

Instrumentation. The thermocouple circuit diagram is shown in Figure 9. The method of calibrating and attaching the thermocouples to the test piece will be described in Chapter IV.

The test piece was electrically grounded and the thermocouples were arc welded to the test piece; therefore, it was not possible to read differential thermal emfs on the potentiometer. However, this disadvantage of not being able to gain more sensitivity in the  $\Delta t$  determinations was more than offset by having fixed thermocouple positions (see Chapter V).

Forty-four thermocouples consisting of 30-gauge (0.010-in.-dia) platinum and platinum plus ten per cent rhodium alloy wires were used in the experiment and located on the test piece and guard tube as shown in Figure 7. The 30-gauge Pt/90Pt+10Rh lead wires were joined to 22-gauge Pt/90Pt+10Rh wires at a Jones terminal strip. Each of the two respective wire sizes were wrapped around the same terminal screw and clamped together. The 22-gauge wires proceeded through the vacuum chamber wall in eight-hole Conax packing glands (see Figure 1 in Chapter II). To aid in minimizing and canceling extraneous thermal emfs, high-purity copper wire (22-gauge stranded, internal instrument hookup wire supplied by Minneapolis-Honeywell Corporation) was joined to the 22-gauge Pt/90Pt+10Rh wires by inert gas arc welding. The two junctions per thermocouple so formed were placed in glycerine-filled glass tubes and immersed in an ice bath. By this procedure, the cold junction and zone control were combined in one bath. The copper leads were connected to twelve low-thermal emf Leeds and Northrup rotary switches arranged in a gradient-free switch box. Lead

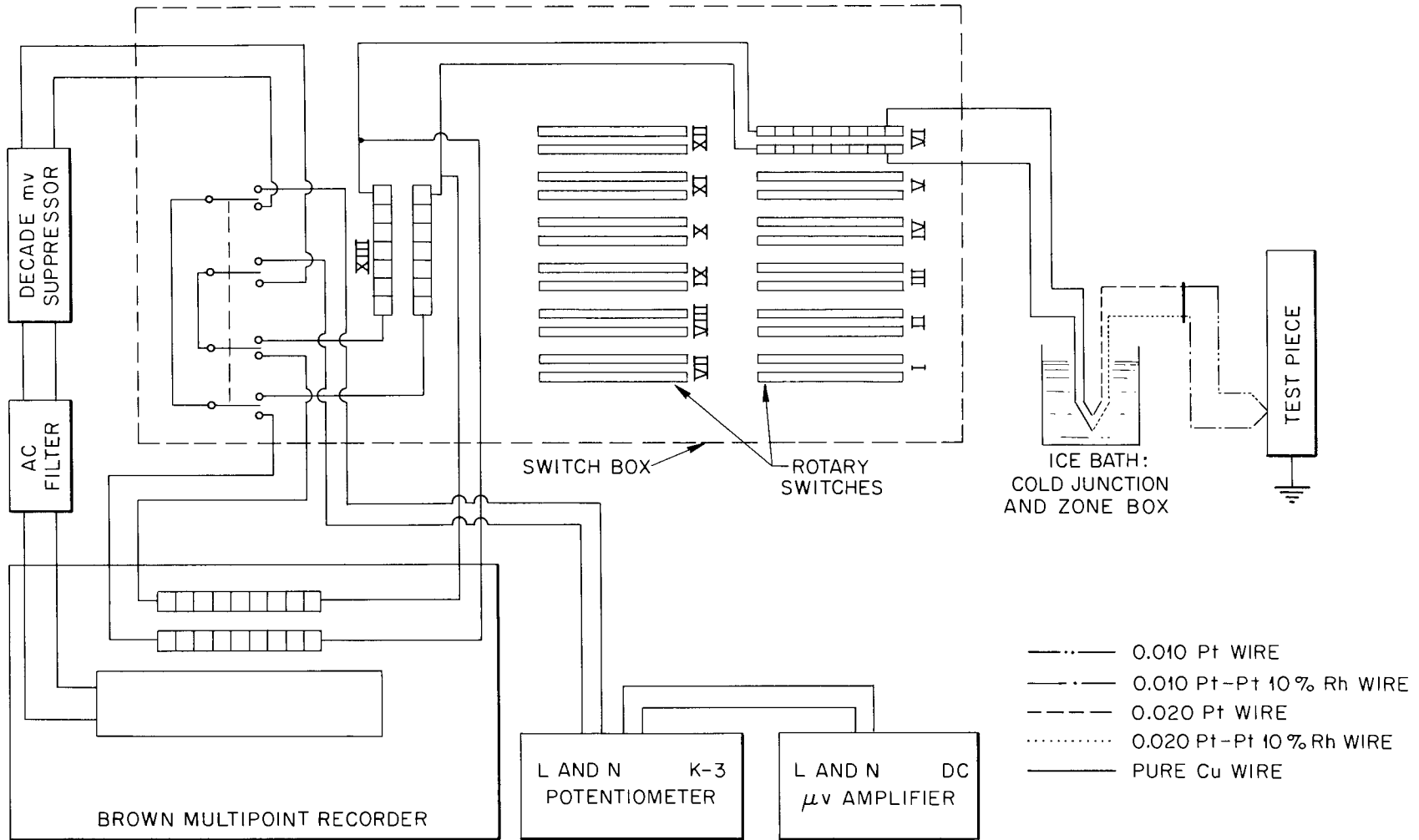


Figure 9. Thermocouple Circuit Diagram.

wire junctions outside of the switch box were kept to a minimum and were insulated to minimize extraneous thermal emfs.

The thermal emfs were either measured by a Leeds and Northrup K-3 potentiometer or recorded on a Brown multipoint recorder. The Brown recorder, which was completely bypassed during the emf measurements, was used to observe the temperature profiles during the guard heater balancing. The K-3 potentiometer and d-c  $\mu\text{v}$  amplifier along with the battery and standard cell (see Table V in Appendix B for specifications) were guarded by the use of special circuitry, insulated from ground, to provide freedom from adverse effects of leakage-current paths between critical circuit points. The system was also well shielded to reduce electrostatic and electromagnetic radiation effects.

Vacuum system. The evacuation of the gas surrounding the thermal conductivity apparatus was performed by a National Research Corporation evaporator system. The evaporator system consisted of a bell jar (which contained the apparatus), a diffusion pump, a forepump, and pressure measuring instrumentation (see Table V in Appendix B for specifications). One ionization gauge ( $1 \times 10^{-6}$  to  $5 \times 10^{-3}$  mm of Hg range) and two thermocouple gauges ( $1 \times 10^{-3}$  to 1.0 mm of Hg range) were used to measure the system pressure and were located as shown in Figure 3. The second water-cooled sink of the apparatus doubled also as a water-cooled baffle to prevent the backflow of diffusion oil vapor. Using Octoil S, this system was able to maintain a pressure of 3 to  $8 \times 10^{-5}$  mm of Hg during operation of the apparatus at the location of the ionization gauge. Of course, the pressure in the immediate vicinity of the test piece was probably several times the measured pressure.

## CHAPTER IV

## PROCEDURE

As considerable time and effort were required in filling the test piece with a sample of purified lithium metal, the procedure is described in much detail in this chapter. The calibration and installation of the many thermocouples and the operation of the apparatus is also discussed.

Filling of the test piece. The cavity of the test piece was filled with a purified sample of lithium metal supplied by the Foote Mineral Company. The weight per cent of impurities in the lithium sample as determined by the spectrochemical analyses before and after the thermal conductivity determinations are presented in Table I. From these analyses, the purity of the lithium sample was estimated, by difference, to be 99.82 weight per cent before and 99.81 weight per cent after the conductivity determinations.

The fill procedure was concerned with minimizing the possibility of further contaminating the lithium, leaving voids in the test piece cavity, and over or underfilling the test piece. To accomplish these requirements, a vacuum transfer system shown in Figure 10 was designed. The main part of this system was the transfer container which was connected by 0.25-in.-dia tubing to the top of the test piece expansion tank. A riser tube inside the transfer container was used to accurately gauge the quantity of lithium to be forced into the test piece cavity. The transfer container and test piece were ultrasonically cleaned and then baked at 1800°F in a hydrogen atmosphere to remove surface impurities. Tape heaters were wound

Table I. Spectrochemical Analyses of the  
Lithium Sample Before and After Thermal  
Conductivity Determinations

Impurity	Weight Per Cent	
	Before	After
Na	0.015	0.015 <sup>a</sup>
K	0.060	0.060 <sup>a</sup>
Ca	0.0001	0.0001 <sup>a</sup>
Al	0.0005	0.0005 <sup>a</sup>
Si	0.001	0.0058
Cl	0.04	0.04 <sup>a</sup>
N	0.012	0.012 <sup>a</sup>
Ni	<0.0015	0.0022
Cr	<0.0015	<0.001
Ti	<0.0010	<0.0010 <sup>a</sup>
N <sub>2</sub>	0.0063	0.0063 <sup>a</sup>
O <sub>2</sub>	0.00033	0.00033 <sup>a</sup>
Mn	-	<0.002
Fe	0.0027	0.0024
Other (estimated)	0.025	0.025 <sup>a</sup>
Li (by difference)	99.82	99.81

<sup>a</sup>These values were assumed to remain unchanged.

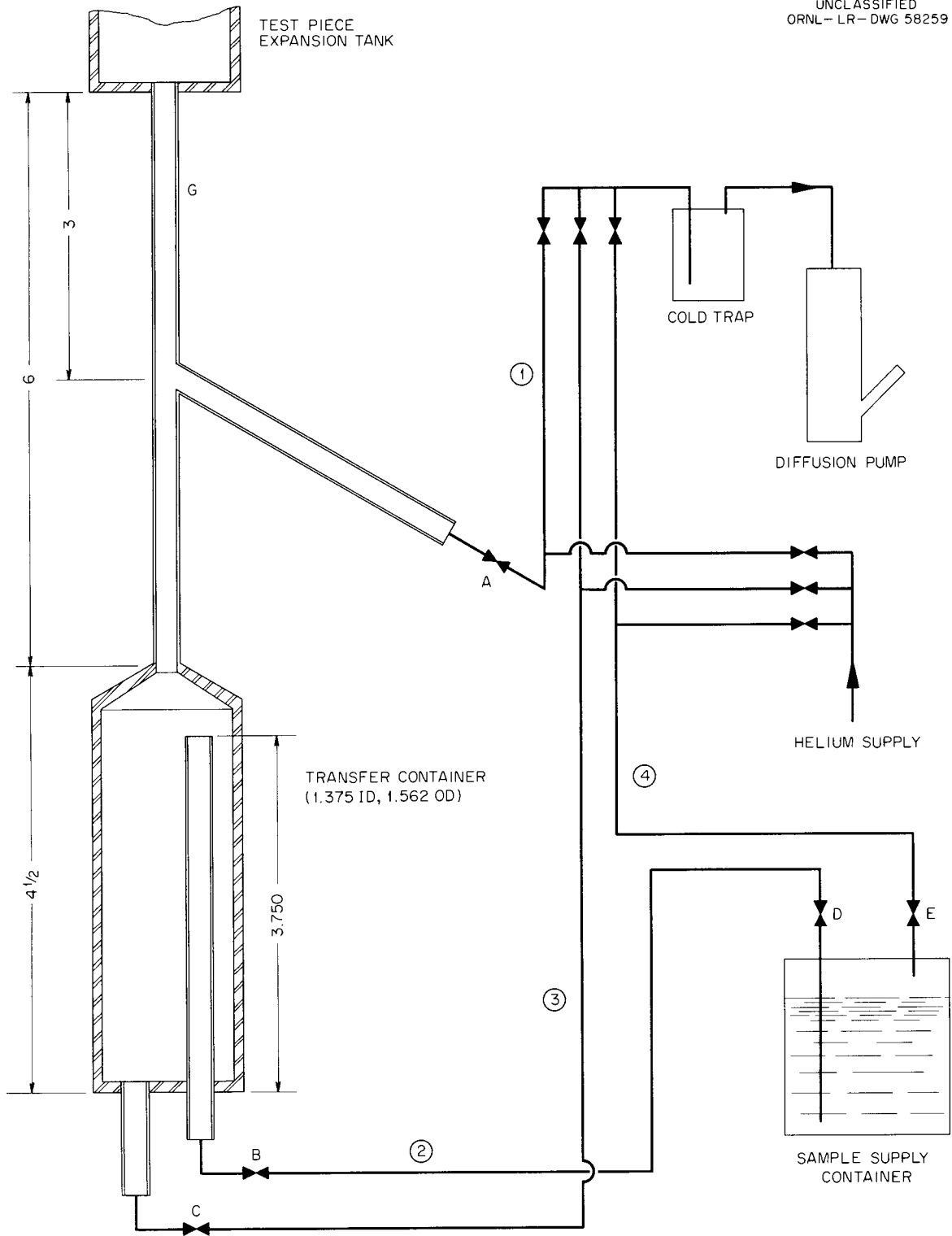


Figure 10. Details and Schematic Flow Diagram of Fill System.

around the test piece, transfer container, and connecting tubing. To complete the vacuum transfer system, a vacuum source, helium supply, and lithium sample supply container were connected to the transfer container with the test piece and transfer container assembly in an inverted position as shown in Figure 10.

The following steps were used to operate the vacuum transfer system. With all valves open except D and E, the system was alternately evacuated and purged with helium several times. The transfer container, sample supply container, and line (2) were heated to 400°F and valves D and E opened with valve C closed. Line (4) was pressurized forcing the lithium into the transfer container. The weight of the supply container was monitored sufficiently to tell when the lithium level was at least over the riser tube in the transfer container. A vacuum was pulled on line (4) draining the lithium from the transfer container until the level of the riser tube opening was reached. All heat was then turned off allowing the lithium to freeze. Valve C was opened and line (3) evacuated.

With the transfer container now filled with an accurately measured supply of solid lithium, the test piece and transfer container were turned upright. All valves except A were closed and the test piece was heated to 500°F and evacuated through line (1) to a pressure  $<1 \times 10^{-5}$  mm of Hg for 24 hr. After evacuation, valve A was closed and heat also applied to the transfer container and connecting tubing. After the lithium in the transfer container had melted, valve C was opened and line (3) pressurized to 20 psig forcing all the lithium into the test piece. All heat was turned off and the system allowed to cool slowly to room temperature. The transfer container was evacuated and the connecting tubing pinched into and

sealed by Heliarc welding at position G.

X-ray photographs taken after the test piece had cooled to room temperature disclosed a 3/4-in.-dia spherical void at the upper interface of the lithium cavity as can be seen in Figure 11a. This void was caused by the lithium prematurely freezing in the 0.125-in.-dia fill hole as the test piece cooled to room temperature. It was expected that by reheating the test piece to 800°F and then cooling by immersion of the lower end in a dry ice-acetone bath (to maintain a large axial temperature gradient), the void could be reduced in size. However, as can be seen in Figure 11a, the void was not centered and only part of the void was pushed out of the cavity by reheating to 800°F. Furthermore, vibrating and tilting the test piece to angles approaching the horizontal did not aid in repositioning the void. At this point, it was conceded that although the upper interface of the cavity was tapered toward the center, concentric machine marks left on this surface coupled with the high-surface tension of the lithium were holding the void in a fixed position.

To obtain a greater force on the void, the test piece was rotated about its own centerline. Unfortunately, the rotational speed was not easily controlled and the speed was exceeded at which the lower surface of the void was pulled below the thermocouple wells. Therefore, small voids were left clinging to the bottom surfaces of the upper and middle thermocouple wells. These voids proved to be equally as stubborn to remove. In fact, when the test piece was rotated about an axis perpendicular to the x-axis of the test piece at a high rpm (sufficient to produce an acceleration of 20 gees on the voids) and the voids were still not removed (see Figure 11b), this test piece was discarded.

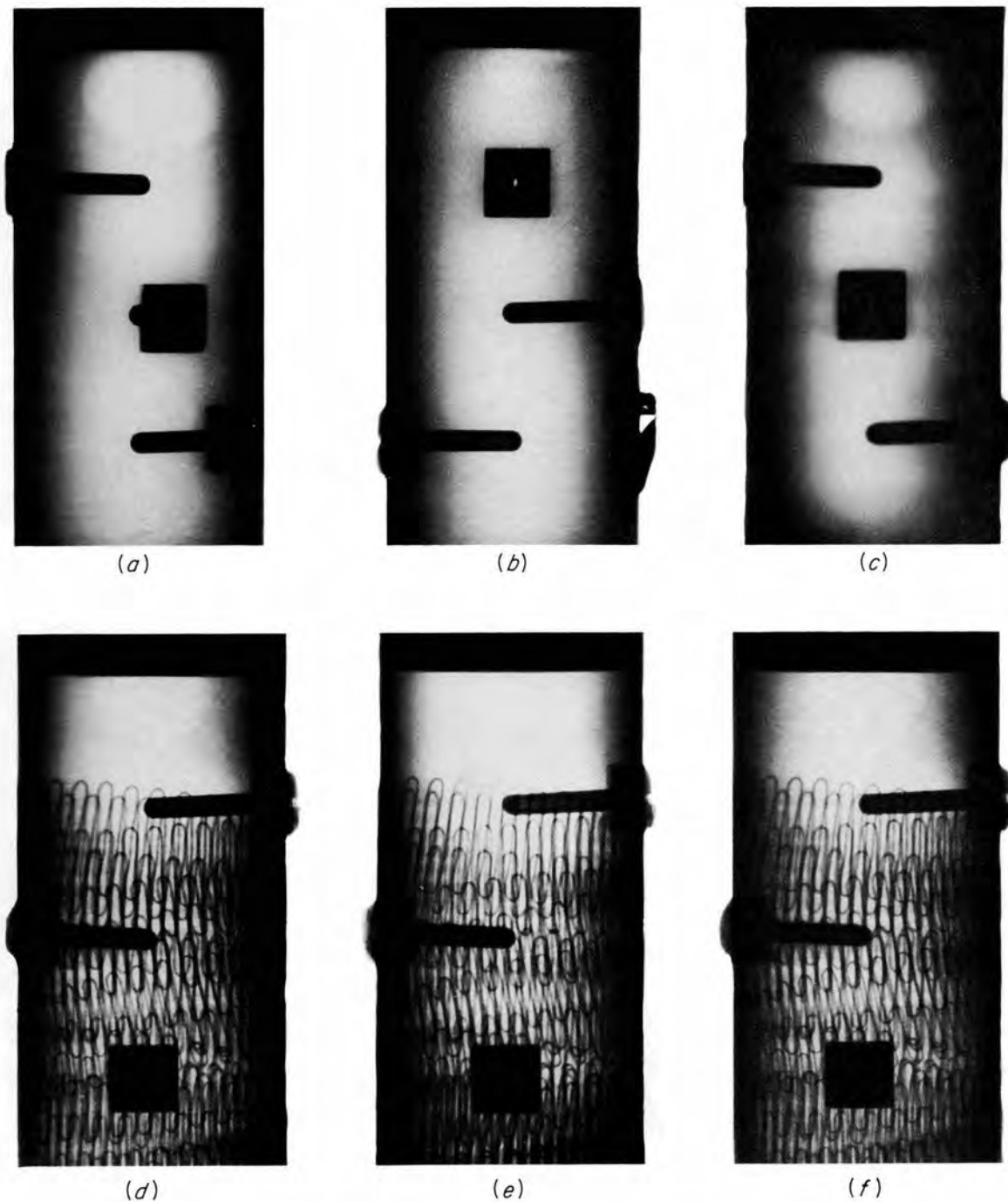


Figure 11. X-Ray Photographs of Test Piece Showing Void in Lithium Sample for Test Piece No. 1 (a) After Filling and (b) After 20 gees Acceleration; and for Test Piece No. 2 (c) After Filling, (d) At 550°F, (e) At 650°F, and (f) As Installed in Apparatus [All X-Rays Except (d) and (e) Taken at Room Temperature].

The upper interface of the cavity of a second test piece was polished to a mirror finish. After following the identical procedure as used in filling the first test piece, an X-ray photograph was taken of the second test piece and is shown in Figure 11c. The void was of similar size; however, it could now be freely moved about by tilting the test piece very slightly and could be centered by merely keeping the test piece vertical.

The test piece was reheated and X-ray photographs taken every 50°F above the melting point of lithium. Somewhere between 600°F and 700°F the void was completely pushed out of the cavity as shown in Figures 11d and 11e. Heating was continued to 800°F at which point the lower end of the test piece was immersed in a dry ice-acetone bath and the heat turned off. The large axial temperature gradient, thus formed, delayed the freezing of the lithium in the fill tube; and the volume of the void in the test piece cavity was reduced to about one-half that of the void left after filling. Calculations showed that this void would be pushed out of the test piece cavity at 520°F, which was well below the average lithium temperature (650°F) of the first thermal conductivity determination.

The void in the test piece as finally installed in the apparatus is shown in Figure 11f. No other voids were detected in the sample cavity. From comparisons with X-ray photographs taken previous to filling and from the density and size of the voids that could be detected in the discarded test piece, it was believed that any voids larger than 1/16 in. in diameter could be detected.\*

---

\*The X-ray photographs made previous to filling the sample cavity were taken at the same angle and exposure as those after filling so that any machine marks, surface blemishes, and shadows would not interfere with the interpretation of the photographs.

Calibration and installation of thermocouples. All critical temperature measurements were made with 30-gauge (0.010-in.-dia) Pt/90Pt+10Rh thermocouples. The Pt and 90Pt+10Rh wires for these thermocouples were purchased under rigid specifications from the Thermo Electric Company. The junctions were made by twisting the ends of the two wires together for three turns and then arcing the junction into and out of a mercury bath situated in a helium atmosphere. In this manner, the junctions were formed into spherical beads of closely controlled diameters ranging from 0.033 to 0.037 in.

Cleaning, annealing, and calibration of the thermocouples were performed by the Instrument and Controls Division of the Oak Ridge National Laboratory. The thermocouples were cleaned with ethyl alcohol, dried, and then annealed in air at 2600°F for 5 min. Next, the beads of as many as eight of the thermocouples at a time were very lightly spot welded to the junction of a 24-gauge National Bureau of Standards Pt/90Pt+10Rh thermocouple. The standard and attached thermocouples were placed in the center of a 24-in. long horizontal furnace. The thermocouples were connected to a high-precision, high-accuracy microvolt emf measuring circuit and calibrated according to established procedures. Thus, eight thermocouples at a time were calibrated relative to each other and to the standard. In this manner, a given group of thermocouples - for example, the four upper-heat-meter and the three sample-region thermocouples - were calibrated relative to each other, reducing the calibration error in the  $\Delta t$  measurements to an estimated  $\pm 0.36^\circ\text{F}$  (see Appendix D).

Upon receipt from calibration, each thermocouple was carefully inspected at 30x magnification under a stereoscopic microscope. Only a

slight indentation could be detected where the beads had been spot welded. The lead wires of several thermocouples were kinked and had slight scratches, but this was to be expected considering the large number of thermocouples being handled. Special care was taken to minimize any further damage, contamination, or cold working of the lead wires during installation of the thermocouples.

The procedure used to install the thermocouples on the test piece and guard tube is shown in Figure 12. A short length of twin bore, 0.051-in.-dia  $\times$  0.015-in. bore, high-temperature porcelain tubing was slipped over the lead wires to insulate them within the 0.055-in.-dia thermowells. The rest of the lead wire was insulated by 1/8-in.-OD  $\times$  1/16-in.-ID quartz sleeving. As an extra precaution against grounding, the test piece and guard tube were each wrapped with a single layer of 1-in.-wide  $\times$  0.016-in.-thick quartz tape. Each thermocouple was arc welded to the bottom of its respective thermowell. The porcelain tubing extended approximately 0.032 in. beyond the surface of the test piece and guard tube; at this point, the lead wires were turned 90 degrees and wrapped a suitable distance around the test piece and guard tube to minimize thermocouple conduction error (see Appendix D). The lead wires were then continued vertically upward. Another layer of quartz tape was wrapped around the test piece and guard tube to hold the lead wires in place.

Operating procedure. After the assembly of the apparatus was completed, the forepump was turned on and the system pulled down to and maintained at  $5 \times 10^{-3}$  mm of Hg pressure. For the next several days, the instrumentation and heater circuits were tested and the system leak checked.

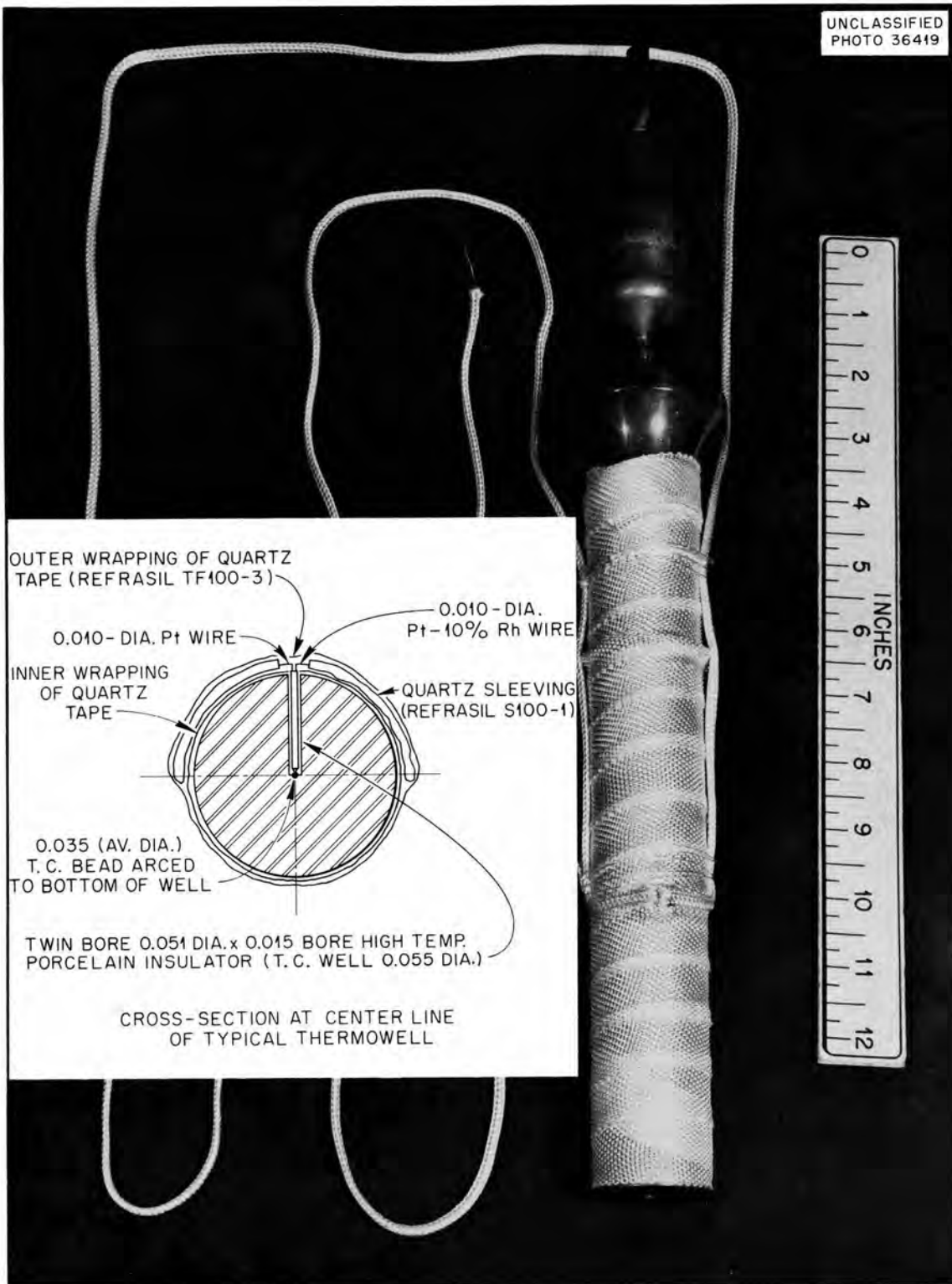
UNCLASSIFIED  
PHOTO 36419

Figure 12. Method of Thermocouple Installation.

The diffusion pump was then started and when the system pressure had been lowered to  $3 \times 10^{-5}$  mm of Hg, the furnace heaters and water to the outer cooling shield were turned on. The increase in furnace heat during the next several days was made gradually so that the diffusion pump could maintain the  $3 \times 10^{-5}$  mm of Hg pressure against the increased outgassing.

When the apparatus reached  $650^{\circ}\text{F}$ , cooling water to the sink cooler and electrical power to the sink heater and main heater were turned on. The sink and main heaters were adjusted to provide an axial temperature gradient down the test piece and to maintain the average sample temperature at  $650^{\circ}\text{F}$ . After an axial temperature gradient had been established in the test piece, the guard heaters were adjusted to obtain a matching axial temperature gradient in the guard tube. To match the two gradients within acceptable limits usually required 8 to 10 hr, and to insure steady state this condition was maintained another 6 to 10 hr before a set of data was taken.

For each thermal conductivity determination, the data were read and recorded in the following order: emf of thermocouples 1 through 32 (in that order), current and voltage of heaters 1 through 17, time to fill weigh tank for each cooling-water circuit, inlet and outlet temperatures of each cooling-water circuit, room temperature, and system pressure.

A check for induced emf was made by reading each thermocouple during a momentary shutoff of all electrical supply to the system. Since the potentiometer was prebalanced for each reading, the disruption required for final balancing was less than a second which had no noticeable effect on the system temperature level. As little inductive effect ( $<0.5 \mu\text{v}$  and all in the same direction) could be detected in the thermocouple emfs,

only spot checks were made during the remaining runs. Also, after the measurements had been completed, an in place, relative calibration of the thermocouples was made. This was performed by use of the furnace heaters only, which could provide a uniform temperature extending over the entire region of the test piece and guard tube at temperatures up to 1200°F.

## CHAPTER V

## RESULTS

Twenty-six determinations of the thermal conductivity of molten lithium were made from 624 to 1527°F. The results of these determinations and other observations related to the accuracy of the results are included in this chapter.

Values of the thermal conductivity of molten lithium. The determinations of thermal conductivity, designated as runs 1 through 14, were made in the order of ascending temperature levels with, in most cases, several runs at each level. The uncorrected and corrected data recorded for these runs are presented in Tables VI and VII in Appendix C. As indicated in the method of calculation in Chapter II, it was possible to calculate the thermal conductivity using the temperature gradients from both the upper and lower heat meters. Therefore, two values of thermal conductivity were determined for every run.

Twenty-six values of the thermal conductivity of molten lithium are tabulated in Table II and shown plotted versus temperature in Figure 13. Two values resulting from the final run (run 14) are also given in Table II but are not plotted in Figure 13 as they were considered to be in error, probably because of the cumulative effects of thermocouple emf drift at this point. Also, the two values from run 9 appeared to be excessively high and were not included in determining the linear least-squares line shown in Figure 13. The average deviation of the twenty-six values, including those from run 9, about the least-squares line was

Table II. Summary of Lithium Thermal Conductivity Calculations

Run No.	Upper Heat Meter			Lithium Sample				Lower Heat Meter			Thermal Conductivity		$\frac{Q_1 - Q_2}{Q_1}$ (%)	$\frac{Q_\theta}{Q_1}$ <sup>a</sup> (%)	$\frac{Q_R}{Q_1}$ <sup>b</sup> (%)	RMS <sup>c</sup> Values of Temp. (°F)
	dt/dx (°F/ in.)	Q <sub>1</sub> (Btu/ hr)	t (°F)	t <sub>1</sub> (°F)	dt/dx  <sub>1</sub> (°F/in.)	dt/dx  <sub>2</sub> (°F/in.)	t <sub>2</sub> (°F)	t (°F)	dt/dx (°F/ in.)	Q <sub>2</sub> (Btu/ hr)	Upper (Btu/hr-ft.°F)	Lower (Btu/hr-ft.°F)				
1	42.40	68.60	681.20	680.00	18.907	19.539	623.79	623.02	43.800	68.47	26.82	25.95	+0.2	+0.15	+0.98	±0.09
2	42.20	68.04	678.39	676.79	19.093	19.660	620.31	619.90	43.837	68.32	26.39	25.79	-0.1	0.0	+0.98	0.11
3	46.15	75.45	711.44	709.29	20.972	21.423	647.50	646.68	47.572	75.02	26.60	25.96	+0.5	+0.2	+0.41	0.13
4	53.33	90.20	793.81	792.04	24.128	24.858	720.59	718.58	54.557	88.73	27.61	26.40	+1.6	+0.2	+0.40	0.29
5	53.37	90.03	786.85	785.15	24.265	24.989	713.34	712.54	55.059	89.28	27.40	26.58	+0.8	0.0	+0.57	0.20
6	53.62	90.45	787.63	785.04	23.947	24.643	714.20	712.83	55.363	89.80	27.92	27.00	+0.7	0.0	+0.55	0.20
7	65.01	116.11	928.35	927.79	29.728	30.565	839.79	838.22	66.730	113.96	28.71	27.48	+1.8	0.0	+0.33	0.22
8	65.11	116.25	929.88	929.07	29.573	30.422	841.51	839.36	66.854	114.22	28.92	27.69	+1.7	0.0	+0.30	0.36
9	71.12	136.07	1114.53	1113.20	29.539	30.478	1025.51	1024.00	72.570	133.10	33.95	32.26	+2.2	0.0	+0.30	0.47
10	69.11	142.62	1330.04	1328.71	30.807	31.575	1237.45	1235.94	70.738	140.08	33.80	32.48	+1.8	-0.3	+0.35	0.48
11	69.76	144.26	1336.31	1334.98	31.065	31.896	1242.87	1241.36	70.513	139.90	33.91	32.08	+3.0	0.0	+0.37	0.43
12	69.92	143.70	1320.07	1318.74	31.038	31.629	1227.07	1225.49	69.944	138.10	33.86	31.93	+3.8	+0.2	-0.70	0.49
13	66.24	145.66	1527.91	1526.48	31.422	32.096	1433.46	1431.94	65.796	140.65	33.62	31.72	+3.4	0.0	-0.34	0.89
14	65.41	144.16	1526.91	1525.48	31.740	32.441	1431.48	1429.96	64.837	137.87	32.83	30.73	+4.5	0.0	-0.30	±1.02

<sup>a</sup>These ratios are the per cent of axial heat flow retained (-) or released (+) by the test piece between center of sample region and center of lower heat meter due to the heat capacity effect.

<sup>b</sup>These ratios are the per cent of axial heat flow loss (-) or gained (+) by the test piece between center of sample region and center of lower heat meter due to the radial heat losses.

<sup>c</sup>The root-mean-square deviations of the three regions of the test piece as calculated from the least-squares analysis were averaged to obtain these values.

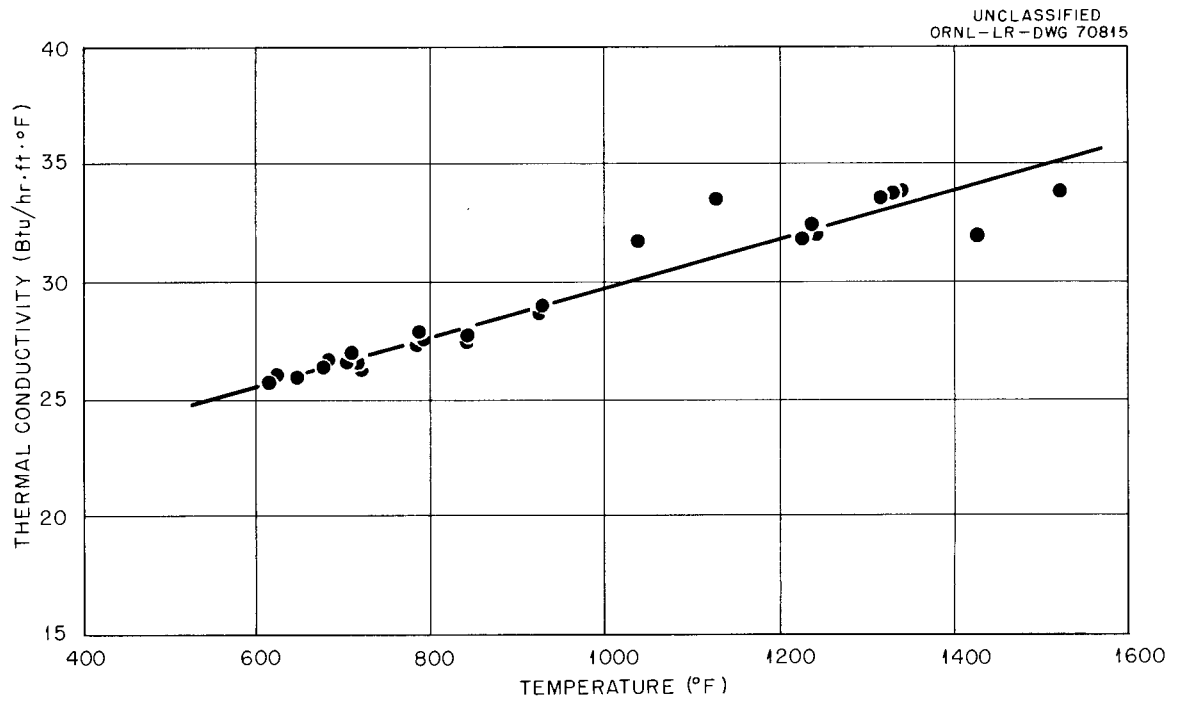


Figure 13. Thermal Conductivity of Molten Lithium as a Function of Temperature - Present Results.

+3.9 and -1.2 per cent.

The sixteen values of thermal conductivity from 624 to 930°F (runs 1 through 8) were calculated as outlined in Chapter II and as shown in the sample calculations in Appendix C. The average deviation of these values about the least-squares line shown in Figure 13 was only +0.8 and -0.7 per cent. It was necessary, however, to alter the method of calculation outlined in Chapter II for the ten values calculated above 1000°F (runs 9 through 13). Above 1000°F, the behavior of all three of the sample-region thermocouples became erratic. Later, disassembly and investigation disclosed that the inner wrapping of quartz tape had torn away from the protruding bases of the three sample-region thermowells. This allowed the soft platinum lead wires, which were not too well protected at this point (see Figure 12), to be grounded to the test piece. Thus, it became necessary to alter the method of calculation by obtaining the lithium temperature gradient from the interfacial temperatures extrapolated from the two heat-meter regions. The average deviation of these ten values of the thermal conductivity of molten lithium about the least-squares line shown in Figure 13 was +4.8 and -4.7 per cent.

Axial and radial heat flow along the test piece. The axial heat flow at the upper and lower interfaces of the sample region of the test piece as determined from the upper and lower heat meters is tabulated in Table II. Also tabulated is the per cent difference between these two heat flows with the positive sign indicating that the axial heat flow into the sample region was larger. For runs 1 through 8, the per cent difference between the axial heat flow into and out of the sample region varied from

-0.1 to +1.8 per cent. The per cent difference for runs 9 through 13 were somewhat larger, varying from +1.8 to +3.8 per cent.

For purposes of comparison to the axial heat flow, only the radial heat flow along the axial distance between the center of the heat-meter region to the center of the sample region was considered. This is the usual procedure since only the heat lost or gained by the test piece between the position of heat flow measurement and sample temperature gradient measurement has any effect on the thermal conductivity determination. Of course, this radial heat flow was compensated for, as far as possible, by the method of calculation (see Chapter II). The ratio of the radial heat flow to the axial heat flow is tabulated in Table II. The radial heat flow varied between -0.7 to +1.0 per cent of the axial heat flow with an absolute average of 0.6 per cent.

Axial temperature measurements and profiles. The rms deviations of the temperature measurements about the least-squares line fitted to each of the three regions of the test piece were averaged and tabulated in Table II. The rms deviation gradually increased from  $\pm 0.09^{\circ}\text{F}$  from run 1 to  $\pm 1.02^{\circ}\text{F}$  for run 14.

After run 14, the system temperature was gradually increased until parts of the test piece were about  $2200^{\circ}\text{F}$ . Before this temperature was reached, several thermocouples failed. The system was then gradually cooled in preparation for shutting it down. When the average test piece temperature reached  $1084^{\circ}\text{F}$ , an in place, relative calibration of the thermocouples was made using only the furnace heaters. During calibration, the furnace maintained a uniform temperature extending over the entire region of the test piece and guard tube. This was deduced from the close

agreement of the thermocouple readings and the lack of any decreasing temperature trend in either the radial or axial directions. The temperature reading of these thermocouples as a function of their position is shown in Figure 14. The mean deviation of all the thermocouples about their averaged value was  $\pm 0.53^{\circ}\text{F}$ . The maximum difference between any two test piece thermocouples was  $2.5^{\circ}\text{F}$ , or a maximum deviation at  $\pm 1.25^{\circ}\text{F}$  about the mean.

A typical axial temperature profile along the test piece and guard tube is shown in Figure 15 for run 8. (Because of the compressed scale, the slight curvature in the profile is not shown in Figure 15.) The agreement of temperature and gradient between the test piece and guard tube for both the heat meter and sample regions can be seen from this typical profile to be quite good. The two interfacial temperature drops were always in the direction of heat flow and for the first eight runs averaged  $1.7^{\circ}\text{F}$ . No such information could be inferred from runs 9 through 14 as the sample region temperature measurements were too erratic to be considered usable.

Axial location of the thermocouple junctions. As was outlined in Chapter II, the axial location of the junctions of the test piece thermocouples were located by a least-squares analysis of the temperature data from runs 1 through 3. The results of this analysis are tabulated in Table III and compared to the "as-built" measured distances to the centerlines of the thermowells taken from Table VIII in Appendix C. The calculated distances for the first three runs deviated from their mean by a maximum of only 0.006 in.; whereas, the measured centerline distances of the thermowells differed by as much as 0.020 in. from the mean of the calculated distances.

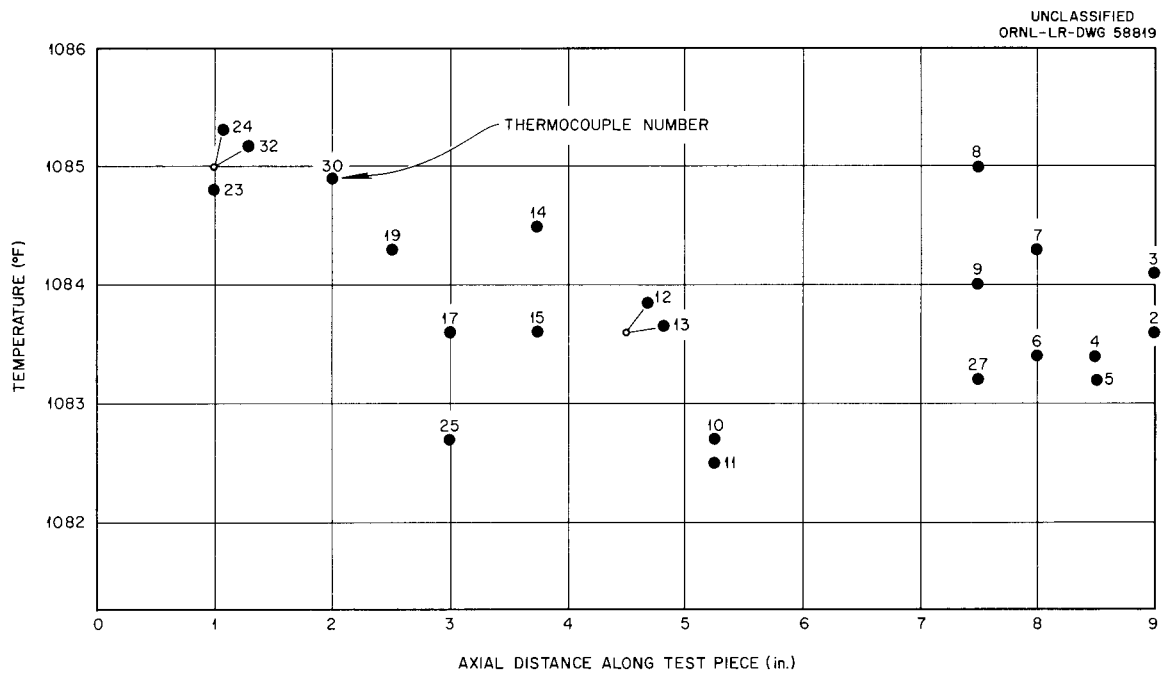


Figure 14. In Place, Relative Calibration of System Thermocouples After Completion of Data Runs.

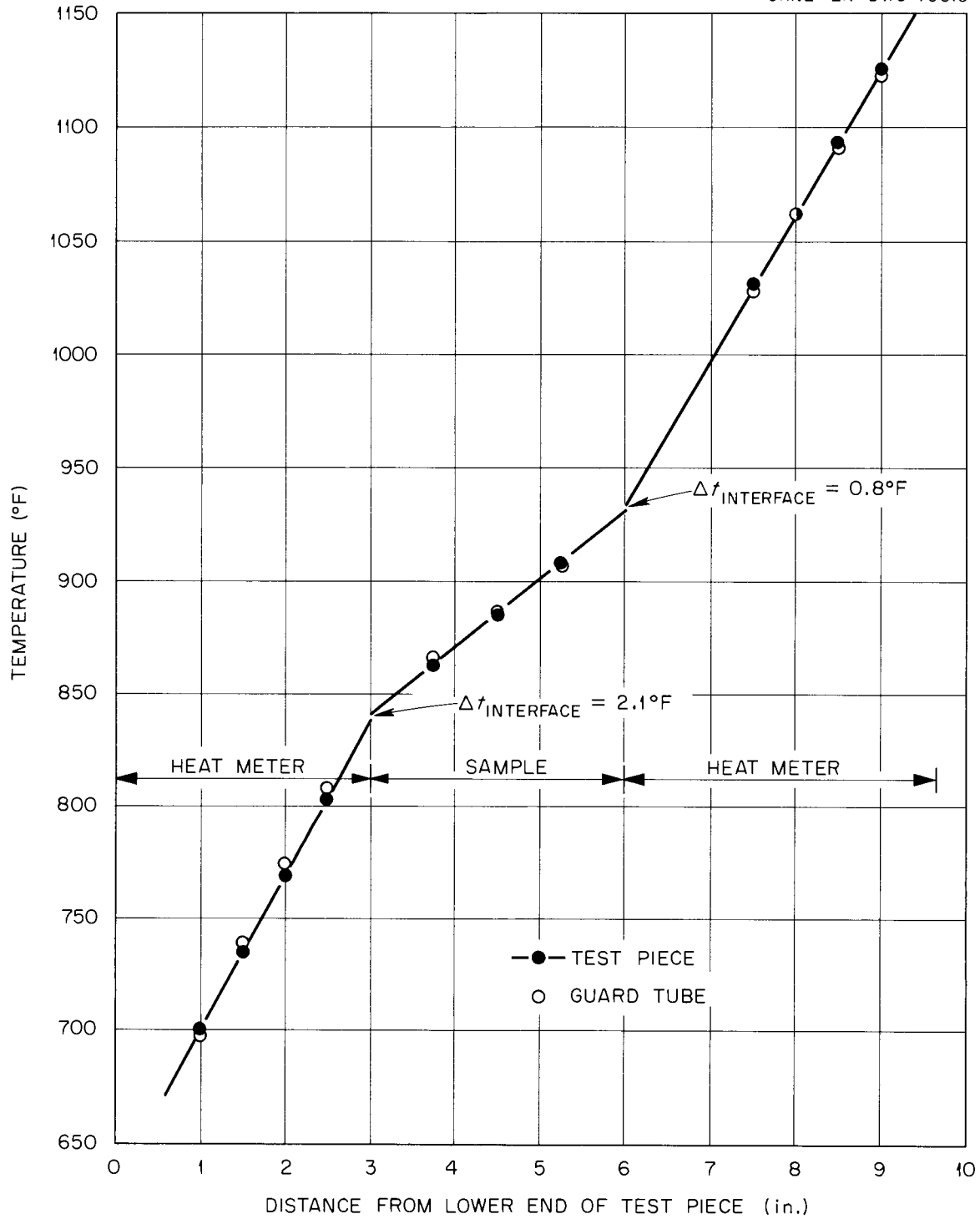
UNCLASSIFIED  
ORNL-LR-DWG 70816

Figure 15. Typical Axial Temperature Profile Along Test Piece and Guard Tube - Run No. 8.

Table III. Summary of Calculated Thermocouple Locations

Run No. → TC No.	Calculated Distances <sup>a</sup>					Max dev from avg	Measured Distances <sup>a</sup> ( $x_m$ )	Deviation of Measured from Calculated ( $x_c - x_m$ )
	1	2	3	Avg ( $x_c$ )				
2	9.1084	9.1076	9.1048	9.1069	0.002	9.103	0.004	
4	8.5971	8.5979	8.6063	8.6004	0.006	8.602	0.003	
6	8.0909	8.0931	8.0847	8.0896	0.005	8.099	0.010	
8	7.6116	7.6093	7.6124	7.6111	0.002	7.604	0.007	
10	5.3491	5.3439	5.3470	5.3467	0.003	5.343	0.004	
12	4.5834	4.5943	4.5878	4.5885	0.005	4.596	0.008	
14	3.8545	3.8489	3.8521	3.8518	0.003	3.848	0.003	
16	2.6006	2.5942	2.5946	2.5964	0.004	2.601	0.005	
29	2.6125	2.6181	2.6160	2.6155	0.003	2.599	0.017	
18	2.0869	2.0810	2.0929	2.0869	0.006	2.100	0.013	
30	2.1045	2.1122	2.1068	2.1078	0.004	2.100	0.008	
20	1.5916	1.5864	1.5908	1.5894	0.003	1.599	0.010	
31	1.5781	1.5861	1.5726	1.5789	0.006	1.599	0.020	
22	1.1111	1.1102	1.1169	1.1127	0.004	1.101	0.012	
32	1.1125	1.1101	1.1075	1.1100	0.002	1.099	0.011	

<sup>a</sup>Distances are from lower end of test piece.

Miscellaneous observations. During the fill procedure and after the thermal conductivity determinations had been completed, the melting point of the lithium sample was obtained from its cooling curves. The primary purpose of obtaining the melting point was to determine before disassembly of the apparatus if the lithium had been further contaminated by either the fill procedure or contact with the stainless steel test piece at high temperatures. (A lower melting point of a pure element usually indicates increased contamination.) The melting point determined during the fill procedure was 357.3°F and after the measurements was 357.5°F. Within the experimental error, these two values can be considered equal (no increased contamination) and in good agreement with the value of 354°F reported by other investigators.<sup>20,21</sup>

After disassembly of the apparatus, three metallographic specimens were cut from the test piece and examined to determine the extent of the attack of the lithium on the type 347 stainless steel. Less than 0.0005 in. of scattered grain-boundary attack was the maximum observed on any of the specimens. Considering that one of the specimens had been in contact with the lithium above 2000°F for 120 hr, above 1500°F for 400 hr, and above 1000°F for 1000 hr, the small degree of grain-boundary attack indicated excellent compatibility of the purified lithium sample with the type 347 stainless steel container.

## CHAPTER VI

## DISCUSSION OF RESULTS

The accuracy and comparisons of the present results with previous determinations, theory, and predictive correlations are discussed in this chapter.

Errors in the present determinations. A detailed error analysis was made for the system in Appendix D. The summary of this error analysis is presented in Table IV. The errors outlined in this table are the maximum uncertainties remaining after all corrections deemed feasible were made to the departure from ideality. These errors were estimated from an unfavorable standpoint, and it is highly unlikely that all the errors would combine in a manner necessary to give the reported maximum error.

The estimated maximum error in the 1500°F determination was  $\pm 14.7$  per cent, which was almost twice as great as the  $\pm 7.6$  per cent error estimated for the 600°F determination. The  $\Delta t$  measurement was largely responsible for this increased error. This was due to the two reasons mentioned previously; i.e., the necessity of calculating the lithium gradient from the extrapolated interfacial temperatures and an apparent drift of the thermocouple output emf away from the initial calibration as evidenced by the calibration of the thermocouples after completion of the data runs (see Figure 14). Some thermocouple drift in the vicinity of the 1500°F measurement was to be expected, since the quartz-sheathed lead wires experienced temperatures of 1900 to 2000°F in passing near the main heater, and the limit of compatibility between platinum and quartz is considered

Table IV. Source and Estimated Magnitude of Experimental Errors

Source of Error	Error at 600°F (Per Cent)	Error at 1500°F (Per Cent)
$\Delta t$ measurements	$\pm 2.8$	$\pm 8.4$
k of heat meters	$\pm 2.1$	$\pm 3.1$
$\Delta x$ measurements	$\pm 1.4$	$\pm 1.5$
Radial heat flow measurement	$\pm 0.5$	$\pm 0.4$
Area measurement	$\pm 0.2$	$\pm 0.2$
Nonsteady state	$\pm 0.0$	$\pm 0.0$
Impurities in lithium sample	-0.2	-0.2
Heat conduction into test piece by thermocouple lead wires	$\pm 0.1$	$\pm 0.1$
Interchange of heat between the test piece and insulation	+0.3 -0.6	+0.5 -1.3
Natural convection in lithium sample	$\pm 0.0$	$\pm 0.0$
Thermocouple conduction error	<u><math>\pm 0.0</math></u>	<u><math>\pm 0.0</math></u>
Total maximum error	+7.4 -7.9	+14.2 -15.2

to be somewhere around 1800 to 2000°F.<sup>22</sup> A large portion of the thermocouple drift may have occurred after the conductivity determinations when the apparatus was heated from 1500 to 1700°F for a few hours just prior to the calibration.

The selection of the thermal conductivity values to be used for the type 347 stainless steel heat meters was narrowed to two investigations, one by Fieldhouse, et al.,<sup>19</sup> and the other by Lucks, et al.<sup>23</sup> These two investigations agreed well with regard to temperature dependency, but the results of Lucks, et al., were approximately 4 per cent higher than those of Fieldhouse, et al., (see Figure 30 in Appendix E). A spectrochemical analysis of the type 347 stainless steel sample used by Lucks, et al., agreed well with that for the heat meters used in this investigation (see Figure 30); however, only the nominal composition sufficient to identify the alloy was known for the sample used by Fieldhouse, et al.<sup>24</sup> Despite the lack of detailed compositional data,\* the determinations of Fieldhouse, et al., were finally selected primarily because their absolute, radial-heat-flow method should have been inherently more accurate than the comparative, axial-heat-flow method used by Lucks, et al. Also, the apparatus used by Fieldhouse, et al., was calibrated using Armco iron, and their results agreed with the elaborate determinations of Powell<sup>26</sup> to within  $\pm 1$  per cent below 700°F and to within  $\pm 2$  per cent above 700°F. The error in the conductivity of the heat meters reported in Table IV ( $\pm 2.1$  per cent

---

\*The thermal conductivities of the 300 series stainless steels are relatively insensitive to minor deviations in nominal compositions as evidenced by only a 6 per cent difference between the measured conductivities of type 301, 304, 316, and 347 stainless steels from 500 to 1600 F.<sup>23,25,19</sup>

at 600°F and  $\pm 3.1$  per cent at 1500°F) was determined considering both the agreement of their calibration with the results of Powell and that Armco iron is a more severe test of the accuracy of the radial flow device than stainless steel (see Appendix D).

The diameters of the test piece were measured to  $\pm 0.001$  in., producing an error of  $\pm 0.2$  per cent in the area measurements. The distances between thermowells were also measured to  $\pm 0.001$  in.; however, there was an additional uncertainty of the thermocouple location within the thermowell. This was minimized by the least-squares procedure described previously. Without such a procedure, the error in the  $\Delta x$  measurements would have been several times larger than the estimated value of  $\pm 1.4$  per cent.

The corrections for radial heat flow and transient heat capacity effects were small, and in the case of the latter did not produce any significant error in the thermal conductivity determination. The most significant uncertainties in the calculation of the radial heat flow were the thermal conductivity of the Fiberfrax insulation and the radial  $\Delta t$  across the insulation. These uncertainties in the calculation of the radial heat flow should not have produced an error greater than  $\pm 0.5$  per cent in the lithium conductivity determination.

The attachment of thermocouples to the test piece introduced the possibility of two other errors. One of these was the usual thermocouple conduction error which was made negligible by the technique described previously and in Appendix D. The other error was caused by the conduction of heat down the thermocouple lead wires and into the test piece. This additional heat flow should not have caused the thermal conductivity of the lithium as determined from the upper heat meter to be low by more

than 0.2 per cent, or from the lower heat meter to be high by more than 0.2 per cent.

The effects of impurities and natural convection in the lithium sample on the thermal conductivity determination were also considered. For the former, an estimation based on Freedman and Robertson's<sup>5</sup> results for the change in the electrical resistivity of sodium with the fractional atomic per cent addition of Li, K, Cs, Rb, Ag, Au, Sn, Cd, and Pb showed that the present thermal conductivity determinations would not be lowered by more than 0.2 per cent because of the impurities (see Appendix D). Considering convection, the large temperature gradients directly opposed to the acceleration of gravity should have had a large inhibiting action on any possible convective currents in the sample. Such convective currents could only occur because of radial temperature gradients, and the net effect of these currents should be only in aiding the radial heat flow, which was measured. The conclusion of the negligible effect of natural convection on the thermal conductivity determination is supported by the experiments of Powell and Tye<sup>27</sup> and Ewing,<sup>25</sup> whose apparatus and methods were similar to those of the present investigation (see Appendix D).

One cause of error not usually considered in the axial-heat-flow apparatus is the interchange of heat between the test piece and insulation, even with perfect matching of guard tube and test piece temperature profiles. The interchange of heat takes place because the axial heat flow in the insulation is not constant along the length of the test piece. It varies because of (1) the step change in thermal conductivity along the test piece and (2) the unequal temperature dependencies of the thermal conductivities of the test piece and insulation. Heat interchange due

to the first cause could result in the thermal conductivity as calculated from both heat meters to be too low. That due to the second cause could result in the thermal conductivity determination corresponding to the upper heat meter to be too low and to the lower heat meter to be too high. In the present investigation, the accumulative error due to these interchanges of heat between the test piece and insulation was estimated to be less than +0.3 and -0.6 per cent at 600°F and +0.5 and -1.3 per cent at 1500°F.

Perturbations due to thermowells in the sample, taper of upper interface, nonuniform test piece heat flux, etc., were considered to be insignificant with regard to the errors discussed above.

Again, it is highly unlikely that all the errors discussed above actually combined in a manner necessary to give the estimated maximum error. This is evidenced by (1) the good agreement between the two independent axial heat flow determinations [the difference varying from 0.1 to 3.8 per cent], (2) the modest amount of radial heat exchange [always  $\leq 0.9$  per cent of the axial heat flow], and (3) the consistency of the test piece axial temperature profiles [see Figure 15]. However, the  $\pm 8$  and  $\pm 15$  per cent estimated deviations are considered to be more realistic as maximum errors than those reported for many other investigations of this nature.

Comparisons with previous determinations. Four experimental investigations of the thermal conductivity of molten lithium have thus far been called to the author's attention. A more detailed review of these investigations is given in Appendix D.

The first reported determination of the conductivity of molten lithium was by Yaggee and Untermyer.<sup>28</sup> Their axial-heat-flow device was

unguarded and uncalibrated and gave only relative values for the conductivity of lithium, sodium, and eutectic NaK. By taking the results of Ewing, et al.,<sup>25</sup> for sodium and eutectic NaK and using the relative values of Yaggee, thermal conductivity values of 22.4 and 26.3 Btu/hr·ft·°F were determined for lithium at 412°F. The average of these two values is plotted in Figure 16 and falls on the linear extension of the present data. This appears to be purely coincidental, since the individual results of Yaggee for lithium varied as much as -17 to +135 per cent from their reported average value and since the authors themselves summarized their results as being only "roughly one-half that of sodium in the neighborhood of 250°C."

Three unpublished determinations were made by Ewing, et al., using an absolute, axial-heat-flow apparatus with compensating guard heaters which was quite similar to the present apparatus.<sup>3</sup> The results are shown in Figure 16 and are, on the average, 4 per cent below the present results. Their experiments above 1000°F were discontinued after a void was discovered at the upper interface of the sample cavity. Such a void was probably caused by filling difficulties similar to those encountered in this investigation. Since the void was present during the conductivity determinations, it would have caused the axial heat flow to diverge toward the wall of the sample cavity. Thus the axial temperature gradient as measured by their thermocouples, which were peened to the cavity wall, would have been greater than the true value. Such an error would not have been easily detected and could account for their values being 4 per cent below the present results.

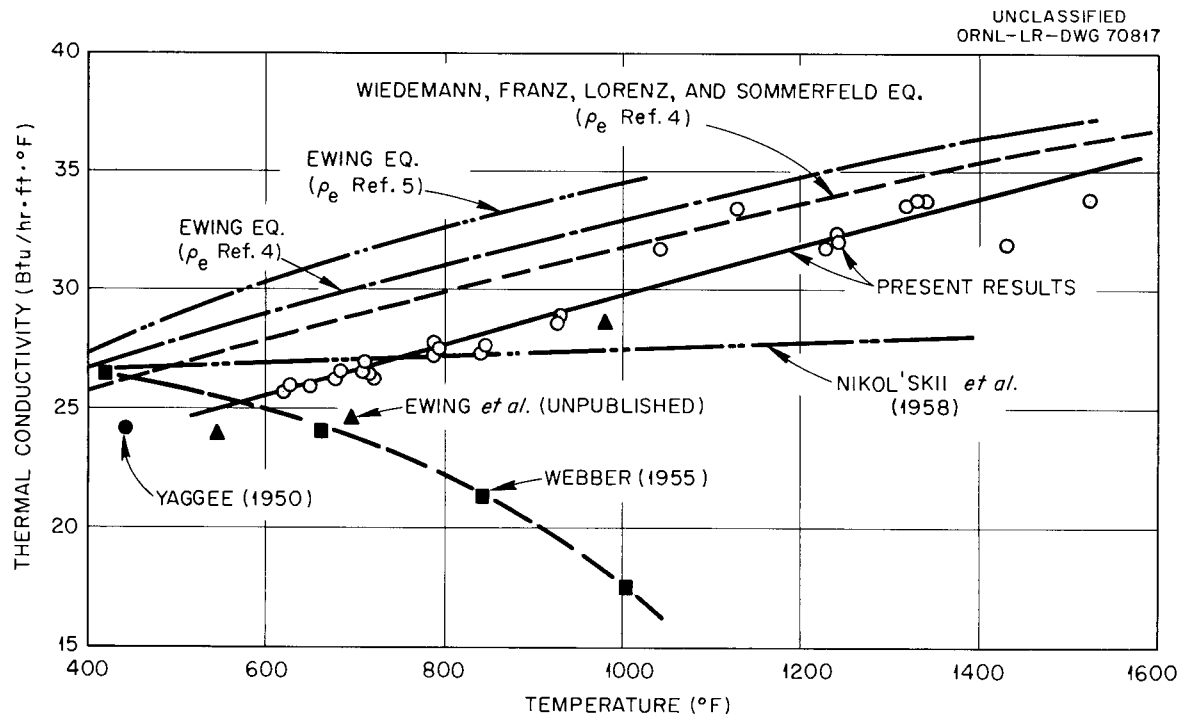


Figure 16. Thermal Conductivity of Molten Lithium as a Function of Temperature - Present, Previous, and Predicted Values.

As can be seen from Figure 16, the results of Webber, et al.,<sup>1</sup> at the higher temperatures are in significant disagreement with the data of all other observers. This is surprising considering (1) that their experimental techniques appeared adequate, (2) that their results are in general agreement with other values below 500°F, and (3) that their comparative, axial-heat-flow apparatus was calibrated using Armco iron. However, several situations may have caused the disagreement. First, the lithium apparently dissolved large amounts of the Armco iron sample container, and this added impurity could have gradually reduced the conductivity of the sample. Second, Sauereisen cement was used to electrically insulate their thermocouples within the heated region of the apparatus. It is now known that the electrical resistivity of certain types of Sauereisen cement decreases sharply at temperatures above 750°F which could have affected their thermocouple readings. Finally, considering the long period of time (20 days) required to obtain their results, the Chromel-Alumel thermocouples could have gradually drifted away from calibration.

A modified axial-heat-flow method - termed the method of successive stationary states - was used by Nikolskii, et al.,<sup>2</sup> to make 74 determinations of the conductivity of molten lithium from 460 to 1364°F, shown in Figures 16 and 17. In this method a coaxial-radiation shield but no compensating guard heating was used. To account for the radial heat flow, two successive steady-state determinations were made with two slightly different axial-heat-flow rates at essentially the same sample temperature. The thermal conductivity was calculated from relationships between the axial-heat-flow and axial-temperature-gradient measurements of the two steady-state conditions. The radial heat losses appeared as a ratio in

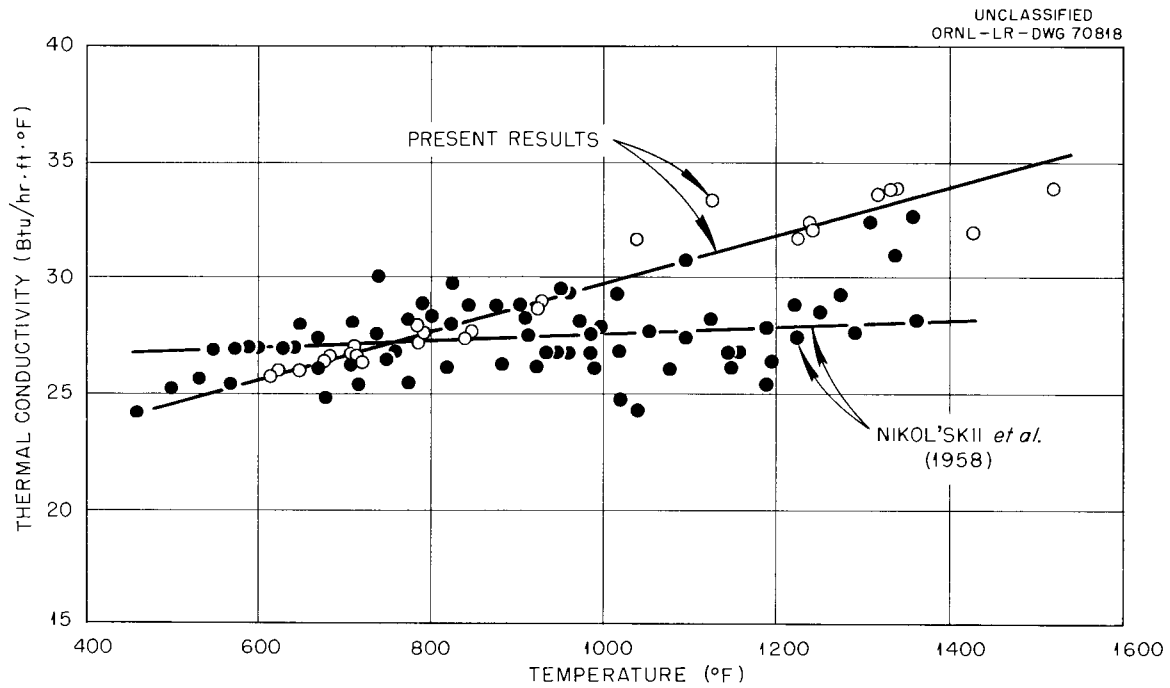


Figure 17. Thermal Conductivity of Molten Lithium as a Function of Temperature - Comparisons Between Recent Russian Data and the Present Results.

these relationships, and the unknown radiation view factor and emissivity were canceled assuming that the emissivity of the test piece and radiation shield surfaces did not vary between the two successive steady states (see Appendix A).

Two features of the method by Nikolskii, et al., are questionable and may account for their data of molten lithium having a large scatter (40 per cent of the data points deviated more than  $\pm 5$  per cent from the mean) and being 17 per cent below the present data at 1400°F. First, filling their apparatus by siphoning from a pool of molten lithium protected only by a surface layer of paraffin could have resulted in the contamination of their sample. Second, the emissivity may not have remained uniform and constant between successive steady states, considering that Richmond and Harrison<sup>30</sup> have shown that the variations of emissivity of Inconel and stainless steel with time and temperature are very erratic even under controlled conditions and high vacuum. Their results for Inconel in a vacuum of  $4 \times 10^{-5}$  mm of Hg showed that the emissivity increased from 0.535 to 0.615 in 1.5 hr at 1050°F and decreased from 0.735 to 0.565 in 2.5 hr at 1475°F. Furthermore, it is interesting to note that the conductivity values of Nikolskii, et al., for sodium and potassium, determined by the same method and equipment as for lithium,<sup>2</sup> are 5 and 12 per cent, respectively, below the results of Ewing, et al., at 1000°F.

Comparisons with predicted values and theory. Several correlations for predicting thermal conductivity were evaluated to show their relative worth in estimating the thermal conductivity of molten lithium. Two of these correlations, the Ewing equation<sup>9</sup> [see Equation (10) in Chapter II]

and the Wiedemann, Franz, Lorenz, and Sommerfeld equation<sup>6-8</sup> [see Equations (8) and (9)], are compared with the present results in Figure 16. Using electrical resistivity measurements for molten lithium obtained by Kapelner<sup>4</sup> (other properties from ref. 29), the WFLS equation predicted values which varied from 9 to 3 per cent higher than the present results from the lower to the higher temperatures, and the values calculated from the equation of Ewing, et al., varied from 13 to 7 per cent higher. The equation of Ewing and co-workers was also evaluated using resistivity measurements by Freedman and Robertson<sup>5</sup> giving values about 20 per cent greater. According to the WFLS theory, experimental thermal conductivity values should always be higher than predicted by the WFLS equation because of the additional conduction due to the lattice and molecules. However, experimental conductivity values for molten sodium, potassium,<sup>25</sup> and other molten metals, as well as the present results, all lie below the values predicted by the WFLS equation. Whether errors exist in these electrical and thermal conductivity determinations or whether the theory is imperfect is uncertain at present. Although there is some minor disagreement in absolute magnitude, the two correlations and the present results are in good agreement in temperature dependency.

Bidwell<sup>16</sup> - using his own determination of the thermal conductivity of solid lithium metal<sup>32</sup> from -418 to + 300°F and using his proposed intercept theory [see Equation (7) in Chapter II] - predicted that the thermal conductivity of molten lithium would be somewhere between 1 to 2 Btu/hr·ft·°F. The large difference between the predicted value and the present results further confirms Powell's conclusions<sup>15</sup> that some of the data used by Bidwell to demonstrate the intercept theory appeared to be

selected and that there was a need for more experimental work before any relationship such as Bidwell's could be accepted.

An expression [see Equations (4), (5), and (6) in Chapter II] has been derived by Mott<sup>13</sup> and Rao<sup>14</sup> to relate the change of the thermal conductivity of a normal metal at fusion to the latent heat of fusion. The results of the calculations for lithium are tabulated below:

$\phi_S$	918°R (ref. 13)
$L_m$	186 Btu/lb (ref. 31)
$T_m$	817.1°F
$f_S$	$10.61 \times 10^{12}$ cps
$f_L$	$9.04 \times 10^{12}$ cps
$(k_S/k_L) = (f_S/f_L)^2 =$	1.4
$(k_S/k_L)$ [with 5 per cent correction]	1.5
$k_S$ (Experimental)	41.1 Btu/hr·ft·°F (ref. 32)
$k_L$ (Experimental)	23.2 Btu/hr·ft·°F
$(k_S/k_L)$ [Experimental]	1.8
Per cent deviation from experimental	16.5 per cent

The values of  $T_m$  and  $k_L$  are from the present investigation. The 5 per cent correction was applied to  $k_S/k_L$  as suggested by Mott to account for the melting temperature of the lithium being near its characteristic temperature. Considering the fundamental nature of the calculation of  $k_S/k_L$ , the agreement with the experimental value is quite good. Kapelner<sup>4</sup> experimentally observed nearly the same increase in the electrical resistivity of lithium upon melting ( $\rho_{eL}/\rho_{eS} = 1.6$  versus 1.8 for  $k_S/k_L$ ).

As concluded in Chapter II, comparisons between experiment and theory for liquid-metal thermal conductivity are difficult to make in the present state of the art. However, from the degree of conformity to the correlations discussed above, it appears that molten lithium conforms to the presently held theory that a considerable degree of crystalline structure is retained in the molten state. This is shown by the agreement between theory and experiment for  $k_S/k_L$  of lithium which tends to lend more weight to Mott's<sup>13</sup> proposal that the decreased thermal conductivity upon melting is due to the greater amplitude of atomic oscillation and not, to any large extent, to the increased irregularities in the atomic arrangement. Also, from electrical resistivity measurements of molten metals, Freedman and Robertson<sup>5</sup> concluded that foreign atoms have about the same scattering power in the molten as in the solid state, showing that the disorder in the molten state for alkali metals is not so great that it cannot be increased by the presence of foreign atoms. Finally, the neutron diffraction measurements of the atomic distributions of molten alkali metals near their melting points by Gingrich and Heaton<sup>12</sup> confirm Mott's proposal that molten crystalline structures consist of small clusters of ordered atoms which gradually merge into one another. Such a gradual change between the crystalline clusters would not scatter the electron waves as they travel through the liquid.

Both the agreement between the present results and the theory of Wiedemann, et al., and between the changes in electrical resistivity and thermal conductivity upon melting tend to confirm that almost all of the heat transferred through molten lithium is by electronic conduction.

Contrary to the results for two other alkali metals, sodium and potassium (no comparative data could be found for cesium and rubidium), the thermal conductivity of molten lithium was found to have a positive temperature dependency. According to the presently held conduction theory (see Chapter II), the thermal capacity and the mean-free path of the conductive electrons should be the only temperature-dependent terms affecting the thermal conductivity of molten lithium, considering that most of its conduction is electronic. The thermal capacity, which increases with temperature, and the mean-free path, which is decreased by the increased amplitude of atomic vibrations, tend to counteract each other. The relative change of the mean-free path with temperature may be found by comparing the coefficient of volumetric expansion, which (like the impedance to the mean-free path of the electrons) depends directly on the amplitude of the atomic vibrations. The average coefficient of volumetric expansion of molten lithium from 400 to 1600°F is almost half that of either sodium or potassium in the same temperature range ( $0.96$ ,  $1.69$ , and  $1.87 \times 10^{-4}$  °F<sup>-1</sup>, respectively, as calculated from the measured densities<sup>33,34</sup>). Thus, there is evidence that the mean-free path of the electrons could decrease sufficiently slowly in molten lithium to cause its conductivity to increase with temperature, as opposed to both molten sodium and potassium.

If lithium behaves as a normal fluid in approaching its critical point, the thermal conductivity of the liquid must reach a maximum and then decline to smoothly merge with the saturated vapor conductivity curve at the critical point. The saturated vapor conductivity was estimated by modified kinetic theory<sup>35</sup> for monatomic gases to be  $\sim 0.1$  Btu/hr·ft·°F at the calculated critical point of 5360°R and 215 atm abs.<sup>36</sup> Furthermore,

from a broad extrapolation of the present experimental data to the calculated critical conductivity (based on the expected tangency of the liquid-vapor conductivity curve to the critical isotherm at the critical point), the conductivity of molten lithium appears to reach a maximum of 45 Btu/hr·ft·°F at 3200°F. This is only an estimate and will require more experimental determinations at high temperatures for verification.

Adequacy of experimental apparatus. The apparatus used in the present investigation functioned extremely well and met most of its design objectives. Several features of the design were especially helpful in providing greater speed and ease of operation by reducing the number of adjustments necessary to obtain a balanced steady-state condition. Some of these were: (1) no adjustment was necessary to match the test piece-guard tube temperatures at the lower end [the test piece and guard tube were each clamped to an isothermal copper cooling pad (see Figure 5 in Chapter III)], (2) no adjustment was necessary to maintain the same test piece-guard tube temperature gradients in the sample region [a nickel alloy was chosen for the composite guard tube which closely matched the conductivity of sample region (see Figure 15 in Chapter V)], and (3) since high-melting tantalum was used for the heater wire, large increments of power could be supplied to rapidly change the system temperature level.

A few changes in the present design and operation are recommended before making further thermal conductivity determinations of molten metals. For reasons noted in Appendix B, the upper heat meter was too far from the sample and should be moved closer. Special cooling should be provided to the lower end of the Alundum refractory heater support to better control

its temperature gradient. Also, a heater should be embedded around the upper guard tube at the level of the main heater to facilitate more rapid test piece-guard tube temperature balances. If the apparatus is to be used to make determinations above 1500°F, all traces of SiO<sub>2</sub> should be removed from the system. This means the substitution of graded Al<sub>2</sub>O<sub>3</sub> powder for the Fiberfrax insulation and Al<sub>2</sub>O<sub>3</sub> tubing for the Refrasil sleeving. Also, the thermocouple lead wires should be brought out of the bottom of the apparatus. Finally, an in place, relative calibration of the thermocouples before each thermal conductivity determination would greatly increase the reliability of the results.

With the above changes, the present apparatus should be able to extend the lithium conductivity results to 2000°F or to the boiling point (~2400°F) if a niobium alloy is used in place of type 347 stainless steel.

## CHAPTER VII

## CONCLUSIONS

A comparative, axial-heat-flow apparatus with compensating guard heating was successfully designed, constructed, and operated to determine the thermal conductivity of a molten sample of 99.82 weight per cent lithium metal. The results can be represented within  $\pm 2.2$  per cent rms deviation by the linear least-squares line,

$$k = 19.76 (1 + 5.01 \times 10^{-4} t) , \quad (22)$$

from 600 to 1550°F. Considerable confidence is placed in the results from 600 to 1000°F; however, increased scatter in the data was encountered from 1000 to 1550°F. It should be emphasized that the present results are relative to the conductivity of the heat meters and thus revert to previous conductivity determinations. From considerations of many sources of error, the maximum error in conductivity was estimated to range from  $\pm 8$  to  $\pm 15$  per cent from the lower to the higher temperatures.

At the melting point, the present values, previous results, and predicted values agree to within  $\pm 7$  per cent. At temperatures above 1000°F, however, the present values do not compare well with any previous experimental determinations but do compare well with predicted values and theory, particularly in temperature dependency. The temperature dependency of the present conductivity results is positive, which is contrary to the data of either molten sodium or potassium. This is consistent with the coefficient of volumetric thermal expansion of molten lithium being almost half that of

either molten sodium or potassium.

From a broad extrapolation of the present data to the calculated critical conductivity, the conductivity of the molten lithium appears to reach a maximum of 45 Btu/hr·ft·°F at 3200°F. This is only an estimate and will require more experimental determinations at high temperatures for verification. The present apparatus, with recommended changes, could be used to extend the conductivity data to the normal boiling point (2400°F).

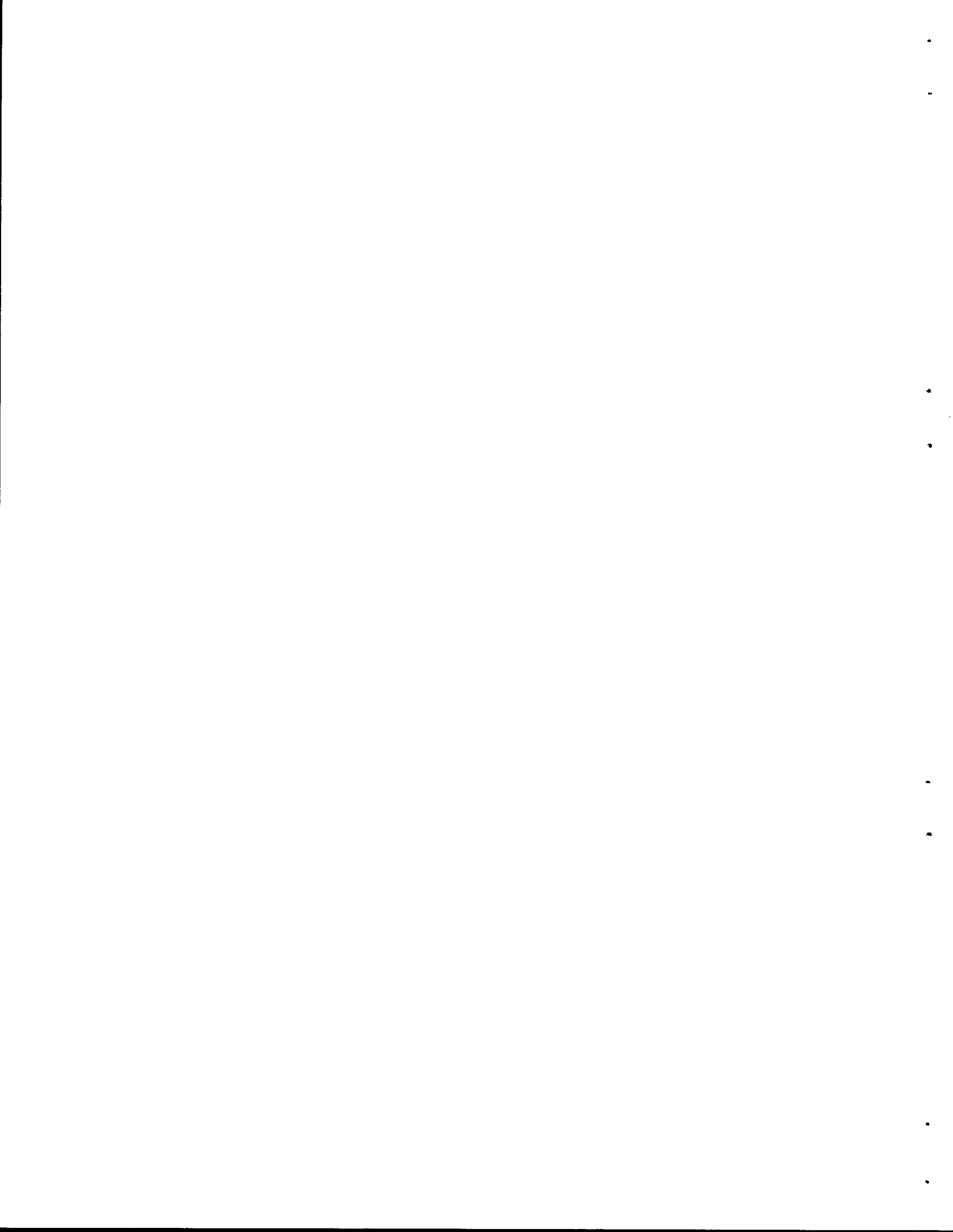
## REFERENCES

1. H. A. Webber, D. Goldstein, and R. C. Fellingner, "Determination of the Thermal Conductivity of Molten Lithium," Trans. ASME 77, 97-102 (1955).
2. M. A. Mikheev, ed., Problems in Heat Transfer, p 1-11, Publishing House of the Academy of Sciences, USSR, Moscow, 1959; translated by U. S. Joint Publications Research Service, New York [AEC-tr-4511 (Jan. 1962)].
3. C. T. Ewing, Naval Research Laboratory, personal communication, Aug. 5, 1960.
4. S. N. Kapelner, The Electrical Resistivity of Lithium and Sodium-Potassium Alloy, PWAC-349 (June 30, 1961).
5. J. F. Freedman and W. D. Robertson, "Electrical Resistivity of Liquid Sodium, Liquid Lithium, and Dilute Liquid Sodium Solutions," J. Chem. Phys. 34, 769-780 (1961).
6. G. Wiedemann and R. Franz, "The Thermal Conductivities of Metals," Ann. Physik 89, 497-531 (1853).
7. L. Lorenz, "The Conductivity of Metals for Heat and Electricity," Ann. Physik 13, 422-447 (1881).
8. A. Sommerfeld, "The Electron Theory of Metals Based on Fermi Statistics," Z. Physik 47, 1-32 (1928).
9. C. T. Ewing, et al., "Thermal Conductivity of Metals," p 19-24 in Chemical Engineering Progress Symposium Series, vol 53, No. 20, 1957.
10. M. Jakob, Heat Transfer, vol I, p 2, John Wiley and Sons, New York, 1949.
11. C. Zwikker, Physical Properties of Solid Materials, p 246-251, Interscience Publishers, Inc., New York, 1954.
12. N. S. Gingrich and LeRoy Heaton, "Structure of Alkali Metals in the Liquid State," J. Chem. Phys. 34, 873-878 (1961).
13. N. F. Mott, "The Resistance of Liquid Metals," Proc. Roy. Soc. (London), Series A, 146, 465-472 (1954).
14. M. R. Rao, "Thermal Conductivity of Liquid Metals," Indian J. Phys. 16, 155-159 (1942).

15. R. W. Powell, "Part II - Thermal Conductivities of Molten Metals and Alloys," J. Iron and Steel Inst. 162, 315-324 (1949).
16. C. C. Bidwell, "A Simple Relation Between Thermal Conductivity, Specific Heat, and Absolute Temperature," Phys. Rev. 32, 311-314 (1928).
17. A. H. Wilson, Semi-Conductors and Metals, University Press, Cambridge, 1939.
18. J. W. Cooke, "Thermal Conductivity of Lithium and Lithium Alloys," ANP Semiann. Prog. Rep. Oct. 31, 1960, ORNL-3029, p 64-69 (Secret).
19. I. B. Fieldhouse, J. C. Hedge, and J. I. Lang, Measurement of Thermal Properties, WADC 58-274, p 1-16 (Nov. 1958).
20. K. K. Kelley, "Heats of Fusion of Inorganic Substances," U. S. Bur. Mines Bull. No. 393 (1936).
21. B. Bohn and W. Klemm, "Zur Kenntnis des Verhhaltens der Alkalimetalle Zueinander," Z. Anorg. Allgem. Chem. 243, 69 (1939).
22. R. Lacroix, "Emploi des metaux de la mine du platine en thermometrie," Revue de Metallurgie 43, 48-56 (1956).
23. C. F. Lucks, J. Matolich, and J. A. Van Velzor, The Experimental Measurement of Thermal Conductivities, Specific Heats, and Densities of Metallic, Transparent, and Protective Materials, USAF Tech. Rep. No. 6145, Part I (March 1954).
24. J. C. Hedge, Armour Research Foundation, personal communication, Aug. 20, 1962.
25. C. T. Ewing and J. A. Grand, Measurements of the Thermal Conductivity of Sodium and Potassium, NRL-3835 (August 1951); also, C. T. Ewing and J. A. Grand, J. Am. Chem. Soc. 74, 11-14 (1952).
26. R. W. Powell, "Further Measurements of the Thermal and Electrical Conductivity of Iron at High Temperatures," Proc. Phys. Soc. (London) 51, 407-418 (1939).
27. R. W. Powell and R. P. Tye, "The Thermal and Electrical Conductivity of Liquid Mercury," p 856-862 in International Developments in Heat Transfer, Part IV, published by ASME, New York, 1961.
28. F. Y. Yaggee and S. Untermyer, The Relative Thermal Conductivities of Lithium, Sodium, Eutectic NaK, and Heat Capacity of Lithium, ANL-4458 (April 21, 1950).
29. R. N. Lyon, ed., Liquid Metals Handbook, 2d ed., p 50, U. S. Government Printing Office, Washington, D. C., 1952.

30. J. C. Richmond and W. N. Harrison, "Equipment and Procedures for Evaluation of Total Hemispherical Emittance," Am. Ceram. Soc. Bull. 39, 668-673 (1960).
31. T. B. Douglas, et al., "Lithium: Heat Content from 0 to 900°, Triple Point and Heat of Fusion, and Thermodynamic Properties of the Solid and Liquid," J. Am. Chem. Soc. 77, 2144-49 (1955).
32. C. C. Bidwell, "Thermal Conductivity of Li and Na by a Modification of the Forbes Bar Method," Phys. Rev. 28, 584-597 (1926).
33. S. A. Been, et al., The Densities of Liquids at Elevated Temperatures: Part I. The Densities of Lead, Bismuth, Lead-Bismuth Eutectic, and Lithium in the Range Melting Point to 1000°C (1832°F), NEPA-1585 (Sept. 7, 1950).
34. C. T. Ewing, et al., Quarterly Progress Report No. 7 on the Measurements of the Physical and Chemical Properties of the Sodium-Potassium Alloy, NP-3040 (May 1948).
35. E. J. Owens and G. Thodos, "Thermal-Conductivity-Reduced-State Correlation for Inert Gases," A.I.Ch.E. Journal 3, 454-461 (1957).
36. D. S. Gates and G. Thodos, "The Critical Constants of the Elements," A.I.Ch.E. Journal 6, 50-54 (1960).
37. N. A. Nikolskii, "A New Method for the Determination of the Thermal Conductivity of Molten Metals," p 54-65 in Heat Transfer and Thermal Simulation (in Russian), ed. by M. A. Mikheev, Academy of Sciences USSR Press, Moscow, 1959.
38. S. Dushman, Scientific Foundations of Vacuum Technique, p 730, John Wiley and Sons, New York, 1958.
39. P. J. Schneider, Conduction Heat Transfer, p 35-40, Addison-Wesley, Cambridge, Mass., 1955.
40. W. H. McAdams, Heat Transmission, 2d ed., McGraw-Hill, New York, 1942.
41. J. A. McCann, Temperature Measurement Theory, KAPL-2067-2, p 56, (April 1, 1962).
42. C. Zwicker, Physical Properties of Solid Materials, p 10, Interscience Publishers, Inc., New York, 1954.
43. J. J. Thigpen, Experimental Analysis of the Mechanisms of Heat Transfer Through Fibrous Insulating Materials, unpublished doctoral dissertation, University of Texas, 1959.
44. W. Przybycien and D. Linde, Thermal Conductivities of Gases, Metals, and Liquid Metals, KAPL-M-WMP-1 (Aug. 6, 1957).

APPENDIX



## APPENDIX

A. PREVIOUS DETERMINATIONS OF THE THERMAL CONDUCTIVITY  
OF MOLTEN LITHIUM

A brief, critical review (in chronological order) of the four determinations of the thermal conductivity of molten lithium that have thus far been called to the author's attention is given in this section of the Appendix.

Determinations by Yaggee and Untermyer.<sup>28</sup> An axial-heat-flow device without compensating guard heating was used to determine the relative conductivities of lithium, sodium, and eutectic NaK and is shown in Figure 18. The liquid-metal sample was held in a stainless steel tube 3/4-in. OD  $\times$  0.033-in. wall  $\times$  7 in. long. Heat was supplied at the top of the tube by a 2-in. long wrapping of nichrome ribbon and was extracted at the bottom of the tube through a heat sink. Surrounding the tube was 3/4-in.-thick 85 per cent MgO pipe insulation. The apparatus was placed in a heated drying oven to reduce heat losses.

The thermal conductivity of the liquid-metal sample was calculated from the power measurement of the heat input and the axial temperature gradient in the liquid-metal sample. The temperature gradient was measured by two iron-constantan thermocouples and two Leeds and Northrup potentiometers. The method of measuring the heat input was not specified.

In an attempt to compensate for unknown heat losses, the apparatus was first calibrated with only a vacuum inside the tube. From measurements of the heat input and temperature gradient, an equivalent heat conductance

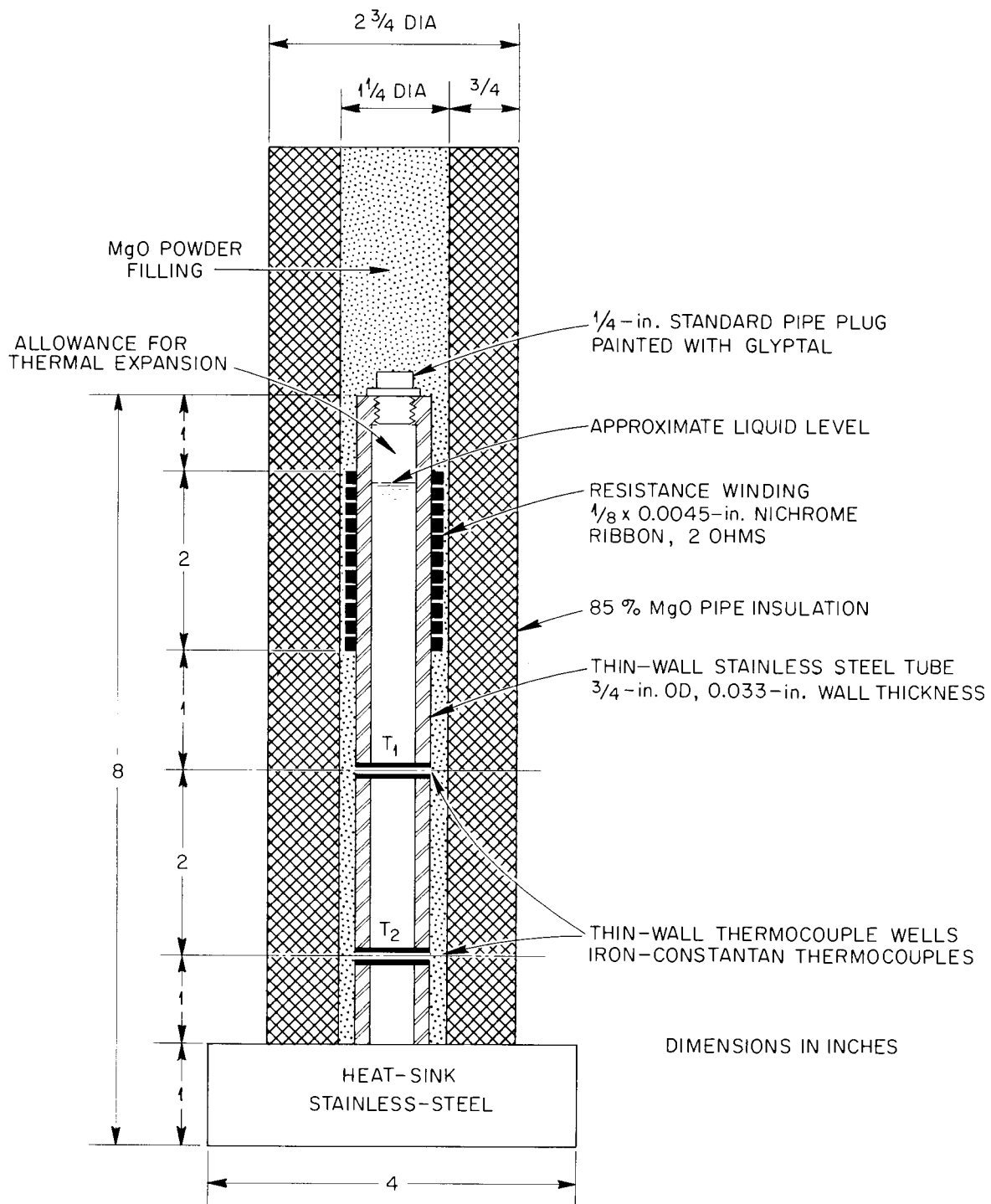


Figure 18. Thermal Conductivity Device Used by Yaggee and Untermyer.

coefficient for the empty apparatus was calculated. Thus when determinations were made with the apparatus filled with the liquid-metal sample under boundary conditions similar to those of the calibration runs, the equivalent heat conductance coefficient would account for the heat flow in the tube wall, in the insulation, and the heat lost to the surroundings.

The conditions which would at least be necessary to fulfill the requirements of similar boundary conditions, mentioned above, are:

(1) the temperature level and temperature gradient would need to be the same for the determinations as for the calibration runs, and (2) the temperature dependency of the thermal conductivities of the sample and the insulation would need to be equal. The latter condition would give the same inherent inaccuracy. The former condition could be controlled by proper operation of the apparatus. However, the calibrations and the thermal conductivity determinations of Li, Na, and NaK were not made at the same temperature levels and gradients. The average temperature levels and gradients for the calibration and for the conductivity determinations with Li, Na, and NaK were 518°F and 970°F/ft, 436 and 430, 392 and 216, and 482°F and 1200°F/ft, respectively. It is little wonder that their individual values for the thermal conductivity of molten lithium varied by as much as -17 to +135 per cent from their mean value of 18.7 Btu/hr·ft·°F. Thus no more significance should be placed in these results than reported by the authors; i.e., "the relative conductivities of Li and NaK are roughly one-half and one-fourth that of Na in the neighborhood of 250°C."

Determinations by Ewing, et al.<sup>3</sup> The determinations of the thermal conductivity of molten lithium by Ewing, et al., have not been published by the investigators. However, the apparatus used previously by Ewing, et al., to determine the conductivities of molten sodium and potassium<sup>25</sup> was essentially the same as that used by him to obtain the lithium conductivity values.<sup>3</sup> The view of the apparatus shown in Figure 19 was taken from the report on the sodium and potassium measurements.

Except for a few details, the method used by Ewing was similar to that used in the present investigation. The major difference was that the heat flow through the sample in their apparatus was measured electrically rather than by a heat meter. Also, instead of using a composite guard tube, Ewing applied heating and cooling directly to the coaxial guard tube to facilitate the equalization of the test piece-guard tube temperature gradients in the sample region (see Figure 19).

The test piece, guard tube, and heat sink were all machined from type 304 stainless steel to form one unit which was positioned within the guard heater tube as shown in Figure 19. The test piece was 1.625 in. in diameter and 20 in. long with a 2-in. long  $\times$  1/32-in.-wall sample cavity and a 3/32-in.-dia fill hole connecting the expansion tank and cavity. Two main heaters, each consisting of a helix of 0.005-in.-dia 90Pt+10Rh wire, insulated and cemented in a spiral groove, were used. The upper heater was used in conjunction with a pair of thermocouples to prevent undesirable heat losses from the lower heater (see Figure 19). The heat was removed from the lower end of the test piece by an air-cooled sink.

The guard tube was 7-in. OD  $\times$  5.5-in. ID and extended well above the top of the test piece. A heater was embedded around the guard

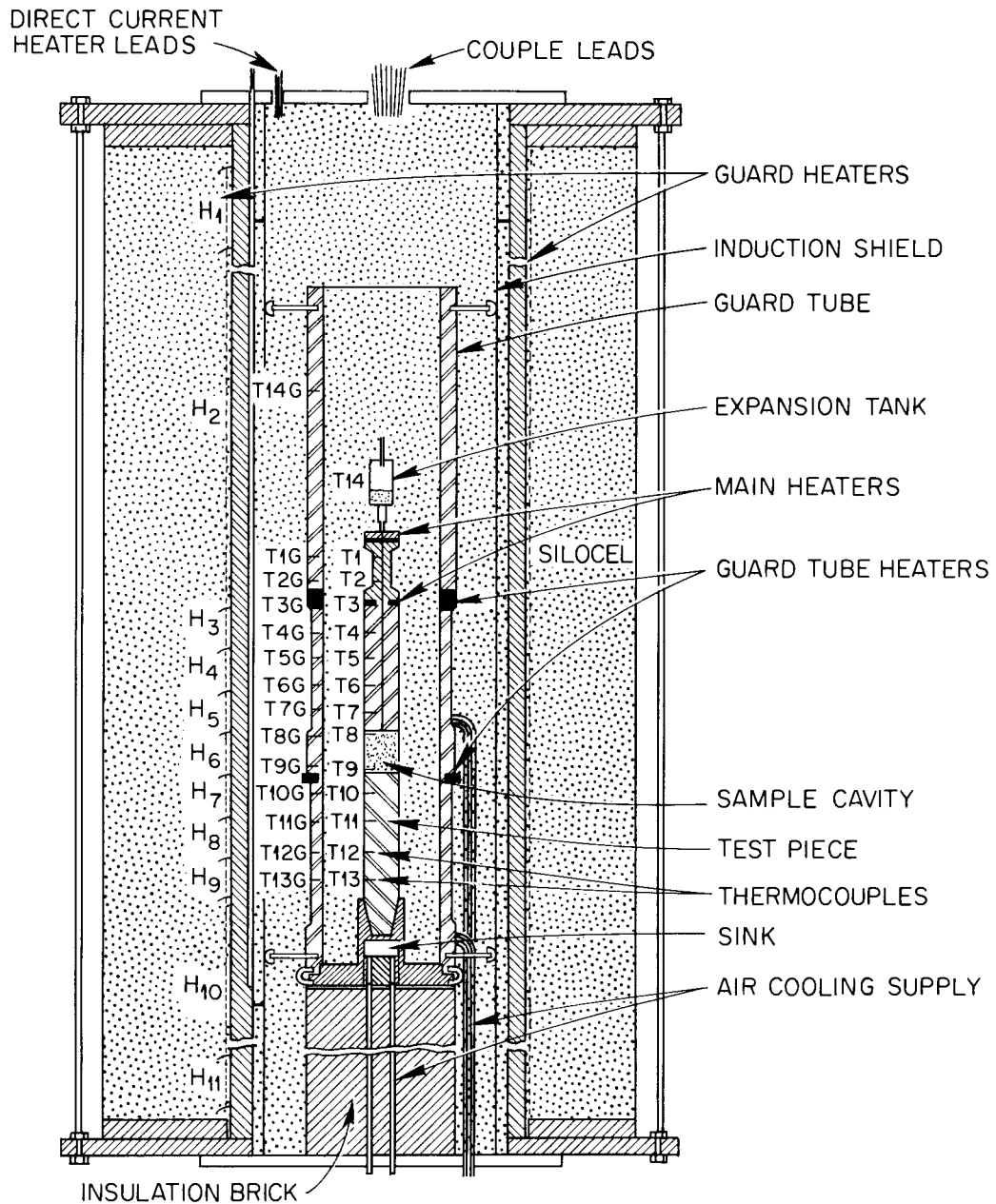
UNCLASSIFIED  
ORNL-LR-DWG 70820

Figure 19. Apparatus Used by Ewing, et al., to Measure the Thermal Conductivity of Molten Metals.

tube wall opposite the main heater. Grooves cut around the guard tube wall opposite the upper interface of the sample cavity were used as passages for thermostatically controlled cooling air. Another heater was embedded in the wall opposite the lower interface and another air cooler located at the end of the guard tube.

Platinum-rhodium heater wire was uniformly wound in eleven sections on a 12-in.-dia Alundum tube for guard heating the test piece (see Figure 19). A grounded metal shield was interposed between the Alundum tube and the guard tube.

Temperature measurements along the test piece were made with 0.005-in.-dia Pt/90Pt+10Rh thermocouples; four were suitably spaced in the test piece above the specimen cavity and four below. Three thermocouples were peened into slots in the wall of the sample cavity. A 0.015-in.-dia Pt/90Pt+10Rh thermocouple was positioned in the guard tube opposite each thermocouple in the test piece. The thermocouple lead wires were insulated and installed in a manner similar to the present investigation (see Chapter IV). Before installation, the thermocouples were calibrated relative to each other and a standard by placing all the junctions in a silver bar supported in the center of a long furnace. After installation, an in place calibration showed that the maximum deviation of the thermocouples near the center of the test piece was only 0.05°F.

The thermocouple emfs during both the calibrations and conductivity measurements were measured with the same well guarded and shielded Rubicon, type C, double-microvolt potentiometer with a Wenner reversing key system. The d-c power to the main heater and guard tube heaters was supplied by a Nobatron power source. The power input to the main heater was determined

from the voltage drop across the heater and across a standard resistor in series with the heater. The voltage measurements were obtained with a Rubicon, type B, potentiometer in conjunction with precision volt boxes.

The test piece cavity was filled with a purified sample of lithium metal by high vacuum distillation. The inlet tube to the expansion tank was then pinched into and welded. The procedures for operation were almost identical to the present investigation. A steady-state axial temperature gradient of  $275^{\circ}\text{F}/\text{ft}$  (as measured in the stainless steel) was established which usually required an adjustment period of several days to attain equilibrium and eliminate drift.

Three determinations of the thermal conductivity of molten lithium were made from 500 to  $1000^{\circ}\text{F}$  and are shown in Figure 16 in Chapter VI. Determinations above  $1000^{\circ}\text{F}$  were discontinued because of irregularities in the data.

The determinations of thermal conductivity of sodium and potassium, and presumably lithium, were made with extreme care. Although their reported accuracy of  $\pm 1$  per cent may be somewhat optimistic, it is the opinion of the author that their measurements for sodium and potassium represent the most accurate determination of thermal conductivity of molten metals that have yet been obtained above  $500^{\circ}\text{F}$ . However, the irregularities in their data for molten lithium (mentioned above) may account for their values being, on the average, 4 per cent below the present results (see Figure 16 in Chapter VI).

After disassembly of the apparatus, it was found that the data irregularities were caused by incomplete filling of the test piece cavity. Considering the similarity between their apparatus and the present

apparatus, the void left in the test piece cavity was no doubt similar to that shown in Figure 11a. Such a void would have been present during the conductivity determinations and would have caused the axial heat flow to be funneled toward the wall of the sample cavity. Thus the axial temperature gradient as measured by thermocouples peened to the cavity wall would be greater than the true value. Such an error would not be easily detected and could account for their data being 4 per cent below the present results.

Determinations of Webber, Goldstein, and Fellingner.<sup>1</sup> A comparative, axial-heat-flow apparatus with compensating guard heating was used to determine the thermal conductivity of molten lithium and is shown in Figure 20. The test piece consisted of a 22-in.-long  $\times$  2.135-in.-dia rod of nickel-plated Armco iron. A 1.997-in.-dia cavity for the lithium sample was bored 10 in. deep into the upper end of the test piece. A 1.75-in.-dia sample heater extended 5 in. deep into the sample cavity and was flanged to the top of the test piece. The sample heater element, consisting of 28-gauge Nichrome V wire wound on a 0.5-in.-dia mandrel, was screwed into the sample heater. The lower end of the bar was cooled by allowing approximately 6 in. of its length to extend outside the heated volume.

Concentric with the test piece was a 4.25-in.-ID  $\times$  4.75-in.-OD mild steel guard tube approximately 15 in. long. At eight approximately equally spaced axial locations along the guard tube, 28-gauge Nichrome V wire was wound directly on the guard tube forming eight 1/4-in.-dia coils. The individual heater wires were insulated from each other and the guard tube by mica and Sauereisen cement. The thermal insulation used for the

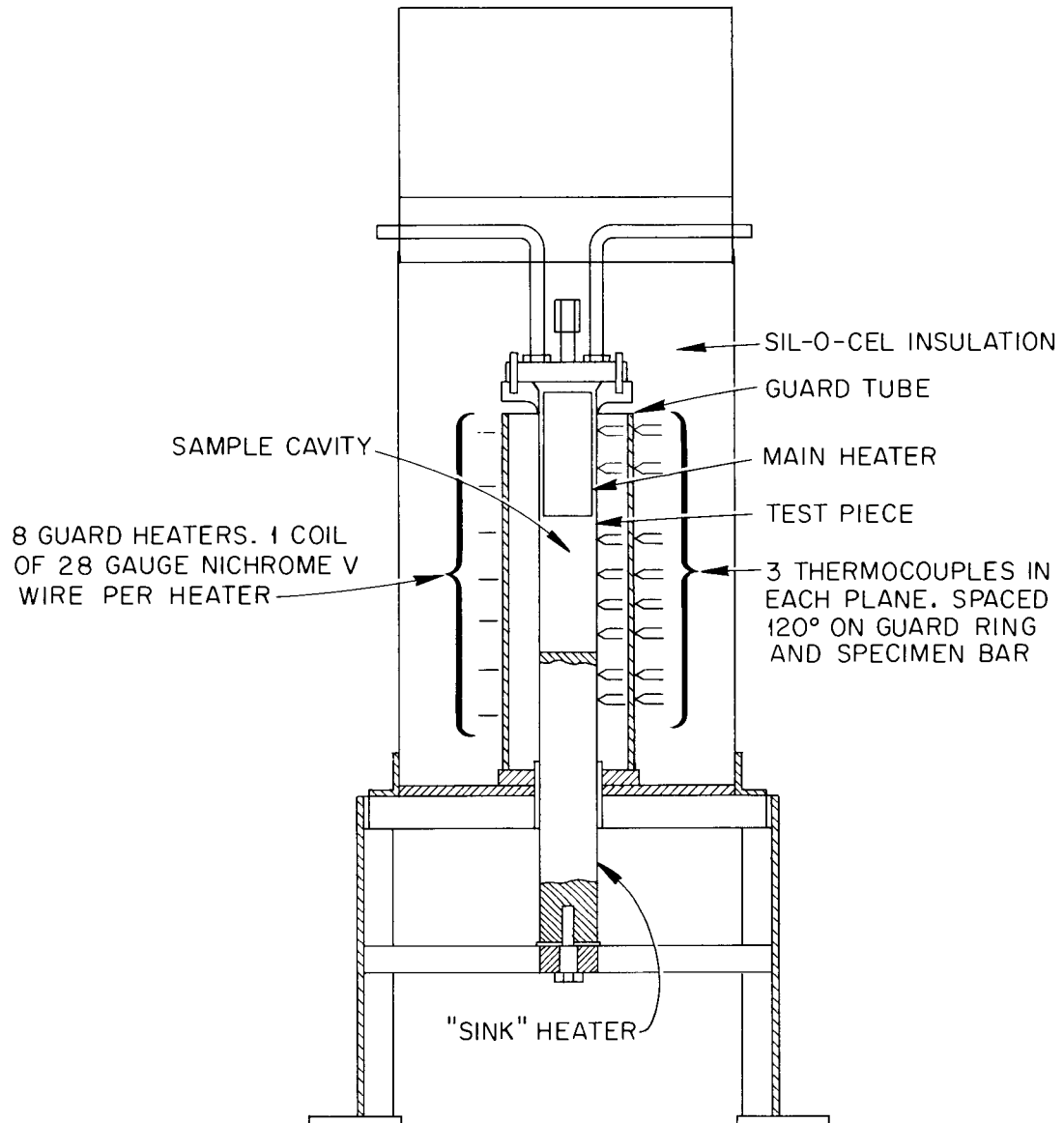
UNCLASSIFIED  
ORNL-LR-DWG 70821

Figure 20. Apparatus Used by Webber, et al., to Measure the Thermal Conductivity of Molten Lithium.

apparatus was Sil-O-Cel.

Three 20-gauge, calibrated, Chromel-Alumel thermocouples were peened into slots spaced 120 degrees apart in each of eight planes on both the test piece and guard tubes as shown in Figure 20. The thermocouple leads were insulated with Sauereisen cement in the heated zone and with glass-fiber braid from the heated zone to the gradient free switch box. The emf was measured with a well-shielded K-2 potentiometer and galvanometer setup. The power for the sample and guard tube heaters was supplied by a shunt-wound 130-volt, 38-amp, d-c generator.

The procedures used to operate their apparatus were similar to those used in the present investigations except that two test pieces were used. The cavity of one test piece (described above) was filled with a sample of lithium metal drained from the bottom of a heated supply container (the supply container was filled by adding pieces of 99.8 weight per cent lithium metal protected from air contamination by a thin coating of benzene). The second test piece was similar to the first, except that the sample region was solid Armco iron (the test piece was bored only deep enough to seat the sample heater against the bottom of the cavity). Thus the thermal conductivity of Armco iron could be measured and compared with reference values to check the experimental and computational methods used in their experiment.

The thermal conductivity of the molten lithium sample was calculated by the usual one-dimensional heat flow equation; i.e.,

$$\begin{aligned} & \left[ (k A \Delta t / \Delta x)_{\text{Li}} + (k A \Delta t / \Delta x)_{\text{Fe}} + (k A \Delta t / \Delta x)_{\text{Ni}} \right]_{\text{SR}} = \\ & = \left[ (k A \Delta t / \Delta x)_{\text{Fe}} + (k A \Delta t / \Delta x)_{\text{Ni}} \right]_{\text{H}} \end{aligned} \quad (23)$$

The conductivity of the Armco iron was calculated by the same equation with the iron substituted for the lithium. Attempts to use the heat input from the main heater as determined from voltage-amperage measurements to calculate the conductivity were not successful (using this method the conductivity of the iron was 100 per cent higher than reference values).

Four determinations of the conductivity of molten lithium from 420 to 1002°F were made and are plotted in Figure 16 in Chapter VI. A leak in the sample container developed while heating to 1200°F, preventing further determinations. Since each determination required five days of adjustment and 12 to 20 hr at equilibrium conditions, the container had been in contact with the molten lithium for 20 days before the leak occurred. Examination after disassembly showed that considerable grain-boundary corrosion had occurred throughout the container.

In calculating the conductivity of lithium, not all of the test piece thermocouple readings could be used since half of them were damaged during assembly of the apparatus. In addition, two of the remaining thermocouples were considered in error and not used.

Two determinations of the conductivity of Armco iron were made at 424 and 944°F and found to be 10 per cent below reference values.<sup>26</sup> No additional details on the calibration results were given.

As can be seen from Figure 16, the results of Webber, et al., at the higher temperatures are in significant disagreement with the data of all other observers. This is surprising considering (1) that their experimental techniques appeared adequate, (2) that their results are in general agreement with other measurements below 500°F, and (3) that their comparative, axial-heat-flow apparatus was calibrated using Armco iron. However,

several situations may have caused the disagreement. First, the lithium apparently dissolved large amounts of the Armco iron sample container, and this added impurity could have gradually reduced the conductivity of the sample. Second, Sauereisen cement was used to electrically insulate their thermocouples within the heated region of the apparatus. It is now known that the electrical resistivity of Sauereisen cement decreases sharply at temperatures above 750°F, which could have affected their thermocouple readings. Finally, considering the long period of time (20 days) required to obtain their measurements, the Chromel-Alumel thermocouples could have gradually drifted away from calibration.

Determinations by Nikolskii, et al.<sup>2,37</sup> A slightly different approach - called the method of successive stationary states - was used by Nikolskii, et al., to determine the thermal conductivity of molten lithium. Their method was essentially an absolute, axial-heat-flow apparatus operated in a vacuum with a coaxial radiation shield but no compensating guard heating. To account for the radial heat flow, two successive steady-state determinations were made with two slightly different axial temperature gradients and at essentially the same sample temperature. Thus the conductivity of the lithium sample, disregarding the effect of a finite container wall thickness, was calculated as:

$$k = \frac{Q_2 \lambda - Q_1}{A [(\Delta t/\Delta x)_2 \lambda - (\Delta t/\Delta x)_1]} , \quad (24)$$

at

$$t = \frac{t_2 (\Delta t/\Delta x)_2 \lambda - t_1 (\Delta t/\Delta x)_1}{(\Delta t/\Delta x)_2 \lambda - (\Delta t/\Delta x)_1} , \quad (25)$$

where

$$\lambda = \frac{Q_{R_1}}{Q_{R_2}} = \frac{\epsilon_1}{\epsilon_2} \frac{\int_0^x (T_{\text{Tube}}^4 - T_{\text{Shield}}^4)_1 dx}{\int_0^x (T_{\text{Tube}}^4 - T_{\text{Shield}}^4)_2 dx}, \quad (26)$$

and where the subscripts 1 and 2 refer to the two successive stationary states. Assuming that the emissivity of the surfaces of the container tube and shield did not vary between the two successive steady states, its influence on Equations (24) and (25) would be canceled by Equation (26).

The apparatus used by Nikolskii, et al., is shown in Figure 21. The lithium sample was contained in a 0.55-in.-dia  $\times$  8-in.-long stainless steel tube (wall thickness not specified) which was sealed by plugs at both ends. The upper plug was welded to the tube and had a 0.15-in.-dia  $\times$  0.788-in.-deep cavity in which the main heater was placed. The lower plug was sealed at the lower edge of the container tube by brazing and had two holes drilled through it. One hole was for evacuating the tube cavity and the other for filling the cavity with lithium (chemical analysis not specified) from a vessel containing the molten lithium under a layer of paraffin.

A thin-walled radiation shield (0.039 in. thick) of Armco iron which was fastened to the cooling jacket surrounded the container tube with an annular spacing of 0.118 in. The shield was heated by an electrical heater of molybdenum wire which was enclosed in single-channel, porcelain tubes. These tubes (22 pieces with a diameter of 0.138 in.) were arranged around the shield with a clearance of 0.012 in. The entire apparatus was placed under a quartz vessel in which a vacuum of the order

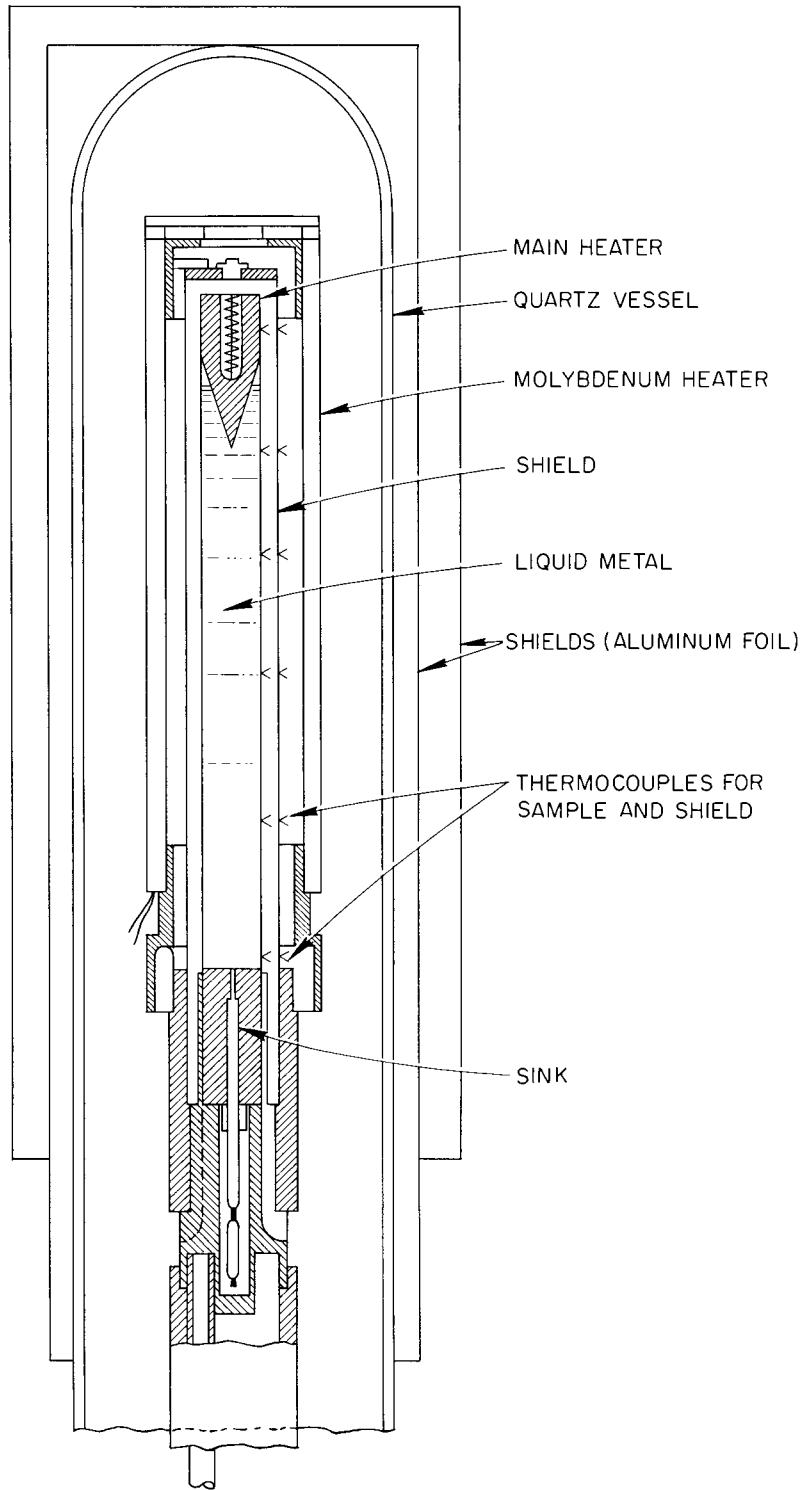
UNCLASSIFIED  
ORNL-LR-DWG 70822

Figure 21. Thermal Conductivity Apparatus Used by Nikolskii, et al.

of  $4 \times 10^{-3}$  mm of Hg was maintained. Aluminum foil shields were placed around the exterior of the quartz vessel.

Thermocouples made of nichrome and constantan wires with diameters of 0.006 and 0.007 in., respectively, were arc welded to the walls of the container tube and the coaxial shield. The container tube and shield thermocouples were arranged opposite to each other at intervals of 1.380 in. along the length of the container tube. The thermocouple wires were enclosed in twin-bore 0.047-in.-dia porcelain tubes which were uniformly distributed along the container tube and shield. The emf measurements were made with a type-K Leeds and Northrup potentiometer.

The main heater in the upper plug of the container tube was made of 0.004-in.-dia nichrome wire. The current measurement for this heater was made by a multivoltmeter with a 0.3 to 0.75 amp shunt. The voltage drop was measured by a voltage divider on a type-K Leeds and Northrup potentiometer. The power supplied by the main heater varied from 10 to 17 Btu/hr.

Seventy-four determinations of the thermal conductivities of molten lithium were made from 460 to 1364°F. A least-squares line through their data points showed that the thermal conductivity of molten lithium remained almost constant with temperature, varying from 27.0 Btu/hr.ft.°F at 600°F to 28.1 at 1350°F. The data scatter was such (see Figure 17 in Chapter VI) that 10 per cent of their data points deviated more than ±10 per cent from the mean least-squares line, 20 per cent more than ±8 per cent, and 40 per cent more than ±5 per cent.

At least two features of the method by Nikolskii, et al., are questionable and may account for their data for molten lithium having a large

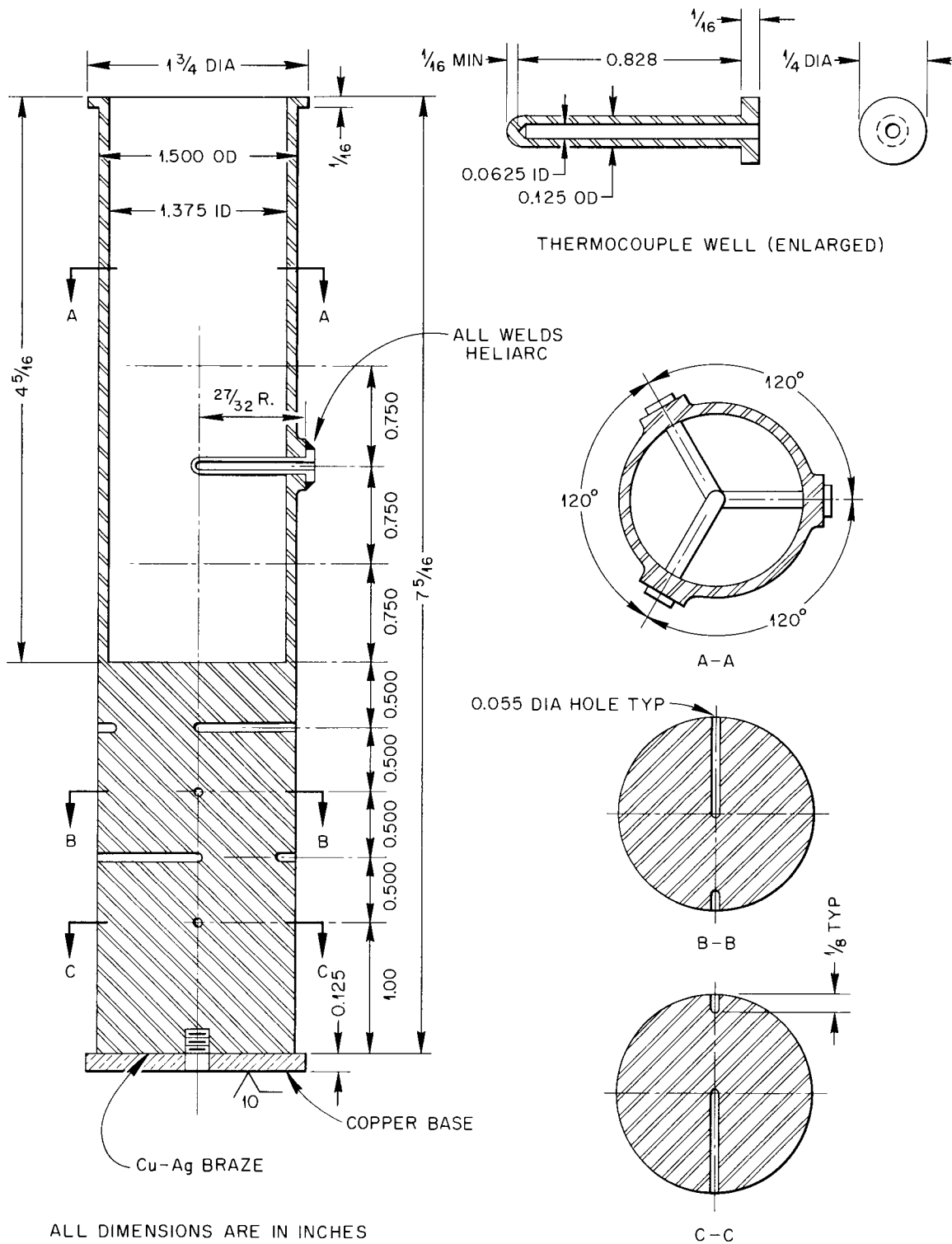
scatter and being 17 per cent below the present data at 1400°F. First, their method of filling their apparatus by siphoning from a pool of molten lithium protected only by a surface layer of paraffin was crude, and, in the absence of a chemical analysis report, there is reason to doubt the purity of their sample. Second, the basic assumption of their method is that the emissivity of both the container tube and the shield surface must remain uniform and constant between successive stationary states. However, Richman and Harrison<sup>30</sup> have shown that the variations of emissivity of Inconel and stainless steel with time and temperature are very erratic even under controlled conditions and pressures of the order of  $10^{-5}$  mm of Hg. Their results for Inconel in a vacuum of  $4 \times 10^{-5}$  mm of Hg showed that the emissivity increased from 0.535 to 0.615 in 1.5 hr at 1050°F and decreased from 0.735 to 0.565 in 2.5 hr at 1475°F. Dushman<sup>38</sup> also states that even at as low a pressure as  $10^{-9}$  mm of Hg and at room temperatures 10 per cent of a surface can be covered by a layer of oxygen molecules in about 3.8 minutes. Either impurities in the sample or a change of emissivity with time could have caused the thermal conductivity values for molten lithium by Nikolskii, et al., to be too low, especially at high temperatures.

It is interesting to note that their results for the conductivity of sodium and potassium, using the same method and equipment as for lithium, are 5 and 12 per cent, respectively, below the data of Ewing, et al.,<sup>25</sup> at 1000°F.

## B. ADDITIONAL DETAILS OF THE DESIGN OF THE APPARATUS

Sufficient detail is given in this section of the Appendix that the test piece, guard tube, guard heaters, and certain other experimental equipment can be duplicated if so desired.

The test piece (consisting of the lower heat meter, sample container, upper heat meter, and expansion tank) is shown in detail in Figures 22 and 23. No rigorous arguments can be given for the particular size and shape selected for the test piece; however, their selection was not completely arbitrary. As can be seen in Appendix D, the geometry of the apparatus has considerable effect upon the accuracy of the conductivity determination. However, in most cases the considerations of gross size, corrosion, high-temperature strength, etc., limited how far the apparatus could be developed to improve accuracy. Most of the effort was centered on minimizing the radial heat flow since the heat-transfer model was one dimensional. Selecting a test piece cylinder with a very small  $L/D$  ratio would accomplish this. However, reducing the  $L/D$  ratio must be compromised with two other factors. First, increasing the diameter of the test piece would of necessity increase the diameter of the application of guard heat. This would in turn increase the system power and cooling requirements and the quantity of precious and semiprecious heater wire. Second, decreasing the length of the apparatus would decrease the number and the spacing of the thermocouples which would increase the uncertainty of the temperature gradient measurement. In addition, the over-all test piece size was limited by the volume which could be conveniently maintained at a low pressure with the vacuum system.



ALL DIMENSIONS ARE IN INCHES

Figure 22. Details of Lower Heat Meter and Sample Container.

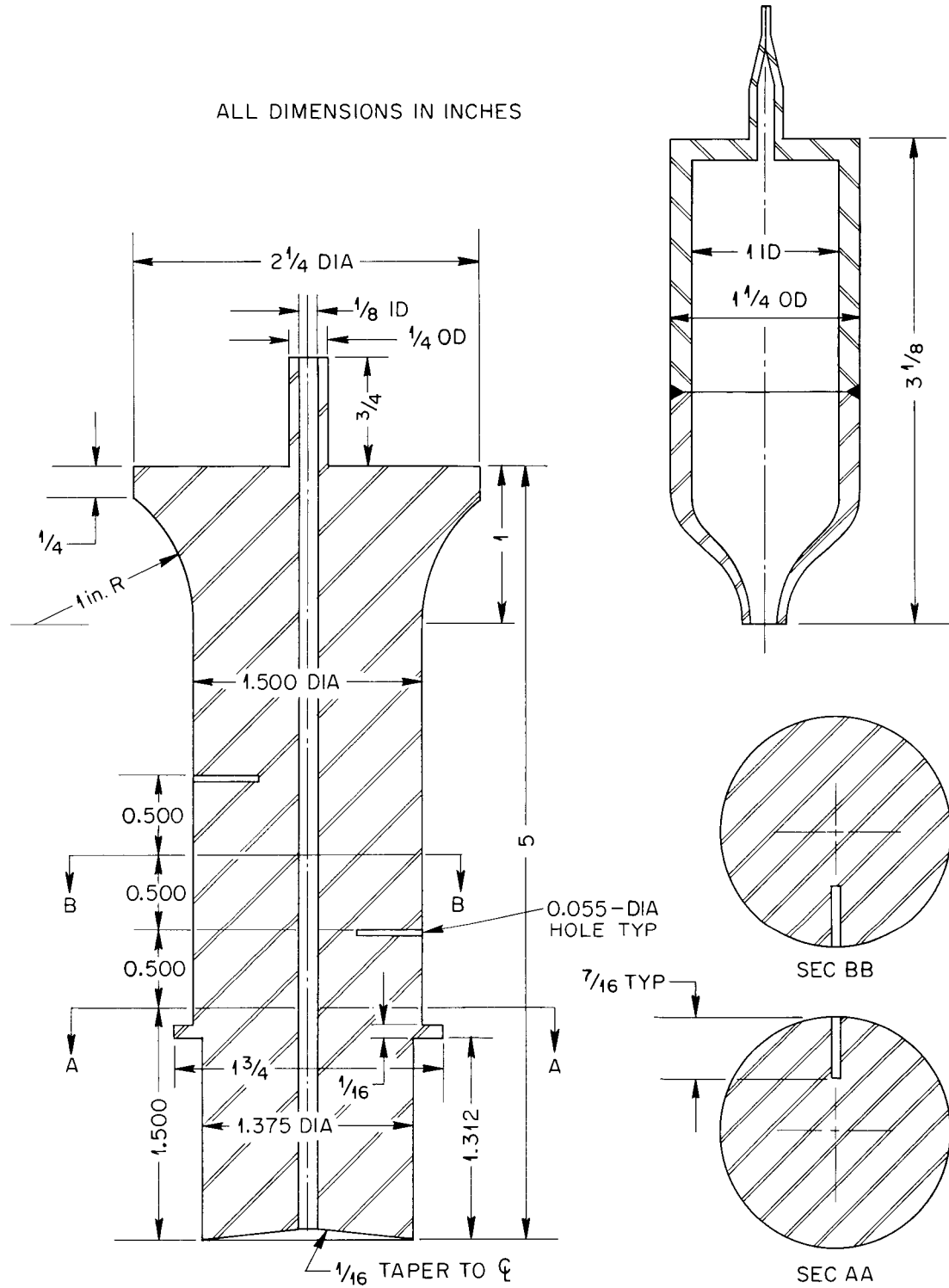


Figure 23. Details of Upper Heat Meter and Expansion Tank.

Another factor in the geometry of the test piece which influences the accuracy of the thermal conductivity determination is the wall thickness of the sample cavity. The thinner the wall the less likely that the accuracy of the determination would be affected. However, due to the severe corrosive nature of molten lithium and to the strength requirements placed on the type 347 stainless steel at 1500°F, 0.065 in. was considered to be a minimum desirable wall thickness. In addition, the cavity wall was required to support the three thermowells.

Thermowells were used in the liquid sample in place of the more usual procedure of peening the thermocouple beads to the exterior of the sample cavity wall. Although the thermowells probably had a slight and essentially unpredictable perturbation on the heat flow through the sample region, this was outweighed by the advantage of measuring centerline temperatures.

The method first considered for filling the test piece was to pour molten lithium into the sample cavity and then to weld the upper and lower parts of the test piece together. As there was a danger of contaminating this weld with lithium vapor, the upper heat meter was separated a greater distance away from the sample region than the lower heat meter. Since the fill procedure actually used (see Chapter IV) was so successful, any future test piece will be constructed with the upper heat meter as close to the sample region as the lower heat meter.

There was also concern that the heat flow pattern into the sink might influence the temperature reading of the first few thermocouples of the lower heat meter. This was checked by electrical analogy using a conductive-sheet model. Although the model design had all the heat flowing

radially out through the heat sink from the test piece, instead of axially, the effect upon the nearest temperature readings (thermocouples 22 and 32) in the lower heat meter was found to be negligible.

Details of the coaxial guard tube are shown in Figure 24. The nominal 3-in. diameter of the guard tube was chosen to provide enough insulation thickness that a mismatch of approximately  $10^{\circ}\text{F}$  in the test piece-guard tube temperatures was required to cause the radial heat loss to exceed 1 per cent of the axial heat flow. Both the test piece and guard tube were clamped to the sink heater plate as described in Chapter III. During operation these three pieces self-welded together and were forced apart during disassembly. The area of self-welding between the upper surfaces was found by inspection to be uniform and to include at least 80 per cent of the total contact surface area.

Details of the guard heaters and main heater are shown in Figure 25. The diameters of the guard heater cylinder and furnace (5 and 10 in.) were selected with respect to the test piece and guard tube diameters (1.5 and 3.0 in.) to provide approximately equal resistances to radial heat flow across the three insulated regions of the apparatus. Threads (10 per in.) were machined along the Alundum cylinder with a diamond cutter. Tantalum heater wire was wound around the cylinder in these threads, and a uniform,  $1/8$ -in.-thick coating of Alundum cement applied over the cylinder. Considerable care was taken in beginning and ending each heater section so that over-all circumferential symmetry was maintained.

The most important experimental equipment used in the present investigation is listed in Table V. Model and serial numbers, capacities, accuracies, and least counts are given when known or applicable.

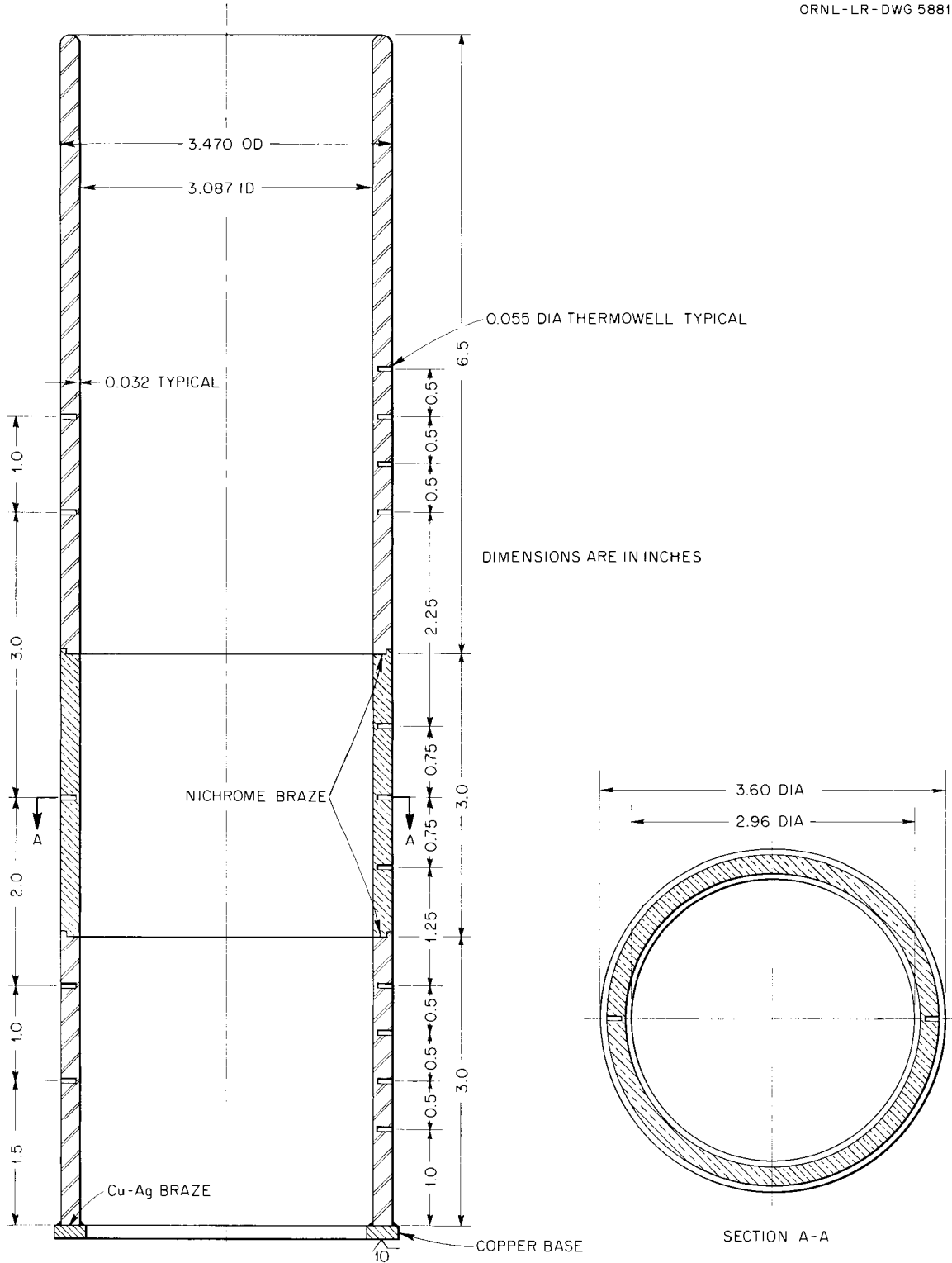


Figure 24. Details of Coaxial Guard Tube.

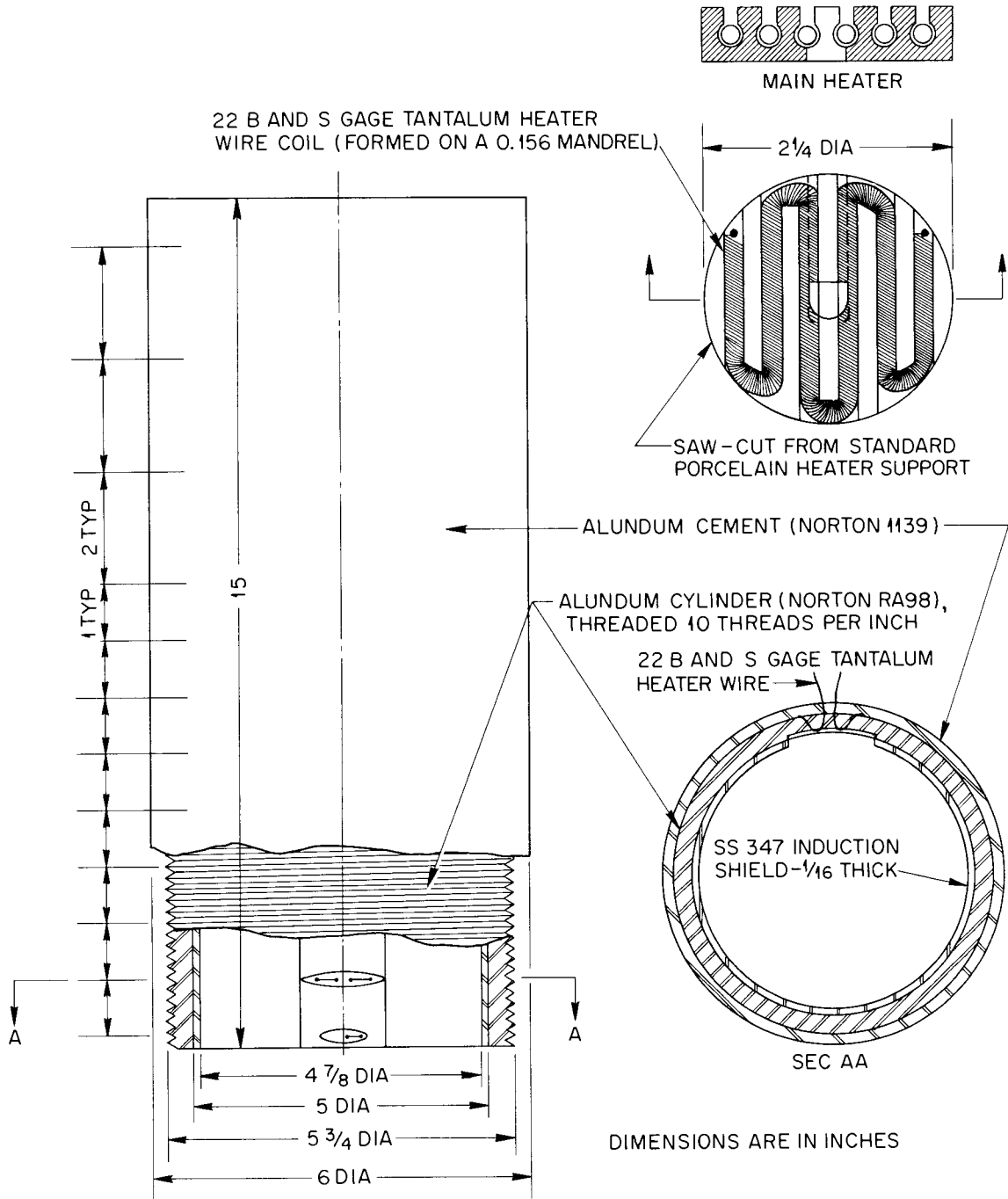


Figure 25. Details of Guard Heaters and Main Heater.

Table V. List of Experimental Equipment Used with Capacities, Ranges, and Accuracies Given When Known

Equipment	Capacity or Range	Accuracy	Least Count
<b>Potentiometer</b>			
L&N 7553 Type K-3, Serial No. 1562629	0-1.611 v	$\pm(0.01\% \pm 20 \mu\text{v})$	50.0 $\mu\text{v}$
Mfg.: Leeds & Northrup Co.	0-0.1611 v	$\pm(0.015\% \pm 2 \mu\text{v})$	5.0 $\mu\text{v}$
	0-0.01611 v	$\pm(0.015\% \pm 0.5 \mu\text{v})$	0.5 $\mu\text{v}$
<b>Null Detector</b>			
L&N 9835-A d-c $\mu\text{v}$ Amplifier	-25 to +25 $\mu\text{v}$	Inherently Stable Zero	1.0 $\mu\text{v}$ (Sensitivity 0.25 $\mu\text{v}$ )
Mfg.: Leeds & Northrup Co.			
<b>Recorder</b>			
Brown, twelve point, Serial No. 5210	0-3000 $\mu\text{v}$	$\pm 45 \mu\text{v}$	10 $\mu\text{v}$
Mfg.: Minneapolis-Honeywell Corp.			
<b>Thermocouples</b>			
0.010-in.-dia Pt/90Pt+10Rh Wires	-	(Uncalibrated $\pm 3^\circ\text{F}$ 0-2000°F)	-
Mfg.: Thermo Electric Co.			
<b>Standard Cell</b>			
Mercury Type, Serial No. 690101	-	-	-
Mfg.: Eppley Laboratory Inc.			
<b>Constant Voltage Transformer</b>			
Type CU-1	2 kva	$\pm 1\%$	-
Mfg.: Sola Electric Co.		(95-125 v)	
<b>Voltmeter</b>			
VOM Meter, Model 260 III	10 v	$\pm 5\%$ of full scale	0.2 v
Mfg.: Simpson Electric Co.	50 v		1.0 v
	250 v		5.0 v
<b>Ammeter</b>			
Panel Meter, Model 476	0-10 amps	$\pm 2\%$	0.2 amps
Mfg.: Weston Electric Co.			
<b>Voltage Adjustments</b>			
Variac	20 amp, 0-100 v	-	0.6 v
Mfg.: General Radio Co.	10 amp, 0-15 v	-	0.07 v
<b>Vacuum System</b>			
Model 31-0121 Evaporator,	-	-	-
18-in.-od X 30-in.-high Bell Jar	-	-	-
Ion Gauge Type 05-0700,	$10^{-3}$ to $10^{-6}$ mm Hg	-	-
TC Gauge Type 05-0100	1 to $10^{-3}$ mm Hg	-	-
Mfg.: National Research Corp.			
	<u>Speed</u>		<u>Blank-Off Pressure</u>
4-in.-dia H-4-P Oil Diffusion Pump	350 liters/sec		$2 \times 10^{-6}$ mm Hg
Mfg.: National Research Corp.	@ $1 \times 10^{-4}$ mm Hg		
Fore Pump, Type VSO	12.5 cfm		$2 \times 10^{-4}$ mm Hg
Mfg.: Kinney Mfg. Co.	@ $1 \times 10^{-2}$ mm Hg		

## C. EXPERIMENTAL DATA AND CALCULATIONS

The uncorrected, "as read", experimental thermocouple emfs, heater amperages and voltages, cooling water flow rates, and system pressures are tabulated in Table VI. The temperature measurements, after conversion and correction, and the calculated heater powers and cooling water flow rates are tabulated in Table VII. Tabulated in Table VIII are the critical "as built" dimensions of the apparatus.

The thermocouple emfs were converted to degrees Fahrenheit using individual curves obtained from the initial thermocouple calibrations. An additional minor correction in the temperature conversion was made to account for the nonsteady state and the noninstantaneous recording of the temperature data. Assuming that each thermocouple emf was changing at the same rate and that the emfs were read at equal increments of time, this correction was made by reading the thermocouple emfs in the order shown in Table VI and then prorating any temperature change in the initial and final recording of thermocouple No. 2 to each of the other thermocouple readings.

The data from runs 1 through 3 were used to determine the position of the thermocouple junctions along the test piece as described in Chapter II. A summary of the results of these calculations are tabulated in Table III. The thermal conductivity of the lithium sample was calculated from the data of runs 1 through 8 as described in Chapter II. For runs 9 through 14, the method of calculating the temperature gradient in the sample region was modified as described in Chapter V. A sample of these calculations using the experimental data from run 1 is given below. Although some of the corrections could have been neglected, their values were left

Table VI. Uncorrected Experimental Data

Run No. →	1	2	3	4	5	6	7	8	9	10	11	12	13	14
Date →	1/20/61	1/21/61	1/23/61	1/24/61	1/25/61	1/25/61	1/27/61	1/27/61	1/30/61	1/30/61	2/1/61	2/1/61	2/1/61	2/3/61
Time Began →	7:02 pm	10:56 am	9:29 am	6:48 pm	9:30 am	3:25 pm	9:17 am	3:17 pm	1:15 pm	6:40 pm	9:37 am	3:41 pm	10:00 pm	8:28 am
TC No.	← emf (mv) →													
1	5.590	5.544	5.887	6.324	6.280	6.302	7.293	7.293	8.369	8.447	9.406	9.440	9.426	10.736
2	3.548	3.528	3.779	4.332	4.294	4.304	5.277	5.290	6.459	6.510	7.715	7.763	7.682	8.890
3	3.488	3.478	3.592	4.318	4.291	4.292	5.272	5.283	6.445	6.503	7.701	7.737	7.601	8.446
4	3.436	3.418	3.656	4.187	4.154	4.161	5.104	5.112	6.259	6.306	7.516	7.559	7.474	8.693
5	3.409	3.400	3.507	4.184	4.157	4.155	5.095	5.105	6.261	6.312	7.546	7.577	7.431	8.707
6	3.324	3.307	3.528	4.045	4.008	4.016	4.921	4.931	6.057	6.101	7.313	7.356	7.268	8.488
7	3.329	3.318	3.421	4.055	4.033	4.028	4.924	4.935	6.082	6.130	7.384	7.412	7.258	8.557
8	3.218	3.201	3.410	3.909	3.872	3.879	4.748	4.760	5.862	5.903	7.115	7.156	7.063	8.291
9	3.212	3.200	3.303	3.902	3.877	3.878	4.734	4.745	5.873	5.916	7.166	7.195	7.034	8.347
10	2.796	2.779	2.940	3.365	3.329	3.330	4.073	4.083	5.148	5.175	6.388	6.423	6.323	7.555
11	2.843	2.827	2.919	3.384	3.355	3.353	4.066	4.076	5.136	5.161	6.377	6.408	6.231	7.538
12	2.723	2.708	2.860	3.271	3.235	3.237	3.954	3.963	5.042	5.065	6.262	6.294	6.193	7.410
13	2.774	2.759	2.848	3.298	3.269	3.267	3.960	3.968	5.008	5.033	6.240	6.269	6.098	7.386
14	2.647	2.630	2.775	3.170	3.134	3.137	3.827	3.839	4.864	4.888	6.080	6.112	6.012	7.230
15	2.709	2.694	2.782	3.209	3.180	3.178	3.844	3.854	4.879	4.901	6.093	6.128	5.955	7.235
16	2.448	2.431	2.557	2.914	2.880	2.881	3.507	3.519	4.504	4.522	5.714	5.742	5.652	6.876
17	2.517	2.501	2.583	2.961	2.931	2.930	3.537	3.548	4.533	4.544	5.748	5.775	5.616	6.867
18	2.331	2.315	2.431	2.761	2.730	2.730	3.319	3.332	4.294	4.306	5.502	5.527	5.441	6.663
19	2.420	2.405	2.479	2.820	2.792	2.790	3.356	3.366	4.321	4.333	5.516	5.543	5.387	6.640
20	2.216	2.201	2.305	2.617	2.582	2.581	3.136	3.147	4.085	4.095	5.292	5.317	5.239	6.463
21	2.283	2.270	2.341	2.656	2.627	2.623	3.162	3.170	4.110	4.116	5.319	5.342	5.195	6.448
22	2.105	2.092	2.185	2.472	2.439	2.438	2.956	2.967	3.879	3.886	5.086	5.109	5.038	6.269
23	2.119	2.108	2.174	2.470	2.443	2.440	2.948	2.955	3.885	3.887	5.121	5.136	5.010	6.269
24	2.260	2.246	2.321	2.644	2.615	2.611	3.153	3.163	4.127	4.138	5.432	5.452	5.246	6.498
25	2.503	2.490	2.569	2.944	2.914	2.912	3.519	3.525	4.513	4.530	5.753	5.778	5.593	6.827
26	2.771	2.757	2.845	3.289	3.263	3.258	3.946	3.958	4.997	5.022	6.234	6.262	6.078	7.355
27	3.215	3.204	3.298	3.905	3.878	3.877	4.739	4.748	5.880	5.928	7.180	7.199	7.035	8.337
28	3.398	3.391	3.492	4.181	4.155	4.153	5.098	5.108	6.271	6.332	7.571	7.588	7.442	out
29	2.446	2.433	2.557	2.910	2.881	2.881	3.511	3.514	4.503	4.520	5.715	5.735	5.644	6.861
30	2.334	2.322	2.432	2.765	2.734	2.734	3.326	3.336	4.297	4.313	5.510	5.535	5.445	6.670
31	2.213	2.202	2.299	2.611	2.579	2.578	3.132	3.140	4.079	4.091	5.292	5.316	5.231	6.465
32	2.105	2.093	2.182	2.471	2.439	2.436	2.955	2.964	3.877	3.886	5.088	5.110	5.035	6.259
2 (Reread)	3.546	3.529	5.877	4.328	4.293	4.303	5.279	5.290	6.454	6.510	7.732	7.763	7.678	8.891
10 (Reread)	2.794	2.799	2.936	3.362	3.329	3.330	4.069	4.083	5.146	5.175	6.396	6.424	6.320	7.556
Time Finish →	7:23 pm	11:17 am	10:05 am	7:14 pm	9:58 am	3:58 pm	9:41 am	3:40 pm	1:38 pm	7:03 pm	10:00 am	4:04 pm	10:21 pm	8:45 am

Table VI. (continued)

Run No. →		1	2	3	4	5	6	7	8	9	10	11	12	13	14
Heater No.															
G-1	volts	26.2	24.3	0.0	47.0	48.5	48.0	61.0	59.0	54.0	54.0	0.0	0.0	0.0	0.0
	amps	2.3	2.2	0.0	3.6	3.6	3.6	4.0	4.0	3.6	3.6	0.0	0.0	0.0	0.0
G-2	volts	0.0	2.5	30.0	10.0	13.0	13.0	20.2	19.5	41.5	42.2	80.0	86.0	85.0	92.0
	amps	0.0	0.2	2.7	0.8	0.8	0.8	1.0	1.0	2.5	2.8	4.2	4.5	4.4	4.8
G-3	volts	0.0	0.0	0.0	0.0	0.0	0.0	0.0	0.0	16.1	14.9	25.5	19.2	19.0	34.0
	amps	0.0	0.0	0.0	0.0	0.0	0.0	0.0	0.0	0.7	0.5	1.3	0.8	0.8	1.8
G-4	volts	0.0	0.0	0.0	0.0	0.0	0.0	0.0	0.0	6.5	6.0	9.5	9.0	9.0	12.3
	amps	0.0	0.0	0.0	0.0	0.0	0.0	0.0	0.0	0.4	0.4	0.8	0.8	0.8	1.1
G-5	volts	0.0	0.0	0.0	0.0	0.0	0.0	0.0	0.0	5.0	6.0	7.0	8.5	8.5	11.0
	amps	0.0	0.0	0.0	0.0	0.0	0.0	0.0	0.0	0.3	0.4	0.5	0.7	0.7	1.0
G-6	volts	0.0	0.0	0.0	0.0	0.0	0.0	0.0	0.0	4.8	5.1	5.1	7.8	7.6	9.5
	amps	0.0	0.0	0.0	0.0	0.0	0.0	0.0	0.0	0.3	0.4	0.3	0.7	0.7	0.8
G-7	volts	0.0	0.0	0.0	0.0	0.0	0.0	0.0	0.0	4.1	4.3	0.0	0.0	0.0	0.0
	amps	0.0	0.0	0.0	0.0	0.0	0.0	0.0	0.0	0.2	0.2	0.0	0.0	0.0	0.0
G-8	volts	0.0	0.0	0.0	0.0	0.0	0.0	0.0	0.0	2.8	0.0	0.0	0.0	0.0	0.0
	amps	0.0	0.0	0.0	0.0	0.0	0.0	0.0	0.0	0.2	0.0	0.0	0.0	0.0	0.0
G-9	volts	0.0	0.0	0.0	0.0	0.0	0.0	0.0	0.0	3.1	0.0	0.0	0.0	0.0	0.0
	amps	0.0	0.0	0.0	0.0	0.0	0.0	0.0	0.0	0.2	0.0	0.0	0.0	0.0	0.0
G-10	volts	0.0	0.0	0.0	0.0	0.0	0.0	0.0	0.0	2.7	0.0	0.0	0.0	0.0	0.0
	amps	0.0	0.0	0.0	0.0	0.0	0.0	0.0	0.0	0.1	0.0	0.0	0.0	0.0	0.0
Main	volts	11.1	10.8	12.0	15.0	16.0	16.2	20.0	19.5	24.0	24.0	27.0	27.0	27.0	29.8
	amps	2.4	2.3	2.7	2.6	2.6	2.6	2.8	2.8	2.9	3.0	3.2	3.1	3.1	3.3
Sink	volts	0.0	0.0	0.0	0.0	0.0	0.0	36.4	36.0	24.2	24.8	27.5	27.5	27.0	34.0
	amps	0.0	0.0	0.0	0.0	0.0	0.0	1.8	1.8	1.2	1.2	1.5	1.4	1.4	2.0
Upper Left	volts	0.0	0.0	0.0	0.0	0.0	0.0	0.0	0.0	0.0	0.0	0.0	0.0	0.0	10.8
	amps	0.0	0.0	0.0	0.0	0.0	0.0	0.0	0.0	0.0	0.0	0.0	0.0	0.0	1.0
Upper Right	volts	0.0	0.0	0.0	0.0	0.0	0.0	0.0	0.0	0.0	0.0	0.0	0.0	0.0	10.6
	amps	0.0	0.0	0.0	0.0	0.0	0.0	0.0	0.0	0.0	0.0	0.0	0.0	0.0	1.0
Lower Left	volts	0.0	0.0	0.0	0.0	0.0	0.0	0.0	0.0	0.0	0.0	0.0	0.0	0.0	37.8
	amps	0.0	0.0	0.0	0.0	0.0	0.0	0.0	0.0	0.0	0.0	0.0	0.0	0.0	7.5
Lower Right	volts	0.0	0.0	0.0	0.0	0.0	0.0	0.0	0.0	0.0	0.0	0.0	0.0	0.0	37.2
	amps	0.0	0.0	0.0	0.0	0.0	0.0	0.0	0.0	0.0	0.0	0.0	0.0	0.0	7.6
Top	volts	0.0	0.0	0.0	0.0	0.0	0.0	0.0	0.0	0.0	0.0	26.6	27.0	27.0	55.0
	amps	0.0	0.0	0.0	0.0	0.0	0.0	0.0	0.0	0.0	0.0	0.7	0.8	0.8	2.2

Table VI. (Continued)

Run No. →	1	2	3	4	5	6	7	8	9	10	11	12	13	14
Sink Coolant No. 1:														
Flow Rate (lb/hr)	-	-	-	-	407.00	387.90	-	2.30	2.19	2.90	off	off	off	off
Temp. Inlet (°F) <sup>a</sup>	-	-	-	44.30	43.70	43.22	-	42.62	42.87	42.80	-	-	-	-
Temp. Outlet (°F) <sup>a</sup>	-	-	-	44.44	43.84	43.36	-	65.26	67.38	67.31	-	-	-	-
Sink Coolant No. 2:														
Flow Rate (lb/hr)	-	-	-	-	445.50	438.70	446.00	457.00	469.00	391.00	391.00	365.30	360.20	357.70
Temp. Inlet (°F) <sup>a</sup>	-	-	-	44.30	43.70	43.22	42.98	42.62	42.87	42.80	43.15	42.98	42.87	43.70
Temp. Outlet (°F) <sup>a</sup>	-	-	-	-	44.66	43.58	43.21	43.30	43.81	42.98	44.24	44.24	44.12	45.32
Vacuum (10 <sup>-3</sup> mm of Hg):														
Pressure	-	0.04	-	0.05	0.03	0.03	0.03	0.04	0.05	0.04	0.05	0.08	0.06	0.10

<sup>a</sup>Water temperatures were measured with uncalibrated thermometers marked with graduations every 0.1°F.

Table VII. Corrected Experimental Data

Run No. →	1	2	3	4	5	6	7	8	9	10	11	12	13	14
Date →	1/20/61	1/21/61	1/23/61	1/24/61	1/25/61	1/25/61	1/27/61	1/27/61	1/30/61	1/30/61	2/1/61	2/1/61	2/1/61	2/3/61
Time Began →	7:02 pm	10:56 am	9:29 am	6:48 pm	9:30 am	3:25 pm	9:17 am	3:17 pm	1:15 pm	6:40 pm	9:37 am	3:41 pm	10:00 am	8:28 am
TC No.	← Temperature (°F) →													
1	1176.97	1169.65	1228.69	1303.8	1296.3	1300.0	1467.1	1467.1	1643.2	1655.7	1807.5	1812.9	1810.7	2011.2
2	809.28	805.57	852.24	953.6	946.7	948.5	1122.5	1124.9	1327.2	1335.9	1537.1	1544.9	1531.6	1726.6
3	797.32	795.42	816.66	950.3	945.3	945.5	1121.1	1123.0	1323.8	1333.6	1533.4	1539.5	1517.0	1718.1
4	788.32	784.80	829.49	927.2	921.2	922.5	1092.1	1093.4	1293.0	1301.0	1504.3	1511.5	1497.5	1695.4
5	782.55	780.80	801.09	926.0	921.0	920.6	1089.7	1091.4	1292.5	1301.2	1508.4	1513.7	1489.5	1696.9
6	767.31	764.09	805.60	901.2	894.3	895.8	1059.4	1061.2	1258.0	1265.5	1469.7	1477.2	1462.6	1662.0
7	768.36	766.13	785.73	903.4	898.9	898.4	1060.4	1062.2	1262.5	1270.7	1481.9	1486.6	1461.2	1673.2
8	747.47	744.10	783.89	876.9	870.0	871.2	1029.4	1031.3	1225.1	1232.2	1437.8	1444.9	1429.5	1631.2
9	746.84	744.41	764.28	875.9	871.0	871.2	1026.9	1028.7	1226.8	1234.1	1445.7	1450.9	1424.2	1639.8
10	666.72	663.32	694.58	775.0	768.0	768.1	906.8	908.4	1100.5	1105.2	1314.9	1321.3	1304.5	1510.5
11	675.87	672.65	690.64	778.8	773.2	772.8	905.5	907.0	1097.9	1102.1	1312.7	1318.5	1288.4	1507.8
12	651.92	648.76	678.42	756.6	749.6	750.0	884.0	885.4	1080.3	1084.1	1292.7	1297.8	1280.7	1485.9
13	661.84	658.77	676.24	761.9	756.2	755.8	885.1	886.3	1074.4	1078.6	1288.4	1293.9	1265.0	1482.1
14	637.77	634.23	662.75	738.2	731.0	731.6	861.6	863.3	1049.6	1053.6	1261.5	1267.7	1250.8	1456.2
15	649.97	646.87	664.22	745.7	740.0	739.6	864.8	866.3	1052.5	1056.3	1263.7	1270.4	1241.1	1456.7
16	598.98	595.41	620.38	689.2	682.5	682.7	801.8	803.6	984.7	987.5	1197.3	1203.0	1187.6	1397.1
17	611.93	608.57	625.13	697.9	691.7	691.5	806.8	808.4	989.1	990.9	1203.2	1208.6	1181.4	1395.1
18	575.87	572.46	595.94	659.9	653.5	653.5	766.3	768.2	946.5	948.5	1160.6	1165.9	1151.3	1360.9
19	592.94	589.70	604.70	670.7	664.8	664.4	773.9	774.2	951.0	952.9	1162.4	1168.0	1141.1	1356.8
20	553.31	550.00	571.19	632.2	624.9	624.7	731.9	733.6	908.6	910.1	1123.7	1129.1	1115.8	1327.3
21	566.71	563.84	578.39	639.8	633.8	633.0	737.0	737.9	913.3	914.1	1128.7	1133.8	1108.4	1324.8
22	531.14	528.20	547.56	604.2	597.3	597.1	697.9	699.5	871.1	872.2	1087.9	1093.0	1081.0	1294.7
23	533.66	531.10	544.99	603.2	597.5	596.9	696.1	696.8	872.5	872.6	1094.0	1097.9	1076.2	1294.8
24	561.47	558.30	573.87	637.1	630.9	630.2	735.7	736.9	915.7	917.4	1147.4	1152.2	1116.5	1332.6
25	609.44	606.55	622.70	695.0	688.6	688.2	803.9	804.3	986.2	988.8	1203.7	1209.3	1177.6	1388.4
26	662.49	659.38	677.10	561.6	756.0	755.1	884.5	886.0	1074.4	1078.5	1288.4	1293.4	1262.6	1477.1
27	747.12	744.68	763.36	875.9	870.3	870.1	1027.2	1028.0	1227.5	1235.4	1446.1	1450.8	1424.0	1637.5
28	780.96	779.20	799.12	926.4	920.6	920.3	1091.2	1092.1	1294.8	1304.6	1510.5	1514.8	1491.3	-
29	599.51	596.50	621.41	688.9	682.9	682.9	802.3	802.1	983.6	986.2	1197.2	1202.2	1186.9	1393.9
30	576.67	573.84	596.62	660.7	654.2	654.2	767.6	768.6	946.7	949.1	1160.6	1166.5	1151.4	1360.9
31	552.69	550.00	570.29	631.1	624.2	624.0	731.2	731.8	907.1	909.0	1122.8	1128.5	1114.3	1326.7
32	531.21	528.20	547.09	603.9	596.9	596.4	697.4	698.3	870.0	871.3	1086.3	1091.8	1079.3	1291.3
2 (reread)	808.91	805.76	-	953.6	946.5	947.3	1123.8	1124.9	1326.9	1335.9	1538.0	1544.9	1530.9	1726.8
10 (reread)	666.20	663.32	694.62	774.9	768.0	768.1	906.2	908.5	1100.5	1105.2	1315.0	1321.5	1303.3	1510.7
Time Finish →	7:23 pm	11:17 am	10:05 am	7:14 pm	9:58 am	3:58 pm	9:41 am	3:40 pm	1:38 pm	7:03 pm	10:10 am	4:04 pm	10:21 am	8:45 am

Table VII. (continued)

Run No. →	1	2	3	4	5	6	7	8	9	10	11	12	13	14
Heater No.	←————— Power (watts) <sup>a</sup> —————→													
G-1	60.0	53.5	0.0	166.9	172.2	170.4	244.0	236.0	196.6	191.8	0.0	0.0	0.0	0.0
G-2	0.0	0.5	81.0	8.0	10.4	10.4	20.2	19.5	102.9	118.9	336.0	387.0	374.0	441.6
G-3	0.0	0.0	0.0	0.0	0.0	0.0	0.0	1.5	11.5	7.5	31.9	15.4	15.2	61.2
G-4	0.0	0.0	0.0	0.0	0.0	0.0	0.0	0.0	2.6	2.4	7.6	6.8	7.2	13.5
G-5	0.0	0.0	0.0	0.0	0.0	0.0	0.0	0.0	1.5	2.4	3.5	6.0	6.0	11.0
G-6	0.0	0.0	0.0	0.0	0.0	0.0	0.0	0.0	1.4	2.0	1.5	5.5	5.3	7.6
G-7	0.0	0.0	0.0	0.0	0.0	0.0	0.0	0.0	0.8	0.9	0.0	0.0	0.0	0.0
G-8	0.0	0.0	0.0	0.0	0.0	0.0	0.0	0.0	0.6	0.0	0.0	0.0	0.0	0.0
G-9	0.0	0.0	0.0	0.0	0.0	0.0	0.0	0.0	0.6	0.0	0.0	0.0	0.0	0.0
G-10	0.0	0.0	0.0	0.0	0.0	0.0	0.0	0.0	0.3	0.0	0.0	0.0	0.0	0.0
Main	26.6	24.8	32.4	38.9	41.6	42.1	56.0	54.6	69.6	72.0	85.1	83.7	83.7	96.9
Sink	0.0	0.0	0.0	0.0	0.0	0.0	65.9	64.4	29.0	29.8	39.9	38.5	37.8	68.0
Upper Left	0.0	0.0	0.0	0.0	0.0	0.0	0.0	0.0	0.0	0.0	0.0	0.0	0.0	10.8
Upper Right	0.0	0.0	0.0	0.0	0.0	0.0	0.0	0.0	0.0	0.0	0.0	0.0	0.0	10.6
Lower Left	0.0	0.0	0.0	0.0	0.0	0.0	0.0	0.0	0.0	0.0	0.0	0.0	0.0	283.5
Lower Right	0.0	0.0	0.0	0.0	0.0	0.0	0.0	0.0	0.0	0.0	0.0	0.0	0.0	282.7
Top	0.0	0.0	0.0	0.0	0.0	0.0	0.0	0.0	0.0	0.0	18.6	20.3	20.3	121.0

<sup>a</sup>Power factor assumed to be unity.

Table VIII. Critical "As-Built" Dimensions of the Apparatus

Diameter of Upper Heat Meter		1.501 in.
Outside Diameter of Sample Container		1.496 in.
Inside Diameter of Sample Container		1.375 in.
Diameter of Lower Heat Meter		1.500 in.
Outside Diameter of Guard Tube		3.471 in.
Inside Diameter of Guard Tube		3.088 in.
Diameter of Thermocouple Wells:		
Both Heat Meters		0.0550 in.
Sample		0.0625 in.
Axial Distances <sup>a</sup> from base of Apparatus to:		
	<u>Test Piece</u>	<u>Guard Tube</u>
Main Heater	10.096 in.	
TC-2	9.103	TC-3 9.099 in.
TC-4	8.602	TC-5 8.602
		TC-28 8.604
TC-6	8.099	TC-7 8.101
TC-8	7.604	TC-9 7.608
		TC-27 7.600
Interface	6.044	Interface 6.047
TC-10	5.343 <sup>b</sup>	TC-11 5.367
TC-12	4.596 <sup>b</sup>	TC-13 4.620
		TC-26 4.588
TC-14	3.848 <sup>b</sup>	TC-15 3.865
Interface	3.142	Interface 3.144
TC-16	2.601 <sup>b</sup>	TC-17 2.606
TC-29	2.599	TC-25 2.589
TC-18	2.100 <sup>b</sup>	TC-19 2.104
TC-30	2.100	
TC-20	1.599 <sup>b</sup>	TC-21 1.605
TC-31	1.599	TC-24 1.589
TC-22	1.101 <sup>b</sup>	TC-23 1.103
TC-32	1.099	

<sup>a</sup>Except as noted, all thermocouple distances were measured to the centerline of the thermowell at the outside diameter of the test piece.

<sup>b</sup>These thermocouple distances were measured to the centerline of the thermowell at the bottom of the thermowell.

in the calculations to show the relative magnitude of their significance.

The radial heat exchange between the test piece and guard tube along the sample region of the test piece was calculated using Equation (19) in Chapter II as follows [for convenience, all the numeral subscripts in the following equations refer to thermocouple positions as shown in Figure 7 in Chapter III]:

$$\begin{aligned}(t_T - t_G) &= (\Delta t_{10-11} + \Delta t_{12-13} + \Delta t_{14-15})/3 = \\ &= (666.72 - 675.87) + (651.92 - 661.84) + \\ &+ (637.77 - 649.97)/3 = -10.42^\circ\text{F}\end{aligned}\quad (27)$$

$$t_{\text{avg}} = (t_{10} + t_{14})/2 = (666.72 + 637.77)/2 = 652.25^\circ\text{F}$$

$$k_I = 0.035 \text{ Btu/hr}\cdot\text{ft}\cdot^\circ\text{F at } t_{\text{avg}} \text{ [see Figure 31 in Appendix E]}$$

$$\begin{aligned}Q_R &= -2 \pi k_I (x_{10} - x_{14})(t_T - t_G)/\ln(D_T/D_G) = \\ &= \frac{-2 \pi (1.500)(0.045)(-10.42)}{(12)(0.743)} = 0.39 \text{ Btu/hr}\end{aligned}\quad (28)$$

The heat retained or released in the sample region of the test piece because of the transient heat capacity effect was calculated from Equation (20) in Chapter II as follows:

$$\left. \begin{aligned}\gamma_{\text{SS}} &= 485 \text{ lb/ft}^3 & ; & \gamma_{\text{Li}} = 30.9 \text{ lb/ft}^3 \\ c_{\text{pSS}} &= 0.125 \text{ Btu/lb}\cdot^\circ\text{F}; & c_{\text{pLi}} &= 1.013 \text{ Btu/lb}\cdot^\circ\text{F}\end{aligned} \right\} \text{ at } t_{\text{avg}} \text{ [see Figures 27 - 29 in Appendix E]}$$

$$\frac{A_W}{A_{Li}} = \frac{(D_o^2 - D_i^2)}{D_i^2} = \frac{(1.496)^2 - (1.375)^2}{(1.375)^2} = 0.1833 \quad (29)$$

$$\frac{\Delta t}{\Delta \theta} = \frac{t_2 \text{ (finish)} - t_2 \text{ (start)}}{\theta \text{ (finish)} - \theta \text{ (start)}} = \frac{3.546 - 3.548}{7:23 - 7:02} =$$

$$= -0.000095 \text{ mv/min} = -1.06^\circ\text{F/hr} \quad (30)$$

$$Q_\theta = -[(V \gamma c_p)_{ss} + (V \gamma c_p)_{Li}] \Delta t / \Delta \theta =$$

$$= \frac{-\pi D_i^2 (x_{10} - x_{14})}{4(1728)} \left[ \frac{A_W}{A_{Li}} (\gamma c_p)_{ss} + (\gamma c_p)_{Li} \right] \Delta t / \Delta \theta =$$

$$= \frac{-\pi (1.375)^2 (1.50)}{4 (1728)} [(0.1833)(485)(0.125) + (30.9)(1.013)] \times$$

$$\times (-1.06) = 0.06 \text{ Btu/hr} \quad (31)$$

The average axial heat flow along the test piece was calculated from the thermal conductivity and temperature gradient of the upper heat meter as follows:

$$t_2 - t_8 = (809.28 - 747.47) = 61.81^\circ\text{F}$$

$$(t_2 + t_8)/2 = 778.38^\circ\text{F}$$

$$k_{ss} = k_o (1 + \beta_{ss} t) = 7.78 [1 + 5.508 \times 10^{-4} (778.38)] =$$

$$= 11.116 \text{ Btu/hr}\cdot\text{ft}\cdot^\circ\text{F} \text{ [see Figure 30 in Appendix E]} \quad (32)$$

$$\begin{aligned}
 Q(x = x_{10}) &\cong Q(x = x_6) \cong \frac{\pi D_o^2 k_{ss} (t_2 - t_8)}{4 (x_2 - x_8)(12)} = \\
 &= \frac{(1.496)^2 (11.116)(61.81)}{(4)(12)(1.50)} = 67.60 \text{ Btu/hr} \quad (33)
 \end{aligned}$$

The axial heat flow along the test piece, at  $x = x_{14}$ , was calculated as follows:

$$\begin{aligned}
 Q(x = x_{14}) &= Q(x = x_{10}) + Q_R + Q_\theta = \\
 &= 67.60 + 0.39 + 0.06 = 68.05 \text{ Btu/hr} \quad (34)
 \end{aligned}$$

The coefficient "a" of Equation (14) in Chapter II was determined from Equation (18) as follows:

$$\alpha_{ss} = 11.5 \times 10^{-6} \text{ }^\circ\text{F}^{-1} \quad [\text{Assumed constant; see Figure 29, Appendix E}]$$

$$\left. \begin{aligned}
 \beta_{Li} &= 4.8 \times 10^{-4} \text{ }^\circ\text{F}^{-1} \\
 k_{oLi} &= 19.4 \text{ Btu/hr}\cdot\text{ft}\cdot\text{ }^\circ\text{F}
 \end{aligned} \right\} \text{estimated from rough calculation of data}$$

$$\begin{aligned}
 k_{SR} &= \left\{ \left[ k_o (1 + \beta t) \right]_{Li} + \left[ \frac{A_W}{A_{Li}} (k_o) (1 + \beta t) \right]_{ss} \right\} \left( \frac{D_i}{D_o} \right)^2 = \\
 &= \left\{ (19.4) [1 + (4.8 \times 10^{-4}) t] + (0.1833)(7.78) [1 + \right. \\
 &\quad \left. + (5.508 \times 10^{-4}) t] \right\} \left\{ (1.375/1.496)^2 \right\} \quad (35)
 \end{aligned}$$

$$k_{SR}(t = t_{10}) = 23.267 \text{ Btu/hr}\cdot\text{ft}\cdot\text{ }^\circ\text{F}$$

$$k_{SR}(t = t_{14}) = 23.046 \text{ Btu/hr}\cdot\text{ft}\cdot\text{ }^\circ\text{F}$$

$$A = \pi D_o^2 (1 + 2 \alpha_{ss} t)/4 \quad (36)$$

$$A (x = x_{10}) = \pi (1.496)^2 [1 + 2 \alpha_{ss} (666.72)]/4 = 1.7845 \text{ in.}^2$$

$$A (x = x_{14}) = 1.7835 \text{ in.}^2$$

$$\left. \frac{Q}{k A} \right|_{\substack{x = x_{10} \\ t = t_{10}}} = \frac{12 (67.60)}{(23.267)(1.7845)} = 19.5375^\circ\text{F/in.} \quad (37)$$

$$\left. \frac{Q}{k A} \right|_{\substack{x = x_{14} \\ t = t_{14}}} = \frac{12 (68.05)}{(23.046)(1.7835)} = 19.8670^\circ\text{F/in.} \quad (38)$$

$$\begin{aligned} \Delta x &= (x_{10} - x_{14})(1 + \alpha_{ss} t_{\text{avg}}) = (5.3467 - 3.8518)[1 + \alpha(652.25)] \\ &= 1.5061 \text{ in.} \end{aligned} \quad (39)$$

$$\begin{aligned} a &= \frac{1}{2 (\Delta x)} \left[ \left. \frac{Q}{k A} \right|_{\substack{x = x_{10} \\ t = t_{10}}} - \left. \frac{Q}{k A} \right|_{\substack{x = x_{14} \\ t = t_{14}}} \right] = \\ &= \frac{19.5375 - 19.8670}{2 (1.5061)} = -0.108^\circ\text{F/in.}^2 \end{aligned} \quad (40)$$

The calculated axial distances between the lower end of the test piece and the thermocouple junctions are tabulated in Table III in Chapter V. The average of the distances calculated for the first three runs were used in the thermal conductivity calculations. These distances were calculated for room temperature and were corrected for thermal expansion as follows:

$$t_e \cong t_{22} - (t_{18} - t_{22}) = 2 (531.14) - 575.87 = 486.41^\circ\text{F} \quad (41)$$

$$t_{il} \cong t_{16} + (t_{16} - t_{18}) = 2 (598.98) - 575.87 = 622.09^\circ\text{F} \quad (42)$$

$$x_{il} = 3.142 \text{ in. [from Table VIII in Appendix C]}$$

$$\begin{aligned} x_{il_t} &= x_{il} [1 + \alpha_{ss} (t_{il} + t_e)/2] = \\ &= 3.142 [1 + \alpha_{ss} (622.09 + 486.41)/2] = 3.162 \end{aligned} \quad (43)$$

$$\begin{aligned} x_t &= (x - x_{il}) [1 + \alpha_{ss} (t + t_{il})/2] + x_{il_t} = \\ &= (x - 3.142) [1 + \alpha_{ss} (t + 622.09)/2] + 3.162 \end{aligned} \quad (44)$$

The two other coefficients of Equation (14) in Chapter II, b and c, were determined by least-squares analysis from the "N" observations of temperature and calculated distances as follows:

$$\begin{aligned} c &= \frac{a \sum x_t^3 - (a \sum x_t^2 - \sum t)(\sum x_t^2 / \sum x_t) - \sum x_t \cdot t}{N (\sum x_t^2 / \sum x_t) - \sum x_t} = \\ &= \left\{ (-0.108)(312.8345009) - [(-0.108)(65.34697988) - 1956.41] \times \right. \\ &\quad \left. \times [4.708199193] - 9073.070258 \right\} / \left\{ 3(4.708199193) - 13.8794 \right\} = \\ &= 560.934^\circ\text{F} \end{aligned} \quad (45)$$

$$\begin{aligned} b &= [a \sum x_t^2 + N c - \sum t] / [-\sum x_t] = [-0.108 (65.34697988) + \\ &\quad + 3 (560.934) - 1956.41] / [-13.8794] = 20.2218^\circ\text{F/in.} \end{aligned} \quad (46)$$

$$\text{Thus: } t = a x_t^2 + b x_t + c = -0.108 x_t^2 + 20.222 x_t + 560.93 \quad (47)$$

$$\text{and } dt/dx = 2 a x_t + b = -0.216 x_t + 20.222 \quad (48)$$

Procedures similar to those above were followed for the upper-heat-meter region of the test piece and yielded the following equations:

$$t = -0.312 x_t^2 + 46.194 x_t + 411.64 \quad (49)$$

$$dt/dx = -0.624 x_t + 46.194 \quad (50)$$

The temperatures and gradients were then calculated at the interface between the upper heat meter and the sample using Equations (44), (47), (48), (49), and (50) as follows:

$$x_{iu} = 6.044 \text{ in. [see Table VIII in Appendix C]}$$

$$t_{iu} \approx t_{10} + (t_{10} - t_{12}) = 2 (666.72) - 651.92 = 681.52^\circ\text{F} \quad (51)$$

$$\begin{aligned} x_{iu_t} &= (x_{iu} - x_{i\ell}) [1 + \alpha_{ss} (t_{iu} + t_{i\ell})/2] + x_{i\ell_t} = \\ &= (6.044 - 3.142) [1 + \alpha_{ss} (681.52 + 622.09)/2] + 3.162 = \\ &= 6.086 \end{aligned} \quad (52)$$

$$\begin{aligned} t_{Li_i} &= -0.108 (x_{iu_t})^2 + 20.222 (x_{iu_t}) + 560.93 = \\ &= -0.108 (6.086)^2 + 20.222 (6.086) + 560.93 = 680.00^\circ\text{F} \end{aligned}$$

$$(dt/dx)_{Li_i} = 0.216 (6.086) + 20.222 = 18.907^\circ\text{F/in.}$$

$$\begin{aligned} t_{H_i} &= -0.312 (x_{iu_t})^2 + 46.194 (x_{iu_t}) + 411.64 = \\ &= -0.312 (6.086)^2 + 46.194 (6.086) + 411.64 = 681.20^\circ\text{F} \end{aligned}$$

$$(dt/dx)_{H_i} = -0.624 (6.086) + 46.194 = 42.396^\circ\text{F/in.}$$

The thermal conductivity of the upper heat meter was determined from the conductivity of the type 347 stainless steel corrected for the 0.125-in.-dia fill hole (assumed to contain lithium) as follows:

$$\begin{aligned}
 k_{ss} &= k_o (1 + \beta t) = 7.78 [1 + \beta (681.20)] = 10.699 \text{ Btu/hr}\cdot\text{ft}\cdot^\circ\text{F} \\
 k_{Li} &\cong 26.5 \text{ Btu/hr}\cdot\text{ft}\cdot^\circ\text{F} \quad \left. \vphantom{k_{Li}} \right\} \text{ estimated from rough calculations} \\
 k_{H_i} &= k_{ss} + \frac{A_{\text{hole}}}{A_H} (k_{Li} - k_{ss}) = 10.699 + \left( \frac{0.125}{1.501} \right)^2 \times \\
 &\quad \times (26.5 - 10.7) = 10.808 \text{ Btu/hr}\cdot\text{ft}\cdot^\circ\text{F} \qquad (53)
 \end{aligned}$$

Finally, the conductivity of the lithium was calculated using the above results and Equation (13) from Chapter II as follows:

$$\begin{aligned}
 k_{Li} &= \frac{(k A dt/dx)_{H_i}}{(A dt/dx)_{Li_i}} - k_{H_i} \left( \frac{A_W}{A_{Li}} \right) = \\
 &= (10.808) \left( \frac{1.501}{1.375} \right)^2 \left( \frac{42.396}{18.907} \right) - 10.808 (0.183) = \\
 &= 26.82 \text{ Btu/hr}\cdot\text{ft}\cdot^\circ\text{F at } 681.20^\circ\text{F} \qquad (54)
 \end{aligned}$$

D. PRECISION AND ERROR ANALYSES; FACTORS AFFECTING  
THE ACCURACY OF THE RESULTS

The final form of the equation used to calculate the thermal conductivity of molten lithium is:

$$k_{Li} = k_{H_i} \frac{A_H}{A_{Li}} \frac{(dt/dx)_{H_i}}{(dt/dx)_{Li_i}} - k_{H_i} \frac{A_W}{A_{Li}} \quad (55)$$

However, in this form it is difficult to analyze all the factors influencing the thermal conductivity determination. A more descriptive form can be developed by realizing that the extremely positioned points of a group of data have the greatest effect on the slope of a curve fitted by a least-squares analysis. Thus the precision and accuracy of the least-squares analysis for the temperature gradients should be no worse, and probably better, than the gradients calculated from the extremely positioned thermocouples of each region; i.e., the thermocouples numbered 2 and 8, 10 and 14, and 16 and 22. Based on such a  $\Delta t/\Delta x$  analysis, the expression for the thermal conductivity of molten lithium is [see Equation (12) in Chapter II]:

$$k_{Li} = k_{H_a} \frac{A_H}{A_{Li}} \frac{(\Delta t/\Delta x)_{H_a}}{(\Delta t/\Delta x)_{Li_b}} - k_{H_a} \left( \frac{A_H}{A_{Li}} - 1 \right) + \frac{C k_I \Delta t_I}{A_{Li} (\Delta t/\Delta x)_{Li_b}} + \frac{Q_\theta}{A_{Li} (\Delta t/\Delta x)_{Li_b}} \quad (56)$$

By taking the total derivative of  $k_{Li}$  in Equation (56) and rearranging terms, the change in  $k_{Li}$  due to a change in any of the quantities in Equation (56) is given by:

$$\begin{aligned}
 dk_{Li} = & \frac{(k A \Delta t / \Delta x)_H}{(A \Delta t / \Delta x)_{Li}} \left( \frac{dk_H}{k_H} + \frac{dA_H}{A_H} + \frac{dA_{Li}}{A_{Li}} + \frac{d\Delta x_H}{\Delta x_H} + \frac{d\Delta x_{Li}}{\Delta x_{Li}} + \right. \\
 & \left. + \frac{d\Delta t_H}{\Delta t_H} + \frac{d\Delta t_{Li}}{\Delta t_{Li}} \right) - \frac{(k A)_H}{A_{Li}} \left( \frac{dk_H}{k_H} + \frac{dA_H}{A_H} + \frac{dA_{Li}}{A_{Li}} \right) + \\
 & + k_H \left( \frac{dk_H}{k_H} \right) + \frac{C k_I \Delta t_I}{(A \Delta t / \Delta x)_{Li}} \left( \frac{dk_I}{k_I} + \frac{d\Delta t_I}{\Delta t_I} + \dots \right) + \\
 & + \frac{Q_\theta}{(A \Delta t / \Delta x)_{Li}} \left( \frac{dQ_\theta}{Q_\theta} + \dots \right), \tag{57}
 \end{aligned}$$

where the change in  $k_I$ ,  $\Delta t_I$ , and  $Q_\theta$  are assumed to be large with respect to the other quantities in the last two terms. For small errors, the symbol  $\delta$ , denoting error, can be substituted for the derivatives. Now, dividing through Equation (57) by  $k_{Li}$ , substituting

$$Q_H = (k A \Delta t / \Delta x)_H, Q_{Li} = (k A \Delta t / \Delta x)_{Li}, \text{ and } Q_R = C k_I \Delta t_I,$$

and adding terms in a manner to obtain the maximum error, the maximum error in  $k_{Li}$  is:

$$\begin{aligned}
\frac{\delta k_{Li}}{k_{Li}} = & \frac{\delta k_H}{k_H} \left( \frac{Q_H}{Q_{Li}} + \frac{k_H}{k_{Li}} - \frac{k_H A_H}{k_{Li} A_{Li}} \right) + \left( \frac{\delta A_H}{A_H} + \frac{\delta A_{Li}}{A_{Li}} \right) \left( \frac{Q_H}{Q_{Li}} - \right. \\
& \left. - \frac{k_H A_H}{k_{Li} A_{Li}} \right) + \left( \frac{\delta \Delta x_H}{\Delta x_H} + \frac{\delta \Delta x_{Li}}{\Delta x_{Li}} + \frac{\delta \Delta t_H}{\Delta t_H} + \frac{\delta \Delta t_{Li}}{\Delta t_{Li}} \right) \left( \frac{Q_H}{Q_{Li}} \right) + \\
& + \left( \frac{\delta k_I}{k_I} + \frac{\delta \Delta t_I}{\Delta t_I} \right) \left( \frac{Q_R}{Q_{Li}} \right) + \frac{\delta Q_\theta}{Q_\theta} \left( \frac{Q_\theta}{Q_{Li}} \right) . \quad (58)
\end{aligned}$$

A detailed investigation of the possible errors will now be made. First, however, a distinction should be made between the types of errors involved. By definition, those errors which are random in nature, such that a statistical average of a large number of independent determinations will tend to reduce their effect, will be termed precision. Those errors which are constant in nature and thus cannot be detected or reduced by repeated determinations will be called accuracy. The precision analysis will be made first.

Examination of Equation (58) shows that of the various terms, the area and  $\Delta x$  terms are constant and thus do not affect the precision. The major contributions to the lack of precision in the remaining terms were the precisions of the temperature measurement and thermal conductivity of the heat meter. These effects on precision were analyzed for runs 1 and 14 and are outlined for thermocouple pairs 16-22 and 10-14 as follows:

Run No. 1

Precision of  $\Delta t$

Precision of emf

Balancing Potentiometer

$\pm 0.20 \mu v$

Rounding of Potentiometer Reading	$\pm 0.50 \mu\text{v}$	
Conversion Factor, $dE/dt$	$\pm 5.01 \mu\text{v}/^\circ\text{F}$	
Precision in Temperature Reading = (0.20 + 0.5)/5.01	$\pm 0.14^\circ\text{F}$	
Precision in Reading Calibration Curve	$\pm 0.05^\circ\text{F}$	
$\delta(t) = (0.14 + 0.05)$	$\pm 0.19^\circ\text{F}$	
$\delta(\Delta t) = 2(0.19)$	$\pm 0.38^\circ\text{F}$	
$\Delta t_{16-22}$	$67.8^\circ\text{F}$	
$[\delta(\Delta t)/\Delta t]_{16-22} = (0.38)(100)/67.8$		$\pm 0.56\%$
$\Delta t_{10-14}$	$29.0^\circ\text{F}$	
$[\delta(\Delta t)/\Delta t]_{10-14} = (0.38)(100)/(29.0)$		$\pm 1.30\%$
Precision of $k_H$		
Precision of temperature, $\delta(t)$ [from above]	$\pm 0.20^\circ\text{F}$	
Change in $k_{ss}$ per $^\circ\text{F}$	0.0043	
$\delta(k_{ss}) = (0.0043)(0.020)$	$\pm 0.0009$	
Average value of $k_{ss}$	$11.2 \text{ Btu/hr}\cdot\text{ft}\cdot^\circ\text{F}$	
$\delta(k_{ss})/k_{ss} = (0.0009)(100)/11.2$		$\pm 0.01\%$
Total		$\pm 1.87\%$

Run No. 14Precision of  $\Delta t$ 

## Precision of emf

Balancing Potentiometer (increased fluctuations)	$\pm 1.0 \mu\text{v}$
Rounding of Potentiometer Reading	$\pm 0.5 \mu\text{v}$
Conversion Factor, $dE/dt$	$6.0 \mu\text{v}/^\circ\text{F}$
Precision in Temperature Reading = (1.0 + 0.5)/6.0	$\pm 0.25^\circ\text{F}$
Precision in Reading Calibration Curve	$\pm 0.05^\circ\text{F}$
$\delta(t)_{16-22} = (0.25 + 0.05)$	$\pm 0.30^\circ\text{F}$
$\delta(\Delta t)_{16-22} = 2(0.30)$	$\pm 0.60^\circ\text{F}$

$\Delta t_{16-22}$	95.3°F	
$[\delta(\Delta t)/\Delta t]_{16-22} = (0.60)(100)/95.3$		±0.63%
$[\delta(\Delta t)_{Li}]_{t'} = 3/2 [\delta(t)_{16-22}] + 3[\delta(t)_{2-8}] =$		
$= 3/2 (0.30 + 3(0.30))$	±1.35°F	
$[\delta(\Delta t)_{Li}]_{t''}$	±0.54°F	
$\Delta t_{Li}$	90°F	
$\delta(\Delta t)/\Delta t_{Li} = (1.35 + 0.54)(100)/90$		±2.10%
Precision of $k_H$ (approximately same as above)		±0.01%
Total		±2.74%

The precision analysis for run 1 is self-explanatory; however, some explanation is necessary for run 14. The temperature drop in the sample region for run 14 was determined from the extension of the temperature profiles from the upper and lower heat meters to the lithium-heat meter interfaces. Thus the precision of the lithium  $\Delta t$  determination was influenced by (1) the precision of the heat meter  $\Delta t$ 's which affected the slope of the extrapolated temperature profiles and by (2) the precision of the radial  $\Delta t$  and the  $\Delta t/\Delta \theta$  measurements which affected the change in the slope of the extrapolated temperature profiles. It is easily seen from the geometry involved that by condition (1) the precision of the temperature determination at the upper interface would be worse than the precision of the upper-heat-meter temperatures by a factor of three, while that of the lower interface would be less than the precision of the lower-heat-meter temperatures by a factor of three-halves. Condition (2) has a ±10 per cent effect on the calculation of "a" [see Equation (18) in Chapter II] which affects the expression for the temperature along the test piece [see Equation (14)] and makes an additional uncertainty in the lithium

$\Delta t$  of  $\pm 0.54^\circ\text{F}$  for run 14.

It will be noted from the above outline that the loss of precision is greatest for the lithium  $\Delta t$  measurement in all cases. Fortunately, the per cent loss of precision of the lithium  $\Delta t$  for run 14 was not significantly larger than for run 1, as the magnitude of the lithium  $\Delta t$  was three times greater. The precision of the thermal conductivity of the heat meter was increased by calculation from an equation rather than by use of a curve. The results of the precision analysis agreed, at least qualitatively, with the actual experimental precision (see Chapter V).

The quantities affecting the accuracy of the thermal conductivity of the lithium are outlined below in their order of appearance in Equation (58) and are tabulated in Table IX.

Accuracy of  $k_H$ . The experimental results of Fieldhouse, *et al.*,<sup>19</sup> (see Figure 30) were selected for the thermal conductivity of type 347 stainless steel for reasons discussed in Chapter VI. No detailed error analysis was given by Fieldhouse, *et al.*, but a calibration of their apparatus was made using Armco iron. Their thermal conductivity values for Armco iron differed from those of Powell<sup>26</sup> by  $\pm 1$  per cent from 200 to  $700^\circ\text{F}$  and by  $\pm 2$  per cent from 700 to  $1500^\circ\text{F}$ . The techniques used by Powell were very elaborate, and a detailed error analysis gave a maximum estimated error of  $\pm 2$  per cent. Furthermore, Armco iron with its higher thermal conductivity provides a more severe test of the absolute radial method used by Fieldhouse than does type 347 stainless steel. Thus from the data of Fieldhouse for Armco iron in the temperature range of 200 to  $1300^\circ\text{F}$ , the average  $\Delta t$  across the sample was  $11^\circ\text{F}$ ; for the type 347 stainless steel, the average  $\Delta t$  was  $22^\circ\text{F}$  from 150 to  $1400^\circ\text{F}$ . It is doubtful

that the accuracy of the  $\Delta t$  measurement could have been better than  $\pm 0.2^\circ\text{F}$ .

Thus, the above can be tabulated as follows:

Temperature		500°F	1400°F
Error in $k_{\text{Fe}}$ , Powell		$\pm 2\%$	$\pm 2\%$
Deviation from $k_{\text{Fe}}$ of Powell by Fieldhouse		$\pm 1\%$	$\pm 2\%$
Total error in $k_{\text{Fe}}$		$\pm 3\%$	$\pm 4\%$
$[\delta(\Delta t)/\Delta t]_{\text{Fe}}$	$(0.2)(100)/11$	$\pm 1.8\%$	
$[\delta(\Delta t)/\Delta t]_{\text{SS}}$	$(0.2)(100)/22$	$\pm 0.9\%$	
		$\pm 0.9\%$	
		$\longrightarrow$	
		$\pm 0.9\%$	$\pm 0.9\%$
Total error in $k_{\text{SS}}$ of Fieldhouse		$\pm 2.1\%$	$\pm 3.1\%$

The type 347 stainless steel used for the heat meters in the present study was procured under rigid specifications with regard to heat treatment and uniformity (see table in Figure 30). Other than the nominal composition, no spectrochemical analyses were available for the sample used by Fieldhouse, et al. However, as discussed in Chapter VI, the thermal conductivity of most 300 series stainless steels is relatively insensitive to minor deviations in nominal compositions. Thus, the error in the thermal conductivity of the heat meter can reasonably be expected to be the same as the error estimated for Fieldhouse's measurement. Therefore,  $\delta k_{\text{H}}/k_{\text{H}}$  in the present measurements is  $\pm 2.1$  and  $\pm 3.1$  per cent for runs 1 and 14, respectively. The weighting function for this error [see Equation (58)] is

$$\left( \frac{Q_{\text{H}}}{Q_{\text{Li}}} + \frac{k_{\text{H}}}{k_{\text{Li}}} - \frac{k_{\text{H}} A_{\text{H}}}{k_{\text{Li}} A_{\text{Li}}} \right), \quad (59)$$

which gives a weighting factor of 1.00 for runs 1 and 14.

Accuracy of  $A_H$  and  $A_{Li}$ . The diameters were measured to  $\pm 0.001$  in.

Therefore, the errors in  $A_H$  and  $A_{Li}$  are:

$$\delta(A_H)/A_H = \frac{[(1.500)^2 - (1.499)^2] 100}{(1.500)^2} = \pm 0.13\% \quad (60)$$

$$\delta(A_{Li})/A_{Li} = \frac{[(1.375)^2 - (1.374)^2] 100}{(1.375)^2} = \pm 0.14\% \quad (61)$$

The weighting function from Equation (58) is:

$$\left( \frac{Q_H}{Q_{Li}} - \frac{k_H}{k_{Li}} \frac{A_H}{A_{Li}} \right), \quad (62)$$

which gives a weighting factor of 0.60 for runs 1 and 14.

Accuracy of  $\Delta x_H$  and  $\Delta x_{Li}$ . The distances from the datum plane (lower end of test piece) to the junctions of the thermocouples were calculated by least-squares analysis from the temperature measurement of runs 1, 2, and 3 and the measured distances to the centerline of the thermowells. A summary of these calculations is tabulated in Chapter V. The calculated distances for runs 1, 2, and 3 were averaged. The maximum deviation from the average of any calculated thermocouple location was 0.005 in.; whereas, the maximum deviation of any measured centerline distance of a thermowell was 0.020 in. The deviation of  $\pm 0.005$  in. was considered to be the maximum uncertainty in a thermocouple junction location. For reasons noted previously, the extremely positioned thermocouples have the most influence on the slope of a least-squares curve. Therefore, the errors in  $\Delta x_H$  and  $\Delta x_{Li}$  for run 1 are:

$$\delta(\Delta x)_H / \Delta x_H = 2(0.005)(100)/1.5 = \pm 0.66\% \quad (63)$$

$$\delta(\Delta x)_{Li} / \Delta x_{ss} = 2(0.005)(100)/1.5 = \pm 0.66\% \quad (64)$$

For run 14, the lithium temperature drop was measured from one interface to the other. Due to the taper on the upper interface and the necessary indirectness of the  $\Delta x$  measurement, the error in the  $\Delta x_{Li}$  was estimated to be  $\pm 0.022$  in. Therefore, the errors in the  $\Delta x_H$  and  $\Delta x_{Li}$  for run 14 are:

$$\delta(\Delta x_H) / \Delta x_H = 2(0.005)(100)/1.5 = \pm 0.66\% \quad (65)$$

$$\delta(\Delta x_{Li}) / \Delta x_{Li} = (0.022)(100)/3.0 = \pm 0.74\% \quad (66)$$

The weighting function is  $Q_H / Q_{Li}$ , which gives a weighting factor of 1.08.

Accuracy of  $\Delta t_H$  and  $\Delta t_{Li}$ . Unfortunately, only one emf reading was made for each thermocouple per calibration point. Since the errors due to lack of precision in the calibration were not reduced by repeated measurements, these errors must be included in the accuracy of the  $\Delta t$ 's. However, since several thermocouples were calibrated together at one time, neither the accuracy of the potentiometer and the standard thermocouple nor the conversion of  $\mu v$  to  $^{\circ}F$  would affect the accuracy of a  $\Delta t$  measurement involving these particular thermocouples. The accuracy analysis of  $\Delta t_H$  and  $\Delta t_{Li}$  for runs 1 and 14 can be broken down as follows:

Run No. 1

$\Delta t_H$

Calibration

Balancing potentiometer

$\pm 0.1 \mu v$

Rounding emf Reading	$\pm 0.5 \mu\text{v}$	
Conversion Factor	$5.0 \mu\text{v}/^\circ\text{F}$	
Precision in Temperature Reading ( $0.1 + 0.5$ )/ $5.01$	$\pm 0.12^\circ\text{F}$	
Accuracy of Potentiometer	} Thermocouples were calibrated together	
Accuracy of Standard Thermocouple		
emf Conversion to $^\circ\text{F}$ (NBS 561)		
Error in Correction Curve due to Straight Line Connection of Calibration Points (every $200^\circ\text{F}$ )	$\pm 0.06^\circ\text{F}$	
$\delta(\Delta t) = 2(0.12 + 0.06)$	$\pm 0.36^\circ\text{F}$	
$\Delta t$ Measurement		
Potentiometer Error = $\pm(0.015\% \Delta t)$	$\pm 0.01^\circ\text{F}$	
emf Conversion to $^\circ\text{F}$ (NBS 561) = $2(0.1)$	$\pm 0.20^\circ\text{F}$	
$\delta(\Delta t) = (0.01 + 0.20)$	$\pm 0.21^\circ\text{F}$	
$\Delta t_{16-22}$	$68^\circ\text{F}$	
$\delta(\Delta t)/\Delta t = (0.36 + 0.21)(100)/68$		$\pm 0.84\%$
$\Delta t_{\text{Li}}$ Calibration		
$\delta(\Delta t)$ [same as above]	$\pm 0.36^\circ\text{F}$	
$\Delta t$ Measurement		
Potentiometer Error = $(0.015\% \Delta t)$	$\pm 0.01^\circ\text{F}$	
emf Conversion (NBS 561)	$\pm 0.20^\circ\text{F}$	
$\delta(\Delta t)$	$\pm 0.21^\circ\text{F}$	
$\Delta t_{10-12}$	$29.0^\circ\text{F}$	
$\delta(\Delta t)/\Delta t = (0.21 + 0.36)(100)/29 =$		$\pm 1.95\%$

Run No. 14

$\Delta t_{\text{H}}$ Calibration		
$\delta(\Delta t)$ [same as before]	$\pm 0.36^\circ\text{F}$	
$\Delta t$ Measurement		
Potentiometer Error = $0.030\% \Delta t$	$\pm 0.03^\circ\text{F}$	

emf Conversion = 2(0.1)	$\pm 0.2^{\circ}\text{F}$
$\delta(\Delta t) = 0.2 + 0.03$	$\pm 0.23^{\circ}\text{F}$
$\Delta t_{16-22}$	$95.3^{\circ}\text{F}$
$\delta(\Delta t)/\Delta t = (0.23 + 0.36)(100)/95.3$	$\pm 0.62\%$
$\Delta t_{\text{Li}}$	
$[\delta(\Delta t)]_{t'} = 3/4 [\delta(\Delta t)_{16-22}] + 3/2 [\delta(\Delta t)_{2-8}]$	
$= 3/4 [0.59] + 3/2 [0.59] =$	$\pm 1.33^{\circ}\text{F}$
$[\delta(\Delta t)]_{t''}$	$\pm 0.27^{\circ}\text{F}$
Uncertainty in upper interfacial $\Delta t$	$\pm 1.67^{\circ}\text{F}$
Uncertainty in lower interfacial $\Delta t$	$\pm 1.23^{\circ}\text{F}$
$\Delta t$	$90.0^{\circ}\text{F}$
$\delta(\Delta t)/\Delta t = (1.33 + 1.67 + 1.23 + 0.27)(100)/90$	$\pm 5.00\%$

The accuracy of the lithium temperature drop for run 14 was determined in the manner described in the precision analysis. In addition to the uncertainties in the slope and curvature of the extrapolated profiles, there was also an uncertainty in the temperature drop across the interfacial boundary between the lithium and the heat meters. Normally, the interfacial resistance between a liquid metal, such as lithium, and a solid metal (stainless steel) would be small and with low heat fluxes would cause a negligible temperature drop. However, an average interfacial  $\Delta t$  of 1.67 and 1.23 $^{\circ}\text{F}$  (as determined from the extrapolated temperature profiles) was found at the upper and lower interfaces, respectively, for runs 1 through 8. Although the interfacial  $\Delta t$ 's for runs 1 through 8 may have been due to inaccuracies in the extrapolated profiles, the average values were used to determine the lithium  $\Delta t$  for runs 9 through 14. Since the heat flux of runs 9 through 14 was twice that of runs 1 through 8, the maximum uncertainty in the interfacial  $\Delta t$ 's for runs 9 through 14 should

have been twice the average  $\Delta t$  and zero; i.e.,  $\pm 1.67$  and  $\pm 1.23^\circ\text{F}$  at the upper and lower interface, respectively. These additional errors are tabulated in the above outline for run 14.

The weighting function for the  $\Delta t$  error is  $Q_H/Q_{Li}$ , which gives a weight factor of 1.08.

Accuracy of  $Q_R$ . The maximum uncertainty in correcting  $k_I$  for operation in vacuum rather than air was determined to be no more than  $\pm 20$  per cent (see Appendix E). Considerable care was taken in placing the insulation in the apparatus, and no additional error due to nonuniform packing should have been created. The error in the  $\Delta t_I$  measurement can be determined, as in the preceding section, for run 1:

$$\frac{\delta \Delta t_I}{\Delta t_I} = \frac{0.57 (100)}{13} = \pm 4.3\% \quad (67)$$

and for run 14:

$$\frac{\delta \Delta t_I}{\Delta t_I} = \frac{0.59 (100)}{5} = \pm 11.8\% \quad (68)$$

The weighting function for these errors is  $Q_R/Q_{Li}$ , which gives a weight factor of 0.009 for run 1 and 0.003 for run 14.

Accuracy of  $Q_\theta$ . The method of measuring  $\Delta t/\Delta \theta$  should not have been subject to any gross errors, and the equations used to correct for  $Q_\theta$  were at least accurate to within  $\pm 20$  per cent. Since the largest value of  $Q_\theta/Q_{Li}$  was 0.003 (see Table II in Chapter V), the error due to heat retained or released due to the heat capacity effect of nonsteady state was

well below 0.1 per cent for all the measurements.

Thermocouple drift from calibration. Since suitable installation techniques were used, the thermocouple emf output for the first few data runs should not have deviated significantly from the calibration values. However, with higher temperatures and increasing time the effects of corrosion, evaporation, etc., appeared to progressively alter the emf output from the original calibration.

To estimate the thermocouple drift from initial calibration, an in place, relative calibration was made at 1100°F after the data runs were completed (see Figure 14 in Chapter V). The results of this calibration indicated that the maximum difference between any two test piece thermocouples was 2.5°F, or a maximum deviation of ±1.25°F from the mean. Of course, there could exist additional thermocouple errors caused by slight differences in the lead wire temperature gradients between the isothermal calibration run and the  $\Delta t$  operational runs. Since in either case the gradients were small, this effect was neglected.

The maximum error in  $\Delta t$ 's for run 14 should not have been greater than ±1.25°F. Of this ±1.25°F error, ±0.59°F has already been accounted for in the accuracy of  $\Delta t_H$  and  $\Delta t_{Li}$ . Thus, the additional error caused by a drift from the initial calibration would be:

$$\frac{\delta(\Delta t_H)}{\Delta t_H} = \left( \frac{1.25 - 0.59}{0.59} \right) \left( \frac{0.59}{95.3} \right) (100) = \pm 0.69\% \quad (69)$$

$$\frac{\delta(\Delta t_{Li})}{\Delta t_{Li}} = \left( \frac{1.25 - 0.59}{0.59} \right) \left( \frac{1.33 + 0.27}{90} \right) (100) = \pm 2.00\% \quad (70)$$

Total ±2.69%

The weighting function for the  $\Delta t$  error is  $Q_H/Q_{Li}$ , which gives a weight factor of 1.08.

Thermocouple conduction error. The concentric tubular arrangement of the guard tube and guard heater cylinder around the test piece required the thermocouple lead wires extend axially along the test piece. Since there was an axial temperature gradient along the test piece, conduction of heat by the leads into the thermocouple junctions could cause an error in the temperature reading. This type of error can be corrected either by calculation or minimized by an adequate length of lead wire passing through an isothermal region just before reaching the thermocouple junction. The latter method was chosen, and the maximum error in temperature was calculated for the installation method described in Chapter IV.

The calculation was made using an accumulation of conservative assumptions. These assumptions were (1) no heat flowed into or out of thermocouple junction from test piece and (2) heat transfer from the lead wires to surroundings was by radiation alone. Two further assumptions were also made: (1) that the lead wires were bent at sharp right angles, and (2) an average value of the radiation heat-transfer coefficient,  $h_r$ , could be used since the  $\Delta t$ 's were small compared to the absolute temperature.

The solution reduced to one dimension can be represented graphically as shown in Figure 26. The differential equation for a wire conducting heat and uniformly losing fractional amounts of heat from its surface can be expressed in terms of the given assumptions and the conditions shown in Figure 26 as:

$$\frac{d^2t}{dx^2} - N^2 (t - t_0) = 0 \quad \text{for } 0 \leq x \leq L , \quad (71)$$

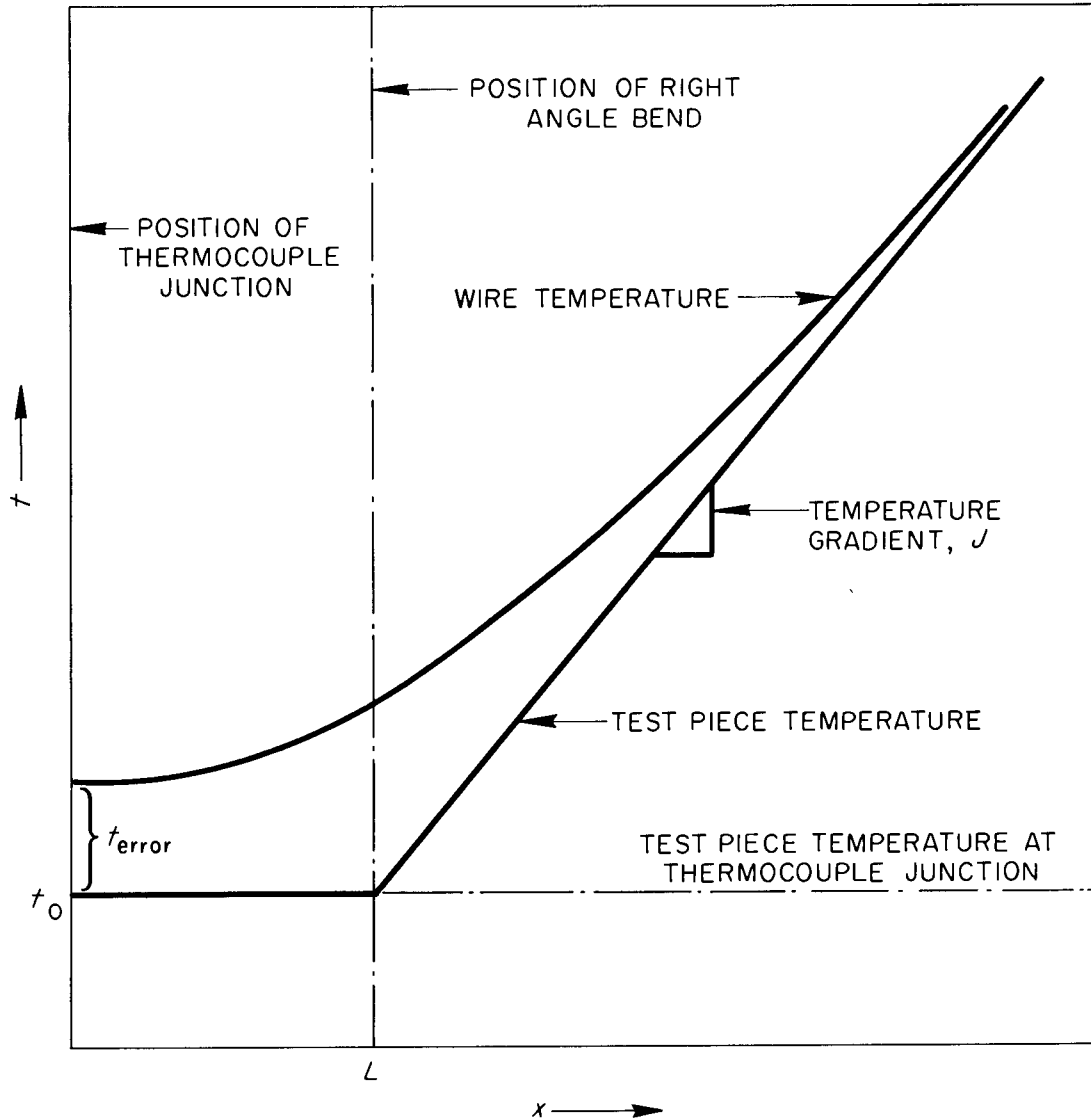
UNCLASSIFIED  
ORNL-LR-DWG 75322

Figure 26. One-Dimensional Representation of the Temperature Distribution Along the Test Piece and Attached Thermocouple Lead Wire.

and

$$\frac{d^2t}{dx^2} - N^2 \left\{ t - [t_0 + J(x - L)] \right\} = 0 \quad \text{for } x > L, \quad (72)$$

where

$$N = \sqrt{h_r \epsilon p / k A}.$$

The solution of Equations (71) and (72) with their associated boundary conditions is similar to that outlined by Schneider<sup>39</sup> and results in

$$t - t_0 = \frac{J}{2N} e^{-NL} (e^{Nx} + e^{-Nx}) \quad \text{for } 0 \leq x \leq L. \quad (73)$$

However,

$$t_{\text{error}} = t - t_0 \quad \text{at } x = 0,$$

and therefore

$$t_{\text{error}} = \frac{J}{N} e^{-NL}. \quad (74)$$

Since the value of  $N$  has a greater effect on Equation (74) than the value of  $J$ , the data from run 1 were used to calculate the thermocouple error.

Thus,  $N$  was calculated as follows:

$$h_r = 12 \text{ Btu/hr}\cdot\text{ft}^2\cdot\text{°F} \quad \text{at } t_{\text{avg}} = 650\text{°F} \quad [\text{Figure 27, p 63, ref. 40}],$$

$$\epsilon \approx 0.2 \quad [\text{Table XIII, p 394, ref. 40}],$$

$$k_{\text{eff}} = 28 \text{ Btu/hr}\cdot\text{ft}\cdot\text{°F} \quad [\text{pair of Pt/90Pt+10Rh wires, ref. 41}],$$

and

$$N = \sqrt{\frac{h_r \epsilon p}{k A}} = \sqrt{\frac{(12)(0.2)(4)(12)}{(28)(0.010)}} = 20.3 \text{ ft}. \quad (75)$$

The minimum length of lead wire in the isothermal region actually used in installing the thermocouples was approximately 2-3/4 in. The gradient,  $J$ , was 500°F/ft. Thus the thermocouple error was

$$t_{\text{error}} = \frac{500}{20.3} e^{-20.3 (2.75)/12} = 0.2^{\circ}\text{F} \quad . \quad (76)$$

Despite the conservative assumptions, this error is already within the magnitude of the other thermocouple errors. Since the thermocouple beads were arc welded to the test piece guard tube and since the lead wires could lose heat by conduction as well as radiation, the actual thermocouple conduction error would be considerably smaller than that calculated above and could clearly be neglected.

Consideration was also given to several other factors which, because of their uncertain nature, were not applied as corrections to the thermal conductivity determination. An estimate of their maximum possible effect is presented below.

Conduction into test piece by the thermocouple leads. Fifteen thermocouples were arc welded to the test piece - four between the center of the upper heat meter and sample and five between the center of the sample and lower heat meter. Thus, an error is involved by the addition of heat to the test piece from the thermocouple lead wires. This can cause the thermal conductivity as calculated by the upper heat meter to be too small, and by the lower heat meter to be too large. The exact magnitude of this error cannot be calculated, as some of the heat flowing down the lead wires is no doubt dissipated to the surrounding insulation. The maximum error, however, can be estimated as follows for run 1:

$$\frac{\delta k_{\text{Li}}}{k_{\text{Li}}} = \frac{k_{\text{Pt}} A_{\text{Pt}} (\Delta t / \Delta x)_{\text{H}}}{k_{\text{Li}} A_{\text{Li}} (\Delta t / \Delta x)_{\text{Li}}} = \left( \frac{28}{26} \right) \left( \frac{2.5 \cdot (0.010)^2}{(1.375)^2} \right) \left( \frac{42}{19} \right) = 0.12\% , \quad (77)$$

i.e., by upper heat meter -0.12 per cent and by lower heat meter +0.12 per cent, and for run 14:

$$\frac{\delta k_{\text{Li}}}{k_{\text{Li}}} = \frac{28}{32} \left( \frac{2.5 \cdot (0.010)^2}{(1.375)^2} \right) \left( \frac{66}{31} \right) = 0.10\% , \quad (78)$$

i.e., upper heat meter -0.10 per cent and lower heat meter +0.10 per cent, where the temperature gradients in the thermocouple lead wires were assumed equal to those of the heat meters.

Interchange of heat between test piece and insulation. An interchange of heat will take place between the test piece and surrounding insulation even though the axial temperature profiles of the test piece and guard tube match perfectly. Such an interchange is caused by two factors: (1) the step change in thermal conductivity of the heat meter and sample at the interfaces, and (2) the differences in the temperature dependence of the thermal conductivity of the insulation and of the test piece. Heat interchange due to the first cause will result in the thermal conductivity of the lithium as calculated by both heat meters to be too low. The exact magnitude of this error cannot be determined, as there is also an interchange of heat between the guard tube and the insulation. The maximum error can be calculated by assuming that the heat-transfer coefficients between the test piece and insulation and between the guard tube and insulation are large and equal. With this assumption, the error for run 1 is given by:

$$\begin{aligned}
\frac{\delta k_{\text{Li}}}{k_{\text{Li}}} &= - \left( \frac{S_{\text{test piece}}}{S_{\text{guard tube}}} \right) \left( \frac{k_{\text{I}}}{k_{\text{Li}}} \right) \left( \frac{A_{\text{I}}}{A_{\text{Li}}} \right) \left( \frac{(\Delta t / \Delta x)_{\text{H}}}{(\Delta t / \Delta x)_{\text{Li}}} - 1 \right) = \\
&= - \left( \frac{1.50}{3.00} \right) \left( \frac{0.035}{26} \right) \left( \frac{(3.0)^2 - (1.5)^2}{(1.375)^2} \right) \left( \frac{42}{19} - 1 \right) = \\
&= -0.29\% , \tag{79}
\end{aligned}$$

and for run 14:

$$\begin{aligned}
\frac{\delta k_{\text{Li}}}{k_{\text{Li}}} &= - \left( \frac{1.50}{2.00} \right) \left( \frac{0.13}{32} \right) \left( \frac{(3.0)^2 - (1.5)^2}{(1.375)^2} \right) \left( \frac{66}{31.5} - 1 \right) = \\
&= -0.79\% . \tag{80}
\end{aligned}$$

Heat interchange due to the second cause mentioned above will result in the thermal conductivity of the lithium as calculated from the upper heat meter to be too low and from the lower heat meter to be too high. Using the same assumption as before, the maximum error is given by:

$$\frac{\delta k_{\text{Li}}}{k_{\text{Li}}} = \left( \frac{S_{\text{test piece}}}{S_{\text{guard tube}}} \right) \left( \frac{A_{\text{I}}}{A_{\text{Li}}} \right) \left[ \frac{k_{\text{I}}}{k_{\text{ss}}} \Bigg|_{t_{\text{a}}} - \frac{k_{\text{I}}}{k_{\text{ss}}} \Bigg|_{t_{\text{i}}} + \frac{k_{\text{I}}}{k_{\text{Li}}} \Bigg|_{t_{\text{i}}} - \frac{k_{\text{I}}}{k_{\text{Li}}} \Bigg|_{t_{\text{b}}} \right] , \tag{81}$$

where the subscripts  $t_{\text{a}}$ ,  $t_{\text{i}}$ , and  $t_{\text{b}}$  refer to the temperatures at planes a, i, and b in Figure 2 in Chapter II. Thus, for run 1:

$$\frac{\delta k_{\text{Li}}}{k_{\text{Li}}} = (0.5)(6.75) \left[ \frac{0.045}{11.12} - \frac{0.037}{10.71} + \frac{0.037}{26.6} - \frac{0.030}{26.2} \right] = 0.28\% , \tag{82}$$

i.e., by the upper heat meter -0.28 per cent and by the lower heat meter

+0.28 per cent, and for run 14:

$$\frac{\delta k_{\text{Li}}}{k_{\text{Li}}} = (0.5)(6.75) \left[ \frac{0.166}{15.0} - \frac{0.139}{14.32} + \frac{0.139}{35.25} - \frac{0.131}{34.8} \right] = 0.51\% \quad , \quad (83)$$

i.e., by the upper heat meter -0.51 per cent and by the lower heat meter +0.51 per cent.

Impurities in the lithium sample. Addition of impurities into a pure metallic substance will invariably lower its thermal conductivity. At present, an accurate estimate of the amount of decrease is not possible. An attempt was made to estimate the decrease by using the results of Freedman and Robertson<sup>5</sup> for the effect of impurities on the electrical resistivity of monovalent, metallic liquids. Their results showed that the incremental change in resistivity per atomic per cent of added impurities could be expressed by:

$$\frac{\Delta \rho_e}{\text{At } \%} = 0.063 \left| \Delta \text{At No.} \right| + 0.53 (\Delta V/V)^2 \quad . \quad (84)$$

The results using this equation are tabulated as follows:

<u>Impurity</u>	<u>Wt %</u>	<u>At %</u>	<u> \Delta At No. </u>	<u>r × 10<sup>8</sup>, cm</u>	<u>(\Delta V/V)<sup>2</sup></u>	<u>\Delta \rho_e, μohm·cm</u>
Na	0.015	0.0046	8	1.91	0.642	0.0038
K	0.060	0.0105	16	2.32	4.972	0.0383
Ca	0.0001	—	—	—	—	—
Al	0.0005	0.0001	10	1.43	0.060	0.00007
Si	0.001	0.0025	11	1.21	0.292	0.0002
Ni	0.0022	0.0003	25	1.25	0.244	0.0005
Cr	0.0015	0.0002	21	1.25	0.244	0.0003
Ti	0.0010	0.0001	19	1.48	0.026	0.0001
Mn	0.002	0.0003	22	1.25	0.244	0.00045
Fe	0.0027	0.0004	23	1.26	0.245	0.0006
Other	0.0250	0.0035	25	1.25	0.244	0.006
Total						0.0504

The weight per cent impurities in the lithium sample are from Table I in Chapter IV, and the atomic radii,  $r$ , are taken from reference 42. The per cent increment in electrical resistivity would be:

$$\frac{\Delta\rho_e}{\rho_e} = \frac{(0.0504)(100)}{25.0} = +0.20\% \quad (85)$$

Now, using the Wiedemann, Franz, Lorenz, and Sommerfeld equation, the error in the thermal conductivity would be:

$$\frac{\delta k_{\text{Li}}}{k_{\text{Li}}} = \frac{L_o T}{L_o T} \left( 1 - \frac{\rho_e}{\rho_e + \Delta\rho_e} \right) = -0.20\% \quad (86)$$

Natural convection. The large temperature gradients directly opposed to the acceleration of gravity should have had a large inhibiting action on any possible convective currents in the sample. Such convective currents could only occur because of radial temperature gradients, and the net effect of these currents should be only in aiding the radial heat flow which was measured. The conclusion of the negligible effect of natural convection on the thermal conductivity determination was shown in experiments of Ewing<sup>25</sup> and Powell,<sup>27</sup> whose apparatus and methods were similar to those of the present investigation.

Ewing, in determining the thermal conductivity of sodium and potassium from 300 to 1000°F, intentionally increased the radial heat exchange by a factor of ten (from 0.1 per cent of axial heat flow to 1.0 per cent) and found no change in the conductivity measurement except for the expected radial heat loss correction. He also increased the axial heat flow by 50 per cent and again found no change in the expected conductivity.

Powell subdivided the sample cavity of his axial-heat-flow conductivity apparatus with a honeycomb of 0.003-in.-thick mica sheets. He obtained the same conductivity values for a mercury sample with or without the honeycomb of mica. From these results, both observers concluded that, if natural convection were present, its effect on the thermal conductivity determination could not be detected.

The results of the error and precision analyses are summarized in Table IX. The total maximum error in the thermal conductivity determination of molten lithium should not have been greater than +7.4 and -7.9 per cent for run 1 to +14.2 and -15.2 per cent for run 14. More than half of this total maximum error resulted from the uncertainties in the conductivity of the heat meters and in the lithium  $\Delta t$  measurement. The rest of the total error was more or less evenly distributed over the other uncertainties discussed in this section. The increased error in the determination for run 14 was primarily due to the necessity of calculating the lithium gradient from the extrapolated interfacial temperatures. The precision analysis showed that the random errors in the thermal conductivity determination should not have amounted to more than  $\pm 1.9$  to  $\pm 2.8$  per cent from run 1 to run 14.

Table IX. Summary of Error and Precision Analyses

Source of Error	Per Cent Error	
	Run 1	Run 14
k of type 347 stainless steel	±2.1	±3.1
$\Delta t_{Li}$ measurement	±2.0	±5.0
$\Delta t_H$ measurement	±0.8	±0.6
Thermocouple drift from calibration	±0.0	±2.9
$\Delta x_{Li}$ measurement	±0.7	±0.7
$\Delta x_H$ measurement	±0.7	±0.7
Area measurements	±0.2	±0.2
Radial heat exchange	±0.5	±0.4
Nonsteady state	±0.0	±0.0
Impurities in lithium sample	-0.2	-0.2
Heat conduction into test piece by thermocouple lead wires		
Upper heat meter	-0.1	-0.1
Lower heat meter	+0.1	+0.1
Natural convection in lithium sample	±0.0	+0.0
Interchange of heat between test piece and insulation		
Due to step change in k	-0.3	-0.8
Due to unequal change of k with temperature		
Upper heat meter	-0.3	-0.5
Lower heat meter	+0.3	+0.5
Thermocouple conduction error	±0.0	±0.0
Total maximum error	+7.4 -7.9	±14.2 -15.2
Precision of $\Delta t$ measurements	±1.8	±2.7
Precision of $k_H$	±0.1	±0.1
Total	±1.9	±2.8

## E. PROPERTIES OF MATERIALS USED IN THE APPARATUS

The electrical resistivity, viscosity, heat capacity, density, and coefficient of volumetric thermal expansion of molten lithium are shown as a function of temperature in Figures 27 and 28. The density, coefficient of linear thermal expansion, and heat capacity of type 347 stainless steel are plotted versus temperature in Figure 29. The properties of the molten lithium and type 347 stainless steel were selected after a careful survey of the literature. This was especially true for the thermal conductivity versus temperature of type 347 stainless steel, shown in Figure 30, which was finally selected for the reasons discussed in Appendix D. The manufacturer's data was used for the thermal conductivity of the Fiberfrax insulation in air, shown in Figure 31. The conductivity in a vacuum was determined in the manner described below.

The total heat flow through the Fiberfrax insulation can be divided into four parts: that due to radiation, air conduction, fiber conduction, and convection. Thus, the total heat flow can be expressed as:

$$\frac{2\pi L k_I \Delta t}{\ln (r_1/r_2)} = A_1 h_r \Delta t + \frac{k_{\text{air}} A_2 \Delta t}{\Delta x_1} + \frac{k_{\text{fiber}} A_3 \Delta t}{\Delta x_2} + Q_{\text{convection}} \quad (87)$$

Since the individual air pockets within the fiber matte are extremely small, the heat transferred by convection should be sufficiently small to be neglected. To investigate the effect of temperature level on Equation (87) when the  $\Delta t$  is quite small ( $\sim 10^\circ\text{F}$ ), the assumption can also be made that all the terms of Equation (87) are constant except  $k$  and  $h_r$ .

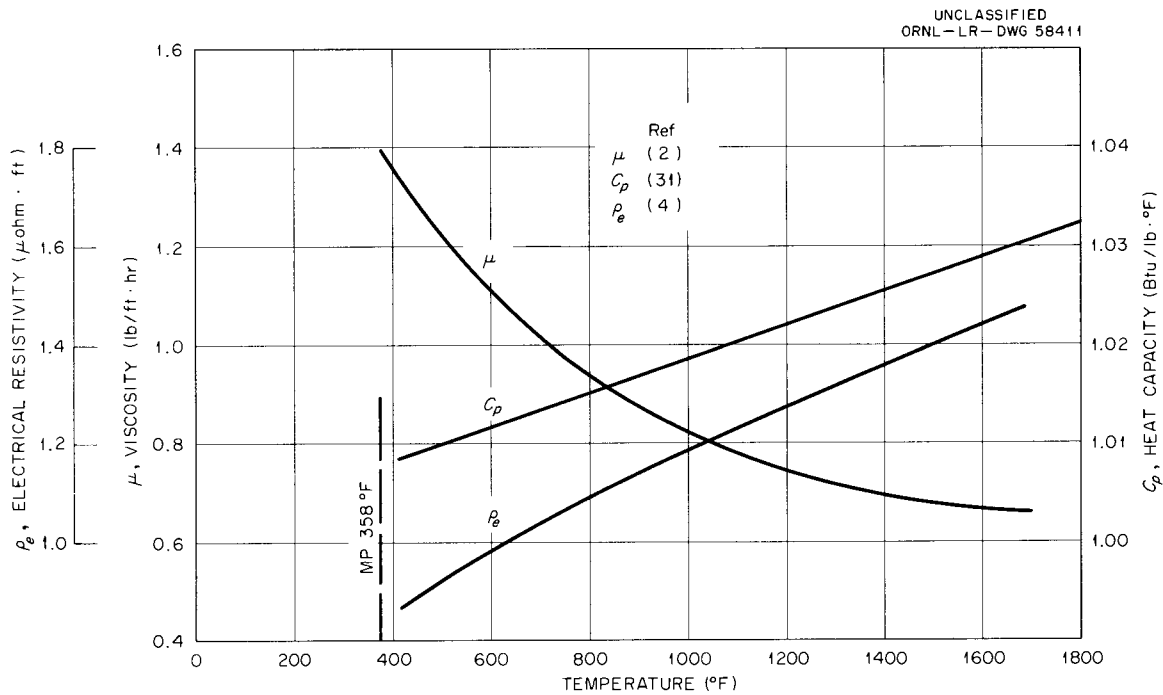


Figure 27. Properties of Lithium as a Function of Temperature - Electrical Resistivity, Viscosity, and Heat Capacity.

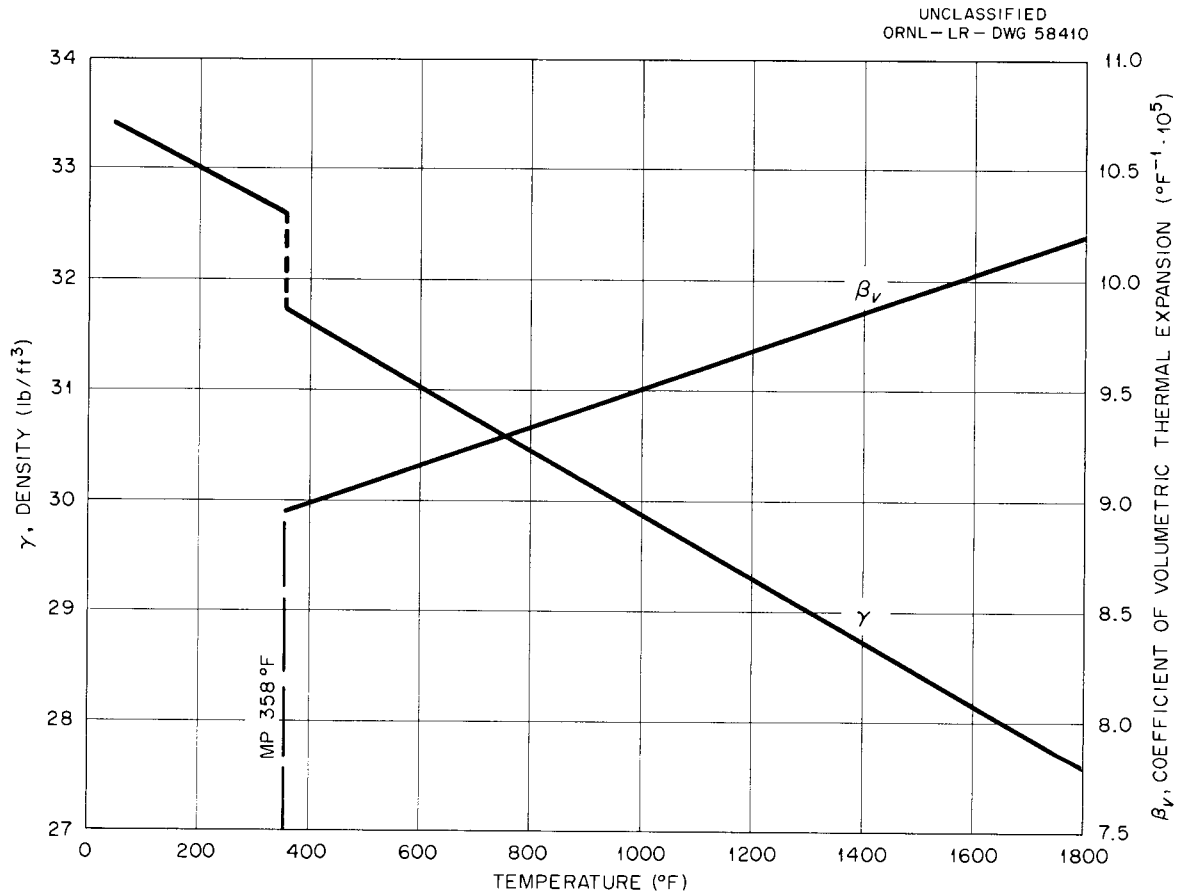


Figure 28. Properties of Lithium as a Function of Temperature - Density and Coefficient of Volumetric Thermal Expansion (Reference 33).

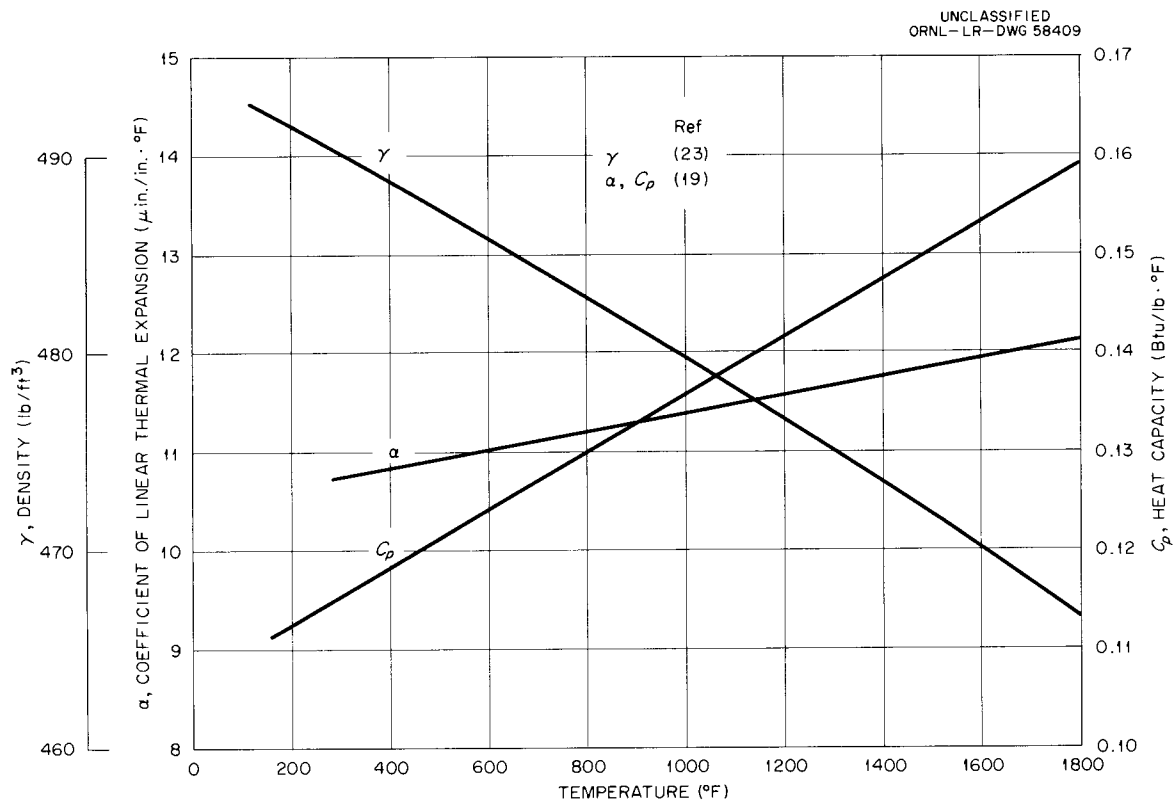


Figure 29. Properties of Type 347 Stainless Steel as a Function of Temperature - Density, Coefficient of Linear Thermal Expansion, and Heat Capacity.

UNCLASSIFIED  
ORNL-LR-DWG 70823R

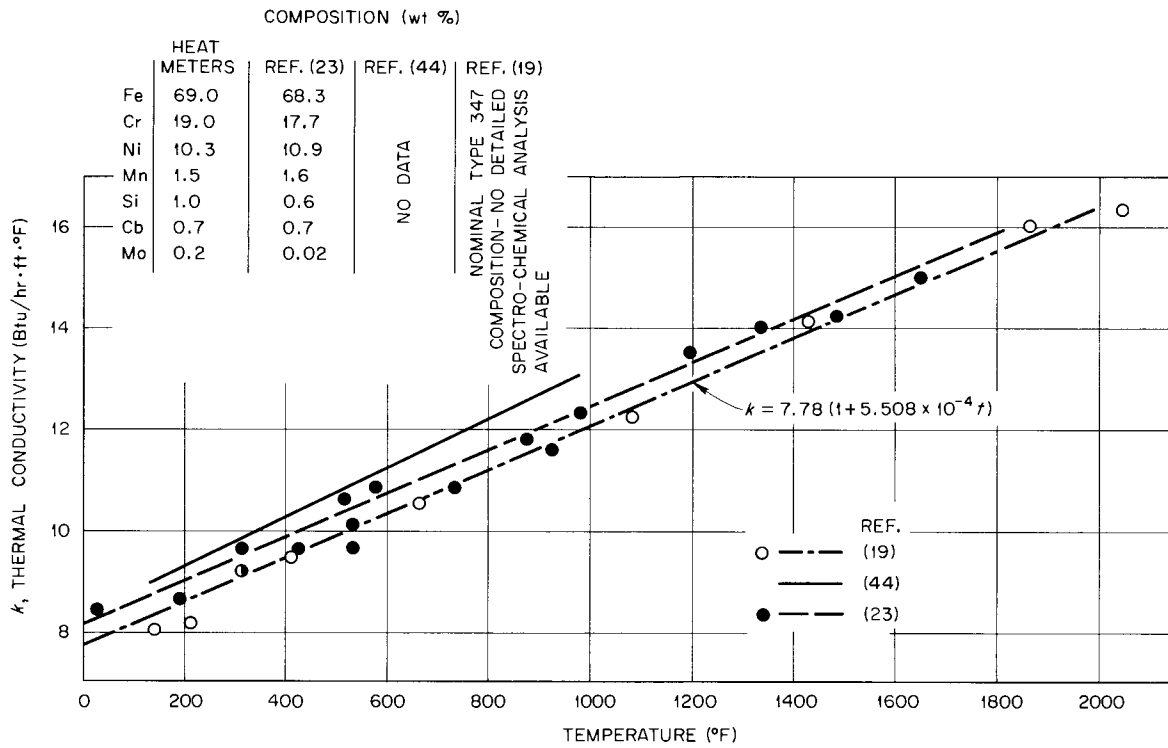


Figure 30. Thermal Conductivity of Type 347 Stainless Steel as a Function of Temperature.

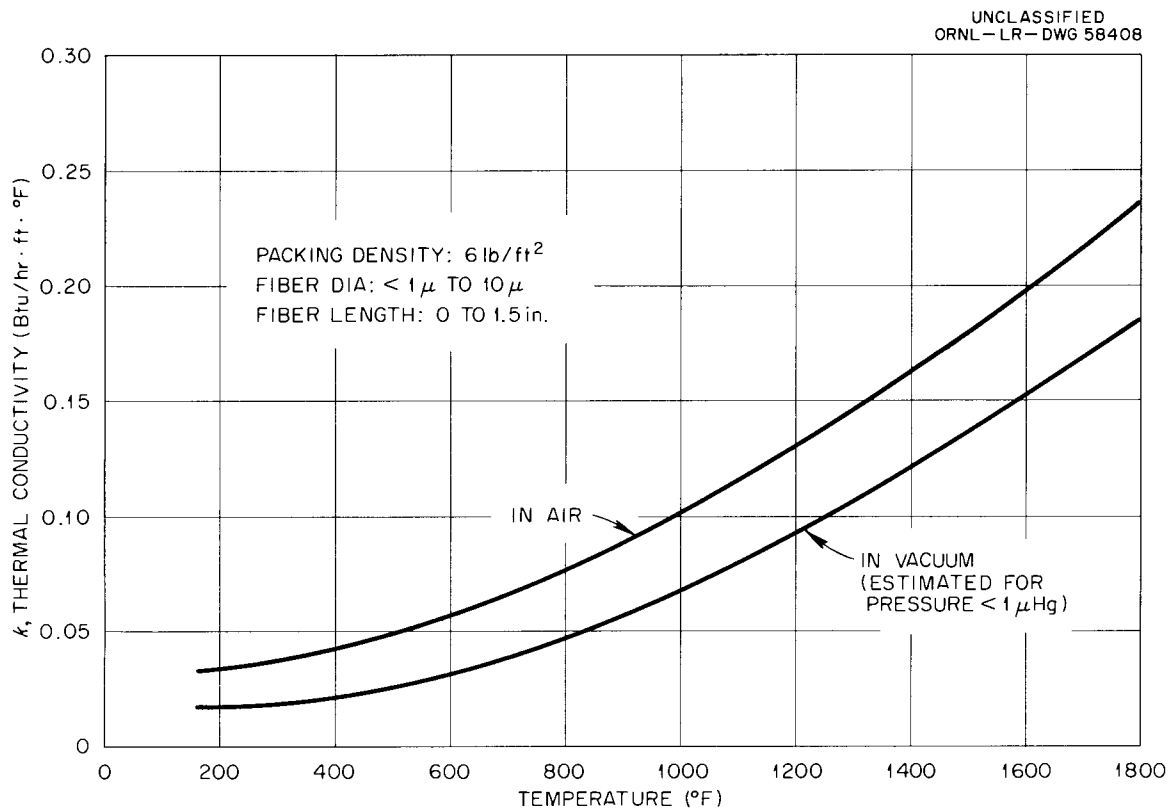


Figure 31. Thermal Conductivity of Fiberfrax Insulation  
(Data for  $k$  in Air Supplied by Mfg: Carborundum Company, Niagara Falls, N. Y.).

Thus Equation (87) can be written as:

$$k_I = C_1 h_r + C_2 k_{\text{air}} + C_3 k_{\text{ceramic}} \quad (88)$$

Since  $h_r \propto T^3$ ,  $k_{\text{air}} \propto T$ , and  $k_{\text{ceramic}} \approx C_7 T + C_8$ , Equation (88) can be further simplified to:

$$k_I = C_4 T^3 + C_5 T + C_9 T + C_{10} = C_4 T^3 + (C_5 + C_9) T + C_{10} \quad (89)$$

With  $C_4 = 11.95 \times 10^{-12}$  Btu/hr·ft·°F<sup>4</sup>,  $(C_5 + C_9) = 0.428 \times 10^{-4}$  Btu/hr·ft·°F<sup>2</sup>, and  $C_{10} = 0.002$  Btu/hr·ft·°F, Equation (89) fits the manufacturer's experimental data, which tends to confirm the assumptions upon which it was based. Since  $C_{10}$  is such a small part of  $k_I$  in the range of interest (600 to 1800°F), it can be ignored.

Because of the multitude of finite contact resistances between the individual fibers, the heat conducted through the ceramic fibers might be neglected, and the entire term  $(C_5 + C_9)T$  could be eliminated at pressures less than 0.001 mm of Hg simplifying Equation (89) to:

$$k_I = C_4 T^3 \quad (90)$$

However, to be conservative, the maximum effect of film conduction (neglecting contact resistance to heat flow) should be considered. Taking the conductivity and density of the ceramic fibers as that of glass, 0.5 Btu/hr·ft·°F and 140 lb/ft<sup>3</sup> (Table IV, page 383, ref. 40), and with a packing density of 6 lb/ft<sup>3</sup>, the maximum apparent conductivity of the fiber matte would be:

$$\frac{6}{140} (0.5) = 0.02 \text{ Btu/hr·ft·°F} \quad (91)$$

at 500°F, which is of the same magnitude as for air. Thus, conservatively,  $C_5$  can be considered equal to  $C_9$ , and in a vacuum of less than 0.001 mm of Hg, the conductivity of the Fiberfrax insulation would be:

$$k_I = C_3 T^3 + (C_5/2) T = 11.95 \times 10^{-12} T^3 + 0.214 \times 10^{-4} T, \quad (92)$$

which was used in the experimental calculations and is plotted in Figure 31.

At 500°F, Equation (92) agrees quite well with the single-value measurement of Thigpen<sup>43</sup> (0.05 Btu/hr·ft·°F at air pressures greater than 100 mm of Hg and 0.02 Btu/hr·ft·°F at air pressures less than 0.1 mm of Hg) for a similar ceramic fiber insulation (type RF 600 manufactured by Johns-Manville with a packing density of 6 lb/ft<sup>3</sup> and 1 to 5 μ dia fibers). Considering that the actual value must at least lie between the manufacturer's data in air and the results of Equation (90) and that Equation (92) agrees with the experimental data, the conductivity values calculated by Equation (92) should be adequate to ±20 per cent.

## F. NOTATION

A	cross-sectional area, $\text{ft}^2$
AC	atomic heat capacity, $\text{Btu}/\text{lb}\text{-atom}\cdot^\circ\text{R}$
a, B, b, C, c	constants
$c_p$	heat capacity, $\text{Btu}/\text{lb}\cdot^\circ\text{F}$
$C_e$	thermal capacity of conductive electrons in unit volume, $\text{Btu}/\text{ft}^3\cdot^\circ\text{R}$
D	diameter, in.
$D_o$	outside diameter of test piece, in.
$D_i$	inside diameter of test piece sample container, in.
e	electronic charge
E	electromotive force, volts
f	frequency of vibration of an atom at melting point, cycles/hr
F	constant
h	Planck's constant ( $1.745 \times 10^{-40}$ $\text{Btu}\cdot\text{hr}$ )
$h_r$	radiative heat-transfer coefficient, $\text{Btu}/\text{hr}\cdot\text{ft}^2\cdot^\circ\text{F}$
J	temperature gradient along test piece, $^\circ\text{F}/\text{ft}$
k	thermal conductivity, $\text{Btu}/\text{hr}\cdot\text{ft}\cdot^\circ\text{F}$
$k_o$	thermal conductivity at $0^\circ\text{F}$ , $\text{Btu}/\text{hr}\cdot\text{ft}\cdot^\circ\text{F}$
$l$	mean-free path of an electron, ft
L	length, ft
$L_m$	latent heat of fusion, $\text{Btu}/\text{lb}$
$L_o$	Lorenz number [ $2.57 \times 10^{-8}$ $\text{Btu}\cdot\text{ohm}/\text{hr}\cdot(^\circ\text{R})^2$ ]
m	electronic mass
M	molecular weight

n	number of conductive electrons per unit volume, $\text{ft}^{-3}$
N	number of data observations
p	perimeter, ft
Q	heat flow, Btu/hr
r	radius, in.
S	surface area, $\text{ft}^2$
t	temperature, $^{\circ}\text{F}$
$t_e$	temperature at the lower end of the test piece, $^{\circ}\text{F}$
T	absolute temperature, $^{\circ}\text{R}$
TC	thermocouple
$T_m$	melting temperature, $^{\circ}\text{R}$
v	effective velocity of conductive electron in unit volume, $\text{ft}/\text{hr}$
V	volume, $\text{ft}^3$
x	axial distance from lower end of test piece, in.
$\alpha$	coefficient of linear thermal expansion, $^{\circ}\text{F}^{-1}$
$\beta$	coefficient of thermal conductivity temperature dependency, $^{\circ}\text{F}^{-1}$
$\beta_v$	coefficient of volumetric thermal expansion, $^{\circ}\text{F}^{-1}$
$\gamma$	density, $\text{lb}/\text{ft}^3$
$\Gamma$	constant
$\delta$	denotes error
$\epsilon$	emissivity, dimensionless
$\theta$	time, hr
$\kappa$	Boltzmann's constant ( $7.27 \times 10^{-27}$ Btu/ $^{\circ}\text{R}$ )
$\mu$	viscosity, $\text{lb}/\text{ft}\cdot\text{hr}$
$\pi$	3.1416...
$\rho_e$	electrical resistivity, $\text{ohm}\cdot\text{cm}$

$\phi$  characteristic temperature, °R

Subscripts

Fe	iron
G	guard tube
H	heat meter
i	interface between sample and heat meter
il	interface between sample and lower heat meter
iu	interface between sample and upper heat meter
I	insulation
L	liquid
Li	lithium
Ni	nickel
Pt	platinum
R	radial
ss	stainless steel
S	solid
SR	sample region
t	temperature dependent
t'	due to an error in $dt/dx$
t''	due to an error in $d^2t/dx^2$
T	test piece
W	wall
$\theta$	time dependent

ORNL-3390  
UC-4 - Chemistry  
TID-4500 (24th ed.)

## INTERNAL DISTRIBUTION

- |                      |  |
|----------------------|--|
| 1. S. E. Beall       | 14. S. E. Moore                        |
| 2. G. E. Boyd        | 15. J. E. Savolainen                   |
| 3. W. L. Carter      | 16. M. J. Skinner                      |
| 4. J. W. Cooke       | 17. J. A. Swartout                     |
| 5. J. H. DeVan       | 18. J. R. Tallackson                   |
| 6. T. G. Godfrey     | 19. W. C. Thurber                      |
| 7. R. L. Heestand    | 20. D. B. Trauger                      |
| 8. H. W. Hoffman     | 21. J. L. Wantland                     |
| 9. M. E. Lackey      | 22. A. M. Weinberg                     |
| 10. C. E. Larson     | 23-25. Central Research Library        |
| 11. A. P. Litman     | 26-27. Y-12 Document Reference Section |
| 12. R. E. MacPherson | 28-62. Laboratory Records Department   |
| 13. H. F. McDuffie   | 63. Laboratory Records, ORNL R.C.      |

## EXTERNAL DISTRIBUTION

64. Research and Development Division, AEC, ORO  
65-66. Reactor Division, AEC, ORO  
67-657. Given distribution as shown in TID-4500 (24th ed.) under Chemistry category (75 copies - OTS)